LASER INDUCED PROCESSES IN MOLECULAR IONS

By

Lee Nickey Morgenthaler

A DISSERTATION PRESENTED TO THE GRADUATE COUNCIL OF
THE UNIVERSITY OF FLORIDA
IN PARTIAL FULFILLMENT OF THE REQUIREMENTS FOR THE
DEGREE OF DOCTOR OF PHILOSOPHY

University of Florida

1979

ACKNOWLEDGEMENTS

This research is the fruit of the effort of many people. The instrument used was designed, fabricated, and assembled by the workers in the electronics and machine shops of the Chemistry Department of the University of Florida. Without their efforts this project would not have been possible. I received financial support from the Chemistry Department, through the ever-smiling Dr. Gerhard Schmit. I would also like to thank Dean Harry H. Sisler for the financial support he provided in 1977-1978. I thank the Tennesee Eastman Company for the financial support provided during my final year of graduate school.

Many of my colleagues at the University of Florida made a significant contribution to this work. Among them are Dr. Dan Reo of ICAAS who assisted me in the use of the curve fitting program, Dr. Milap Mathur of the Chemistry Department who assisted in the "chemical" aspects of this work and Dr. Ed Voigtman of the Fourth Floor who assisted in the design of the computer system. Many thanks also to the other members of Dr. Eyler's research group--especially Ron Daubach, "Bad"Bob Doyle, and Tom Buckley--for many helpful discussions.

Throughout this work I was sustained, both spiritually and materially, by many good friends. I would especially like to thank Aldo Atherton and Kelley and Janet St. Charles for their assistance in times of need. My best friend throughout this project was my wife Andi. She provided me with an unfailing supply of love and very vocal encouragement to complete the work.

Finally I would like to thank Dr. John Eyler for his inspiration, assistance, encouragement, and friendship.

TABLE OF CONTENTS

Chapter Page

ACKNOWLEDGEMENTS. ii

KEY TO IMPORTANT SYMBOLS AND ABBREVIATIONS. . vii

ABSTRACT. ix

1 INTRODUCTION. 1

2 THEORY. 15

Introduction 15

The Motion of Ion in the Trapped Ion Cell 17

The Pulsed Marginal Oscillator Detector. 21

Derivation of the Expression for the Photodissociation Cross Section. . 26

3 THE INSTRUMENT. 37

Introduction 37

The Vacumm System. 37

The Optical System 40

The Digital Electronics. 46

Interfacing the Pulse icr With a KIM-1 Microprocessor 51

Evaluation of the Performance of the Computer Data System 65

4 STUDIES OF THE PHOTODISSOCIATION OF OH^---STANDARDIZATION OF THE CELL. 72

Introduction 72

TABLE OF CONTENTS
(Continued)

Chapter Page

4 (Cont.)
Experimental 74
Results. 78
Discussion 90
Conclusions. 100

5 PHOTODISSOCIATION OF CHLOROETHANE MOLECULAR CATION. 101
Introduction 101
Experimental 104
Results. 112
Discussion 117
Conclusions. 123

6 PHOTODISSOCIATION OF BENZYL CHLORIDE MOLECULAR CATION 125
Introduction 125
Experimental 126
Results. 127
Discussion 130
Conclusions. 137

7 TIME-RESOLVED PHOTODISSOCIATION SPECTROSCOPY OF THE 1,3,5 HEXATRIENE MOLECULAR CATION 138
Introduction 138
Expermental. 144
Results. 152

TABLE OF CONTENTS
(Continued)

Chapter Page

7 (Cont.) Discussion 181

Conclusions. 186

REFERENCED BIBLIOGRAPHY 188

BIOGRAPHICAL SKETCH 193

KEY TO IMPORTANT SYMBOLS AND ABBREVIATIONS

$E(\lambda)$ -- Total energy at wavelength λ in a laser pulse, generally recorded as mV of joulemeter output, this quantity times 2.2 is the energy in mJ.

$E(\lambda)$ -- E( ) in mV times λ in nm, this quantity is proportional to the photon flux in photons $cm^{-2}s^{-1}nm^{-1}$ as derived on p. 26.

f -- The fraction of the ion population actually in the laser beam.

icr -- Ion cyclotron resonance mass spectrometry.

I.P. -- Ionization potential.

k_L -- The rate constant for orbiting collisions introduced on p. 81.

$K'\sigma$ -- The relative cross section for a photoinduced process.

m.o. -- Marginal oscillator.

N_c -- Mean collisional number (see p. 88).

$N(\lambda)$ -- The number of photons of wavelength λ in a laser pulse.

$P(\lambda)$ -- Probability that an ion will undergo a photoinduced process when irradiated at wavelength.

$\rho(\lambda)$ -- Photon flux at wavelength.

R -- The fraction of the ion population that disappears in photolysis.

$\sigma(\lambda)$ -- The absolute cross section for a photoinduced process in cm^2.

Z -- Collision frequency in s^{-1}.

Abstract of Dissertation Presented to the
Graduate Council of the University of Florida
in Partial Fulfillment of the Requirements
for the Degree of Doctor of Philosophy

LASER INDUCED PROCESSES IN MOLECULAR IONS

By

Lee Nickey Morgenthaler

June 1979

Chairman: John R. Eyler
Major Department: Chemistry

The pulsed icr pulsed laser technique is a means of probing a number of physical processes in excited molecular ions in the gas phase. A detailed spectrum, related to the absorption spectrum, of the ion can be obtained at a time when it has undergone anywhere from zero to fifty collisions with the background gas. The spectra of collisionally unstable ions may be studied before they decompose or react and collision induced changes in apparently stable ions can be followed spectroscopically.

Chloroethane molecular ion is an example of a collisionally unstable species that has been investigated successfully by this technique. The photodissociation spectrum indicates that the first excited electronic state

of this ion is weakly bound or flat and that the second excited state is purely repulsive with respect to scission of the carbon-chlorine bond. In addition, there is a strongly energy-dependent competition between two reaction channels. This effect is not predicted by quasi equilibrium theory, which indicates that the dynamics of the decay processes are dictated by the potential surfaces of the excited electronic states of the ion.

Several of the experiments presented here are attempts to probe the dynamics of rearrangement processes that had been discovered by the continuous icr technique. In the first case, benzyl chloride, the results presented here are not the same as those obtained in the continuous icr experiment. A kinetic scheme that reconciles the two results is suggested. Based on the results presented here one cannot be sure that rearrangement has occurred at all.

In the second example, cis trans isomerization in the 1,3,5 hexatriene cation, emission spectroscopy indicated that the structure of the ions formed from the two isomers of the parent compound were different on the time scale of 10^{-8} s. However, continuous icr photodissociation spectroscopy indicated that the two structures were identical on the time scale of several seconds. The results presented here indicate that the ions of the two isomers are the same within 10 ms of ionization. No information about the kinetics of the rearrangement process can be obtained in this case.

The collisional relaxation of vibrationally excited 1,3,5 hexatriene molecular ion was also studied. The rate of quenching by the parent molecule was observed to depend on the ionization energy. Ions formed at the higher ionization energy were quenched on every nonreactive collision with the parent molecule. This result is consistent with other studies of similar processes in molecular ions. Ions formed at the lower ionization energy were quenched less efficiently by a factor of four--an unexpected result. Quenching by argon atoms was also investigated and found to be extremely rapid--about two orders of magnitude faster than the corresponding process in neutrals.

CHAPTER 1
INTRODUCTION

The existence of charged particles arising from ordinary chemical compounds was proposed by Arrhenius in his doctoral dissertation, published in 1884. By 1900 conductivity measurements on electrical discharges and flames had established the presence of similar charged particles in the gas phase. The study of gaseous molecular ions began with the development of the mass spectrograph by J.J. Thomson in 1907. Within a few years several investigators reported evidence of chemical reactions between gas-phase ions and the molecular samples from which they were formed. A few studies of these reactions appeared in the next forty years, but it was not until 1950 that the study of ion-molecule reactions began in earnest.

In more recent times (beginning around 1960) the investigation of ion-photon interactions was begun. This field of study evolved from the study of ion-molecule interactions both in terms of the motivation behind it and in terms of the instrumentation used. Such studies have yielded information about the energetics of electron detachment from negative ions and about the dynamics of photodissociation of both positive and negative ions.

In addition, the technique of photodissociation spectroscopy has shown promise of providing a sensitive probe of the structure of gas-phase ions. The studies reported in this dissertation yield information about the dissociation of several molecular ions. Both the dynamics of the dissociation process itself and the structure of gas-phase ions are probed. In addition, this work is one of the first attempts to study such processes in a fully pulsed mode of operation. The research presented here examines some of the capabilities of the pulsed technique.

A number of experimental techniques have been developed for the study of ion-molecule reactions and ionic decomposition. All of them were based upon mass spectrometers that were modified to study the specific process of interest. These modifications have included variable pressure sources (1), photoionization sources (2), various coincidence techniques (3), and various schemes for kinetic energy analysis of fragments (4). A further development was the use of two mass spectrometers in series, so-called tandem mass spectrometers, to study the ionic products of the reactions of a specific ion with a neutral gas (5). Another type of mass spectrometer, the ion cyclotron resonance (icr) mass spectrometer, also proved to be very useful in these studies (6,7). The long residence times and the low sample pressures that can be achieved in these instruments make them ideally suited to the investigation of gas-phase ion-molecule reactions.

Studies of ion-molecule reactions have had three important impacts on chemistry as a whole. Studies of the unimolecular decomposition of ions have played a major role in the development of the theory of unimolecular decomposition (8). This in turn has been an important input to the transition state theory of chemical reactions since the decay of the intermediate complex is treated as a unimolecular decomposition.

Gas-phase ion-molecule reactions are often similar to reactions hypothesized in liquid-phase chemistry. Many reactions in solution are thought to proceed via ionic intermediates which have very brief lifetimes and whose existence in solution can only be inferred. Elaborate theories relating the structure of these ionic intermediates to their stability and chemistry have been developed and inflicted upon generation after generation of unsuspecting organic chemistry students. The study of gas-phase ion-molecule reactions provides a means of examining directly the chemistry of these legendary species in the absence of "solvent" effects. It has provided a test for many theories of reaction mechanisms (9).

Although it is a powerful analytical technique, electron impact mass spectrometry has the serious drawback that it only measures the mass-to-charge ratio of the ions arising from a given sample. Many different compounds, particularly structural isomers of complex molecules, yield indistinguishable electron impact mass spectra. The third major impact of studies of ion-molecule interactions is a powerful technique for overcoming this difficulty: chemical ionization mass spectrometry (10). In this approach the sample is ionized in an ion-molecule reaction. It may be hoped that a further elucidation of the properties of gas-phase ion-molecule interactions will lead to new developments in this field.

Beyond the confines of chemistry itself, there are many fields where the study of ion-molecule reactions may lead to important new insights. Among them are aeronomy, combustion technology, and radiation biology. Of course the analytical technique of chemical ionization mass spectrometry is of importance in many more fields of investigation than can be enumerated here.

A second class of gas-phase ion-particle interactions that has aroused considerable interest may be called ion-photon interactions. Principal among these are photodetachment of negative ions and photodissociation of either positive or negative ions. Such processes are of basic physical and chemical interest. Studies of photodetachment, for example, are thought to yield extremely accurate values of the electron affinity of many molecular species (11). The study of the photodissociation of positive ions has yielded information about the location, stability, and dynamics of the decomposition of excited states of molecular ions. In addition, since a photon must be absorbed for photodissociation to occur, the study of ionic photodissociation provides a means of examining the spectroscopy of gas-phase ions. Such information is very difficult to obtain by spectroscopic techniques normally employed in the study of neutral species.

The development of gas-phase ion spectroscopy has been greatly accelerated by the advent of lasers. In general ion densities are low in the gas phase and consequently very intense light sources are required. Prior to the introduction of laser light sources the spectral resolution of studies of ion-photon interactions was limited by this need for a high photon flux. Lasers with their high intensity and spectral resolution are particularly well suited to the study of gas-phase ion spectroscopy.

Instrumentation used to study ion-photon interactions has been developed from that used to study ion-molecule reactions. The simplest modification consisted of opening a window into the ion source of a mass spectrometer and irradiating the sample there (12,13). Such techniques may be classified as "high pressure swarm" techniques using a classification scheme introduced by Henchman (14). A number of such studies have been described. They are, with few exceptions, of principally historical interest. For one thing, these techniques were not specific as to which ion was in fact being dissociated or detached. Under normal source conditions the daughter particles from the photoinduced process might undergo as many as 100 collisions prior to mass analysis. Since these species are almost by definition high energy (in the chemical sense) species, there is the possibility that these techniques may sample secondary or higher-order products of reactions between the daughter and neutral species. In addition, the spatial distribution of the ion population in these instruments is not known, making quantitative measurements of absolute cross sections impossible.

Techniques based on the tandem mass spectrometer, "beam techniques" in Henchman's scheme, have provided a far more detailed picture of ion photodissociation and photodetachment. Both crossed laser-ion beam (15) and coaxial laser-ion beam (16) instruments have been constructed. In both systems particle densities and spatial distributions are reasonably well defined and absolute cross sections can be measured with some confidence. Coaxial beams can be Doppler-tuned to provide extremely high spectral resolution. In crossed beam instruments the measurement of the angular distribution and kinetic energy of photofragment ions and photodetached electrons can be measured. Both of these techniques provide extremely detailed data on the dynamics of the photoinduced process. To date both have been applied principally to simple ions.

Ion cyclotron resonance mass spectrometry can be classified as a "low pressure swarm" technique. Such instruments have been modified for studies of the photodetachment and photodissociation of gas-phase molecular ions.

Because the icr technique allows for irradiation and mass analysis in the same chamber of the instrument and because operating pressures are often so low that an ion undergoes only a few collisions per second, some of the difficulties encountered in the high pressure swarm techniques are minimized in continuous icr mass spectrometry. However, this is not always the case and must be considered on a case-by-case basis. Unfortunately the spatial distribution of ions in the icr cell is difficult to analyze (17) making the determination of absolute cross sections nearly impossible. In general, photodissociation and photodetachment studies in icr instruments have involved a wider variety of ions than those using other techniques. A number of studies of large and complex ions have appeared (18,19).

The wavelength dependence of the cross section for photodissociation or photodetachment, the photodissociation or photodetachment spectrum, yields truly spectroscopic information. The threshold for photodetachment can be related to the electron affinity of the neutral species (11). The onsets for detachment to excited states of the neutral species can be identified by abrupt changes in the photodetachment cross section with wavelength. The photodissociation of gas-phase ions with visible light proceeds via excited electronic states of the ion. This can be confirmed by comparison of the photodissociation spectrum to the photoelectron spectrum (20) of the parent neutral.

In the photoelectron spectrum the lowest ionization potential corresponds to ionization to the ground state of the ion. The higher ionization potentials correspond to formation of excited states of the ion. The difference between a given ionization potential and the lowest yields the energy of the given excited electronic state of the ion. This analysis is confirmed by the fact that almost all photodissociation spectra that have appeared so far correspond closely to the photoelectron spectra of the parent molecules.

The photodissociation spectrum is related to the absorption spectrum of the ion since photodissociation involves the absorption of a photon. However, photodissociation also involves dissociation. Every photon that is absorbed may or may not cause dissociation. As a result the photodissociation cross section is only an lower limit to the absorption cross section.

The most elegant and complete study of photodissociation of a molecular ion was, ironically perhaps, the first to appear using the crossed ion-laser beam technique (21). A fixed frequency laser was used to dissociate H_2^+ and D_2^+. The fragment ion kinetic energy was obtained along with the angular distribution of ionic photofragments. Such results yield detailed information about the orientation of the electronic transition moment and the lifetime of the excited state. For H_2^+ and D_2^+, these results could be compared to theoretical predictions (excellent agreement was observed).

Moseley and his co-workers (16) have employed Doppler-tuning of their coxial ion-laser beams to examine the rovibronic structure of a long-lived ($^4\Pi_u$) state of O_2^+. This study highlights the extremely detailed information that can be obtained in favorable cases by photodissociation spectroscopy.

The most important results obtained to date by icr photodissociation spectroscopy have been related to the identification of the structure of molecular ions in the gas phase. Numerous ions of the same mass but arising from different neutral precursors have been investigated. According to Lineberger (11) these studies have provided the most convincing evidence as yet available that the structure of a molecular ion in the gas phase is related to the structure of the parent molecule. This result is important, for if it were not so, the comparison of gas-phase ion chemistry to solution chemistry would have little validity. A variation on this theme is provided by a recent study of reactively produced chloropropene ($C_3H_5Cl^+$) molecular ions (22). Different isomers of $C_3H_5Cl^+$, identified by their photodissociation spectra, were shown to arise from several ion-molecule reactions. Prior to this study the actual structure of the products of an ion-molecule reaction could only be inferred. Such investigations promise to yield new and more detailed information about the mechanisms of gas-phase ion-molecule reactions.

A second interesting area of investigation, currently being pursued by steady state icr techniques, is multiphoton dissociation of molecular ions (23). Because of the low operating pressures employed in the continuous icr, radiative decay (24) is often the only mode of relaxation for excited ions. If radiative decay is slow, many photons may be absorbed by an ion even at relatively low light intensities. In addition to providing information about the excitation and de-excitation of gas-phase ions, such studies may lead to new insights into the phenomenon of sequential photon absorption.

Pulsed icr mass spectrometry (25) was developed somewhat more recently than steady state icr mass spectrometry. Few studies of photodetachment or photodissociation have been carried out with this technique (26,27). Furthermore, none of these studies has attempted to exploit the time resolution of the pulsed icr. Although several investigators have used a technique that they call "time resolved photodissociation spectroscopy" (28,29) they have not obtained a time resolved photodissociation spectrum. Rather they have measured the rate of disappearance of an ion when irradiated with a continuous light source. The term "exhaustive photodissociation" used in one report (29) about this technique more accurately reflects the truth of the matter.

In a sense the experiments reported below are "technique" oriented rather than "problem" oriented. Each is an attempt to use the time resolution of the pulsed icr technique to obtain information that cannot be obtained in the continuous icr. Each represents a different facet of the instrument's capabilities. The first study (Chapter 4) is essentially a calibration experiment. The photodetachment of OH^- has been well studied (30,31) and no new information is reported here. The cross section for a photoinduced process is shown to vary slowly with ion residence time between the first few and at least the fortieth collision. Some effect of magnetic field strength and laser alignment are observed and procedures are developed to correct for them.

The study of chloroethane molecular ion presented in Chapter 5 uses the time resolution of the pulsed icr to investigate an unstable ion whose abundance is very low in a steady state icr instrument (32). The photodissociation spectrum yields interesting information about the excited state potential surfaces of the ion. In addition, data on the competition between dissociation channels were obtained. A similar study of the butene molecular cation has been reported by Riggin (33). His results are explained successfully by the quasi equilibrium theory (8) of unimolecular decompositions. In contrast, the results obtained in the study of chloroethane molecular ion reported here bear no resemblance to the predictions of quasi equilibrium theory.

A study using the exhaustive photodissociation technique (29) suggested that the population of the parent ion (m/e = 126) of benzyl chloride consisted of two molecular structures one of which dissociated at a wavelength of 600 nm (30 percent of the population) and one of which did not. The results presented below suggest that this analysis is simplistic. The maximum percent dissociation observed is at least 65 percent. Moreover, the apparent cross section is unchanged for at least 2.5 s corresponding to roughly 100 collisions. No evidence of rearrangement is observed. A kinetic scheme consistent with all of these observations (both pulsed and steady state studies) is presented.

Another well studied molecular cation is that of 1,3,5, hexatriene. Evidence obtained by emission spectroscopy (34) indicated that there were two distinct isomers of the molecular ion in the gas phase. One arose from the cis isomer of the molecule and one from the trans. A study of ions formed from both molecules carried out in a continuous icr (35) indicated that no matter which neutral precursor was used the structure of the molecular ion was the same. The results presented below also suggest that the parent ion is identical no matter which isomer of the parent molecule is ionized. This indicates that the ion rearranges rapidly after ionization.

A hot band at 646 nm was reported in both the emission spectrum and the steady state photodissociation spectrum of

1,3,5 hexatriene molecular ion. This band was also observed in the photodissociation spectrum reported in Chapter 7. The decrease in the intensity of this band relative to a transition from the ground vibrational state of the ion with time was obtained. From this the rates of quenching of the vibrationally excited ions in collisions with the parent molecule and with argon atoms were obtained. Although several measurements of the rate of comparable processes have appeared based on indirect evidence, this is the first direct measurement of the rate of V-T transfer in a molecular ion. The results, in general agreement with those obtained by indirect means (23,36,37), show collisional quenching of vibrational excitation in molecular ions to be very rapid compared to similar processes in neutral species.

In addition to the inherent value of each of these results as a measurement of a basic physical process, these studies outline the capabilities and limitations of the pulsed icr instrument. The pulsed icr is not particularly well suited to the study of the kinetics of unimolecular decomposition. Many unimolecular reactions occur much faster than the minimum time resolution (about 1 ms) of the instrument. However, the pulsed icr is more useful than the continuous icr for the study of the competition between reaction channels because product ions can be detected within a few ms of irradiation (before they undergo any collisions). Thus, only the products of the unimolecular decomposition of the excited ion are sampled. Because of the narrow bandpass of the laser output, a precisely known amount of excitation energy is applied in this experiment. Subtle differences in the probability of a reaction with excitation energy can thus be probed.

The ability to obtain a complete photodissociation spectrum at a specific time after the formation of an ion makes the study of the rearrangement of gas-phase ions possible. Such processes have been shown to occur using steady state icr photodissociation spectroscopy (29). However, such studies yield little information about the dynamics of the rearrangment process. Pulsed icr techniques complement the steady state technique and offer considerably more flexibility in the study of rearrangement processes.

The real forte of the pulsed icr is the study of collisional processes because the time resolution of the instrument is comparable to the collision lifetime of an ion at normal operating pressures. The study of V-T energy transfer in 1,3,5 hexatriene reported in Chapter 7 below is one example of this capability. It may be hoped that the study of ion-photon interactions will prove to be as interesting as that of ion-molecule reactions. Studies of ion-photon interactions in the gas phase should answer some questions raised by the study of ion-molecule reactions. Moreover, the study of ion-photon interactions promises to yield considerable information about physical and chemical processes in excited molecular species.

CHAPTER 2
THEORY

Introduction

The instrument used in these experiments was a pulsed ion cyclotron resonance (icr) mass spectrometer (25) employing a trapped ion cell (38) and coupled to a flash-lamp pumped dye laser in an intracavity configuration (39). The specific mechanical, optical, and electronic layout of the instrument is described in Chapter 3. In this chapter the motion of ions in the trapped ion cell is considered; the principle of mass analysis using a pulsed marginal oscillator detector (40) is described. In the final section the relationship between the quantities measured experimentally and the physical observable of interest, the relative cross section for a photoinduced process, is derived (41).

Figure 2.1 is a schematic of a trapped ion cell. The axes shown are referred to throughout the text and the origin is labelled. ICR mass spectrometry is based on the principle that a charged particle, in this case an ion, in crossed magnetic and electric fields executes a circular

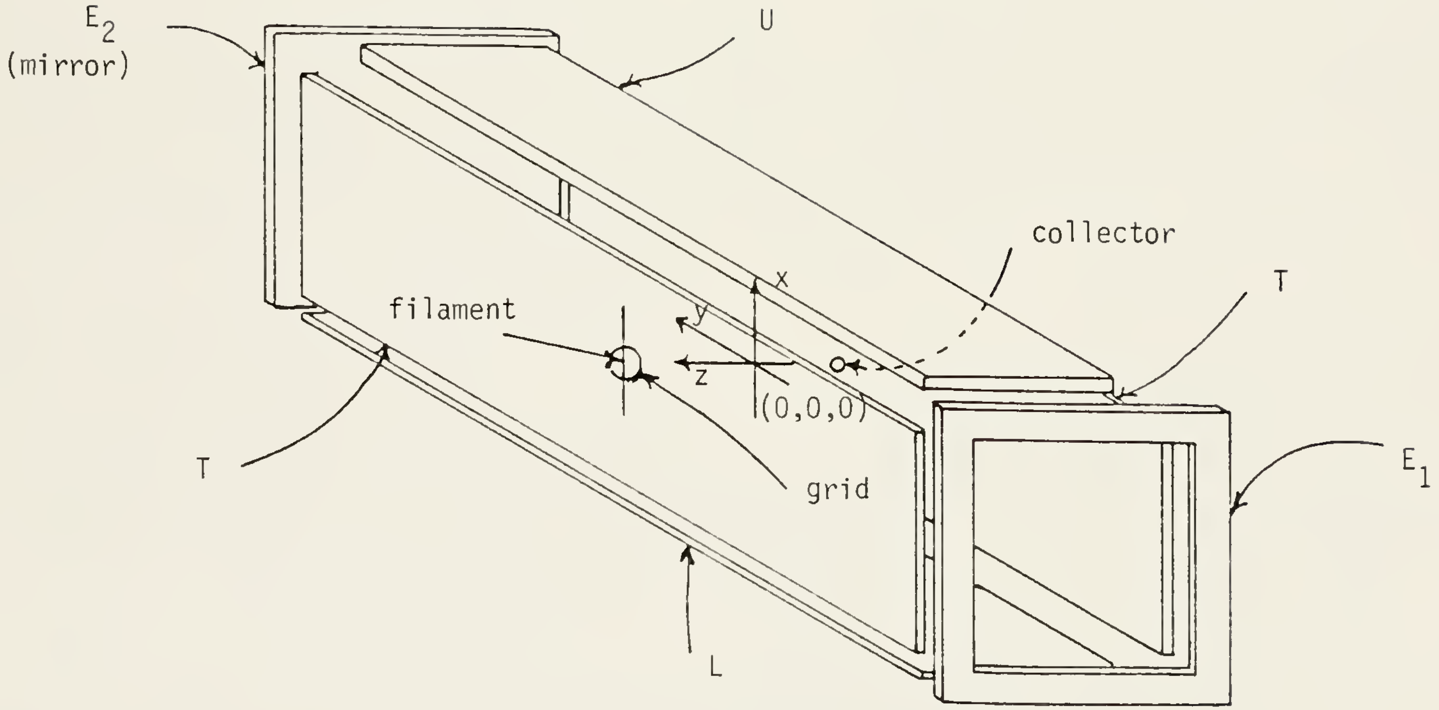

Figure 2.1. Diagram of Trapped Ion Cell

motion perpendicular to the magnetic field the frequency of which, ω_f, is given by:

$$\omega_f = qB/m \qquad 2.1$$

where q is the charge of the ion, m is its mass, and B is the magnetic field strength. If an oscillating electric field of the same frequency as the ion motion is applied perpendicular to the magnetic field, the ions absorb energy from it and are accelerated to larger orbits. The power loss from the oscillating circuit is proportional to the number of ions of a given mass-to-charge ratio in the cell. In the absence of the oscillating electric field the imposition of the appropriate potentials on the walls of the cell forms an efficient ion trap (38). The usefulness of such a system for the study of ion-molecule reactions has been reviewed recently (6,7).

The Motion of Ions in the Trapped Ion Cell

The equations of motion for an ion in a trapped ion icr cell have been obtained (17). The force, $\vec{F}$, acting on an ion with initial velocity $\vec{v}$ in crossed magnetic and electric fields ($\vec{B}$ and $\vec{E}$, respectively) is given by the Lorentz equation:

$$\vec{F} = q(\vec{E} + \vec{v} \times \vec{B}). \qquad 2.2$$

Here, q is the charge on the ion. In the trapped ion cell the potentials on the upper, lower, and end plates of the cell (labelled as U, L, and E, respectively, in Figure 2.1) are typically -1.0 V and those on the side plates (T) are +1.5 V for positive ions. The polarity of these potentials is reversed for negative ions. The magnetic field is applied parallel to the z axis and the oscillating electric field is applied along the x axis. The laser beam is parallel to the y axis in the photochemistry experiments. The potential on the side plates repels ions as they oscillate parallel to the magnetic field as described more fully below.

The electric field can be approximated by a two-dimensional quadrupole field for ions close to the origin of the cell (17) and the magnetic field is constant over the ion trap region. The motion of an ion trapped in such a potential has three characteristic components. The most important of these is the cyclotron motion in the x,y plane. It has the characteristic frequency:

$$\omega_c^2 = (qB/m)^2 - 4qV_T/md^2 \qquad 2.3$$

where ω_c is the observed cyclotron frequency of the ion motion. The first term on the right hand side is the ideal cyclotron frequency and the second term is a correction for the effect of the trapping potential, V_T. The separation between the upper and lower cell plates is d.

The second aspect of the ion motion is a rapid simple harmonic oscillation parallel to the z axis about the origin of formation of the ion. The frequency of this motion is a function of the trapping potential.

The third component is a slow drift of the generating center for the two oscillations described above. In the absence of collisions and space charges, this drift causes the cross section of the ion "cloud" to oscillate between being a circle in the x,y plane and an ellipse in the x,y plane with the long axis parallel to the y axis. The greater the kinetic energy of an ion the larger the amplitude of the drift motion.

In the experiment ions are formed initially in a band along the z axis of the cell by the electron beam emitted by a hot filament. The initial acceleration of the electrons is due to the negative potential on the filament and this is given as the nominal electron energy. However, the trapping potentials affect the electron's motion so the true energy of the ionizing electron is a function of its position in the cell.

At the time of formation the generating centers for the ion motion form a circular cylinder across the cell parallel to the z axis. The frequency of the drift motion is given by:

$$\omega_d = \Omega/2\Pi \qquad 2.4$$

$$\Omega = 2(V_T - V_o)(\alpha\beta)^{1/2}/a^2B. \qquad 2.5$$

The constants α and β are related to the geometry of the cell and a is the length of the cell parallel to the x axis. The trapping potential is again given as V_T and V_o is the potential applied to the upper and lower plates of the cell. Values of α and β have been reported for a cell similar to the one used here (17). Substituting the appropriate values of V_T and V_o from our experiments yields a frequency for the drift motion of approximately 190 Hz at 8000 G. The frequency of the change in shape of the ion "cloud" is twice the frequency of the motion. Thus, the time associated with the change in shape is 2.7 ms at 8000 G and less at lower fields. In all the experiments described here ions are formed for at least 5 ms. Consequently, the effects of the oscillation of the shape of the ion "cloud" are cancelled out because ions are formed for at least two periods of the oscillation. The resultant drift path is best described as a quasi-ellipse in the x,y plane with the long axis parallel to the y axis. Both of the fast oscillations--the cyclotron motion in the x,y plane and the simple harmonic parallel to the z axis--originate from centers travelling this complicated drift path.

The Pulsed Marginal Oscillator Detector

In the pulsed marginal oscillator (m.o.) (40) detection system the mass detection of ions is achieved by applying a gated burst of potential to the upper plate of the cell. This potential has the effect of changing the form of the electric field, E, during the time the burst is applied from the quadrupole potential of the static trap to:

$$\vec{E}(t) = E_1(\sin\omega_i t)\vec{i}. \qquad 2.6$$

The frequency of the applied potential is ω_i, E_1 is the amplitude, t is the time, and $\vec{i}$ is the unit vector in the x direction. Solving the Lorentz equation with this new potential yields a function for the ion velocity that is time dependent. The kinetic energy, T, obtained from this velocity, v, is:

$$T = 1/2\ mv^2 = [q^2E_1^2/2m(\omega_i-\omega_c)^2]\ \sin^2(1/2)(\omega_i-\omega_c)t. \qquad 2.7$$

For the singularity, $\omega_i = \omega_c$, the straightforward application of l'Hopital's rule yields:

$$T = q^2E_1^2t^2/8m. \qquad 2.8$$

The power absorbed by a single ion is given by:

$$A(t) = dT/dt$$

$$= [q^2E_1^2/4m(\omega_i-\omega_c)] \sin(\omega_i-\omega_c)t \qquad 2.9$$

and

$$A(t) = q^2E_1^2t/4m, \qquad \text{if, } \omega_i = \omega_c. \qquad 2.10$$

In practical pulsed operation the detect pulse is usually shorter than the collision lifetime of the ion so the effect of collisions on the power absorption can be neglected. The average power absorption per ion is given by:

$$\langle A\rangle = {}_{t_o}^{t}\!\int A(t)dt \qquad 2.11$$

$$= q^2E_1^2\tau/8m, \qquad \text{if, } \omega_i = \omega_c. \qquad 2.12$$

Here, τ is the ion's lifetime in the oscillating field. For a sample of n ions:

$$\langle A\rangle = nq^2E_1^2\tau/8m. \qquad 2.13$$

Measurement of resonant power absorption is obtained with a GCL circuit like the one illustrated in Figure 2.2 (40). This circuit has a resonant frequency:

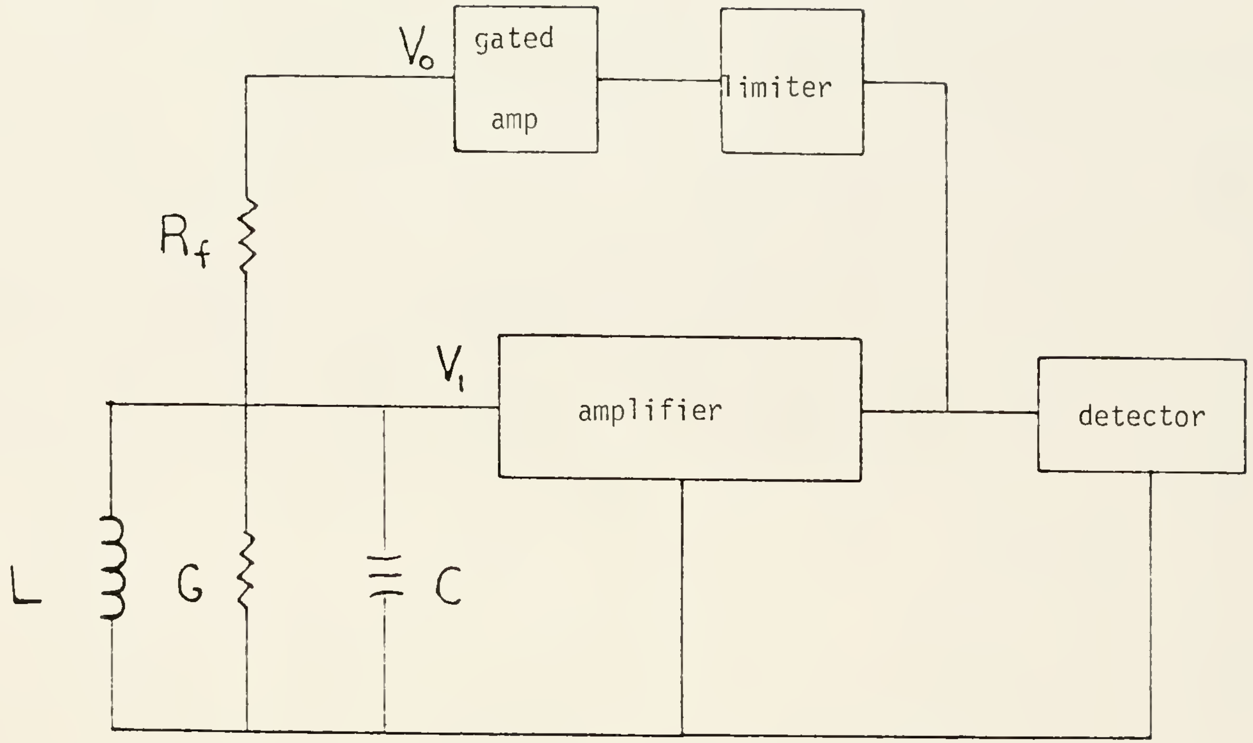

Figure 2.2. Diagram of m.o. Circuit

$$\omega = (LC)^{-1/2} \tag{2.14}$$

where L is the inductance, C the capacitance, and the conductance, G, represents losses due to nonideality of the circuit. A constant amplitude radio frequency voltage is provided to the resonant circuit through the feedback resistor R_f. For pulsed operation this voltage is switched on and off by the gated amplifier. At the resonant frequency the admittance of the resonant circuit is:

$$V_1 = V_0/(1 + GR_f). \tag{2.15}$$

In this equation V_0 is the rms voltage from the limiter and V_1 is the rms voltage across the resonant circuit. The absorption by resonant ions in the cell represents a change in the conductance of the circuit, ΔG. The corresponding change in voltage, ΔV, is just:

$$\Delta V = V_0\{1/(1 + GR_f) - 1/[1 + (G + \Delta G)R_f]\} \tag{2.16}$$

$$= V_1 \Delta G[R_f/(1 + (G + \Delta G)R_f]. \tag{2.17}$$

If ΔV is small the incremental power absorption, A, due to ΔG is given by:

$$A = V_1^2 \Delta G. \tag{2.18}$$

If ΔG is small and Expression 2.18 above is substituted into Expression 2.17 then:

$$\Delta V = (A/V_1)(R_f/1 + GR_f). \qquad 2.19$$

If the expression for power absorption obtained above (Equation 2.10) is substituted into Equation 2.19 the instantaneous voltage change due to a single resonant ion is obtained as:

$$\Delta V = (q^2E^2t/4mV_1)(R_f/1 + GR_f) \qquad 2.20$$

The average value of the voltage change induced by an ensemble of n ions is then:

$$<V> = (nq^2E^2/8mV_1)(R_f/1 + GR_f). \qquad 2.21$$

In practical operation the output of the m.o. is integrated by a switched integrator circuit as described in Chapter 3. The final measured signal is thus $<V>$ and V_1, R_f, and G are constants of the analysing circuit. It can be seen that the magnitude of an ion signal is directly proportional to the number of ions of a particular mass-to-charge ratio in the cell. The magnitude is also shown to be inversely proportional to the ion's mass. This correction must be applied routinely in pulsed icr work (25).

Derivation of the Expression for the Photodissociation Cross Section

From this experiment one obtains a signal proportional to the number of ions of a given mass-to-charge ratio in the icr cell when no laser irradiation is applied, a signal proportional to the number of such ions with the laser flashing, and the total energy in each flash of the laser. In this section the relationship between these measured quantities and the quantity of interest, the relative photodissociation cross section, is derived and discussed.

The probability that an ion will photodissociate at wavelength λ, $P(\lambda)$ is given by:

$$P(\lambda) = 1 - \exp[-kt\int\rho(\lambda)\,\sigma(\lambda)\,d\lambda] \qquad 2.22$$

where k is an overlap factor between the laser and the ions, t is the laser pulse duration, $\rho(\lambda)$ is the flux of photons of wavelength λ and $\sigma(\lambda)$ is the absolute cross-section for photodissociation at λ. The integration is carried out over the bandwidth of the laser output.

If $E(\lambda)$ equals the energy in a laser pulse at wavelength λ then $N(\lambda)$, the number of photons of wavelength λ in the pulse, is:

$$N(\lambda) = E(\lambda)\,\lambda/hc \qquad 2.23$$

and

$$\rho(\lambda) = N(\lambda)/at \qquad 2.24$$

where a is the cross-sectional area of the laser beam. The number of ions, A, which dissociate from a sample B at wavelength λ is:

$$A = fBP(\lambda) \qquad 2.25$$

where f is that fraction of the ion population actually irradiated by the laser. The experimental fractional dissociation, R, is then:

$$A/B = fP(\lambda) = R. \qquad 2.26$$

Substituting 2.22 into 2.25 yields:

$$A = fB\{1 - \exp[-kt\int\rho(\lambda)\sigma(\lambda)d\lambda]\}. \qquad 2.27$$

Since the bandwidth of the laser output at any grating setting is small, ca. 0.3-0.5 nm, it can be assumed that $\rho(\lambda)$ and $\sigma(\lambda)$ are constant over the bandwidth of the laser output. It may also be assumed that the bandwidth is constant at all grating settings. Thus,

$$\int\rho(\lambda)\sigma(\lambda)d\lambda = \rho(\lambda)\sigma(\lambda)\ m \quad (m = \text{constant}) \qquad 2.28$$

and with these assumptions 2.27 becomes:

$$A = fB\{1 - \exp[-kt\, \rho(\lambda)\sigma(\lambda)m]\}. \qquad 2.29$$

Substituting 2.23 and 2.24 into 2.29 yields:

$$A = fB\{1 - \exp[-(km/hca)E(\lambda)\ \lambda\sigma(\lambda)]\}. \qquad 2.30$$

Taking logarithms and rearranging yields:

$$-\ln(1-A/fB) = (km/hca)E(\lambda)\lambda\ \sigma(\lambda). \qquad 2.31$$

Setting km/hca = K', substituting 2.26 into 2.31 and solving yields:

$$K'\sigma(\lambda) = [\ln(f/f-R)]/\lambda E(\lambda). \qquad 2.32$$

The term k in Expression 2.22 above is loosely described as an "overlap factor." As discussed in Chapter 1, the laser ion interaction region in this experimental apparatus is poorly defined. In our particular apparatus this problem is compounded by the fact that routine maintenance of the mass spectrometer necessitates frequent realignment of the laser. The ion packet orbiting in the trapped ion cell is probably considerably smaller than the laser beam diameter, so k should be related to the fraction of the laser beam that irradiates the ions. Since the ions drift along the long axis of the cell k is also related to the degree of overlap between the laser beam and the ion "cloud." As such it can be expected to change somewhat with laser alignment. Qualitatively k can be thought of as a measure of the relative size of the laser-ion interaction region.

In the discussion above f is described as that fraction of the ion population actually irradiated by the laser; i.e., if 95 percent of the ion population is irradiated, f = 0.95. However, a second factor may lead to an f value less than unity. If some fraction of the ion population is not dissociable then f will appear to be less than 1.0. Figures 2.3 and 2.4 illustrate the behavior of Equation 2.32 with changes in K' (2.3) and f (2.4).

An important pair of assumptions is introduced in Equations 2.24 and 2.25. The quantity $\rho(\lambda)$ is set equal to the total number of photons in the laser pulse divided by the cross-sectional area of the beam and the duration of the pulse. As such it is an average flux. Equating this with the local flux through the sample is correct only if the cross-sectional area of the beam is constant at all $E(\lambda)$. If the area is a function of the geometry of the lamp and optics, this will be true. If not, a serious distortion of the intensity dependence may result. This effect is illustrated in Figure 2.5. Here Curve A

Figure 2.3. Curves Predicted by Equation 2.32 ($f = 1.$)

$A - K'_\sigma = 1 \times 10^{-4}$

$B - K'_\sigma = 6 \times 10^{-5}$

$C - K'_\sigma = 3 \times 10^{-5}$

$D - K'_\sigma = 1 \times 10^{-5}$

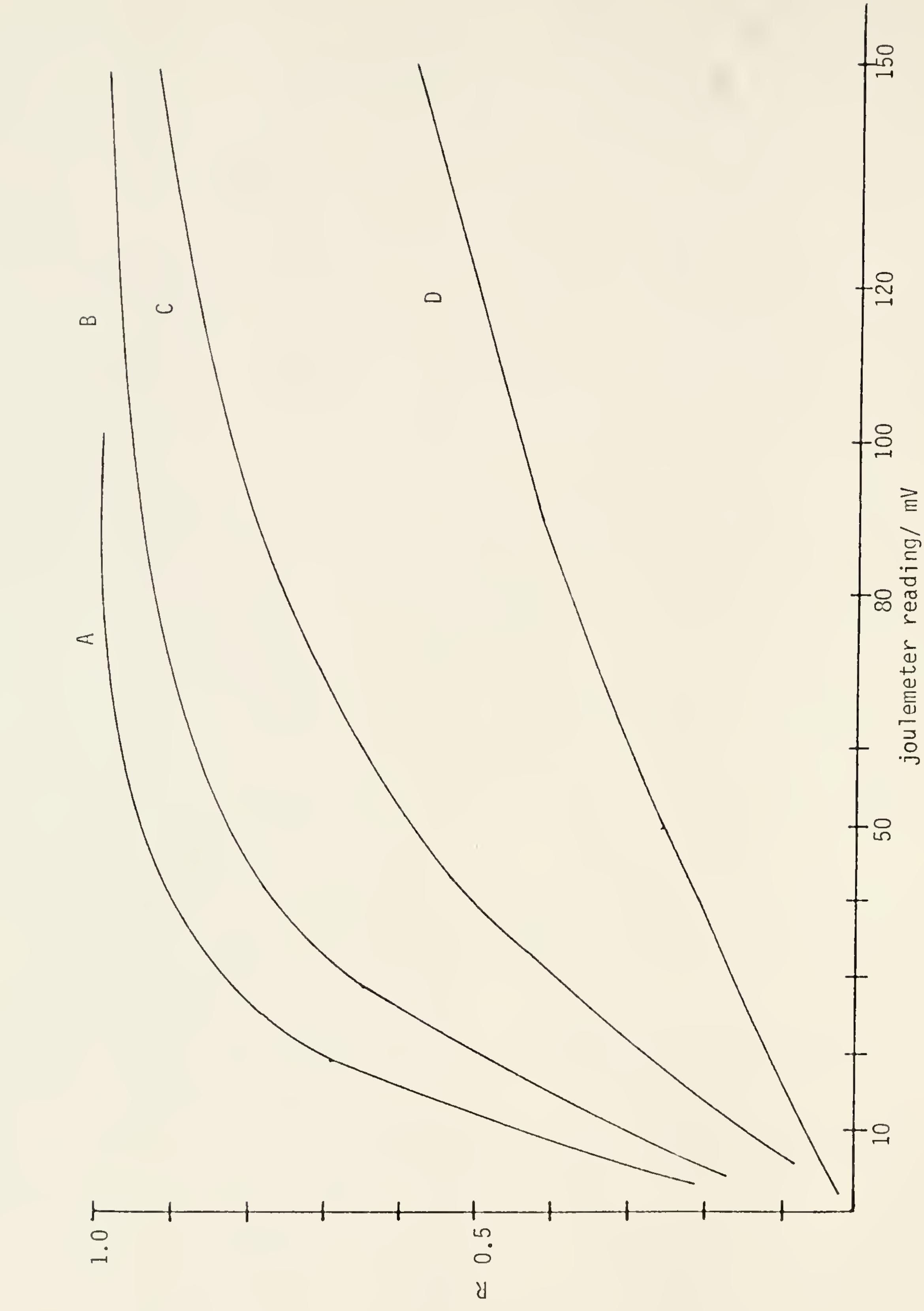
1.0
R 0.5
10
50
80
100
120
150
joulemeter reading/ mV
A
B
C
D

Figure 2.4. Curves Predicted by Equation 2.32: A - $f = 1.$; B - $f = 0.9$; C - $f = 0.75$; D - $f = 0.50$

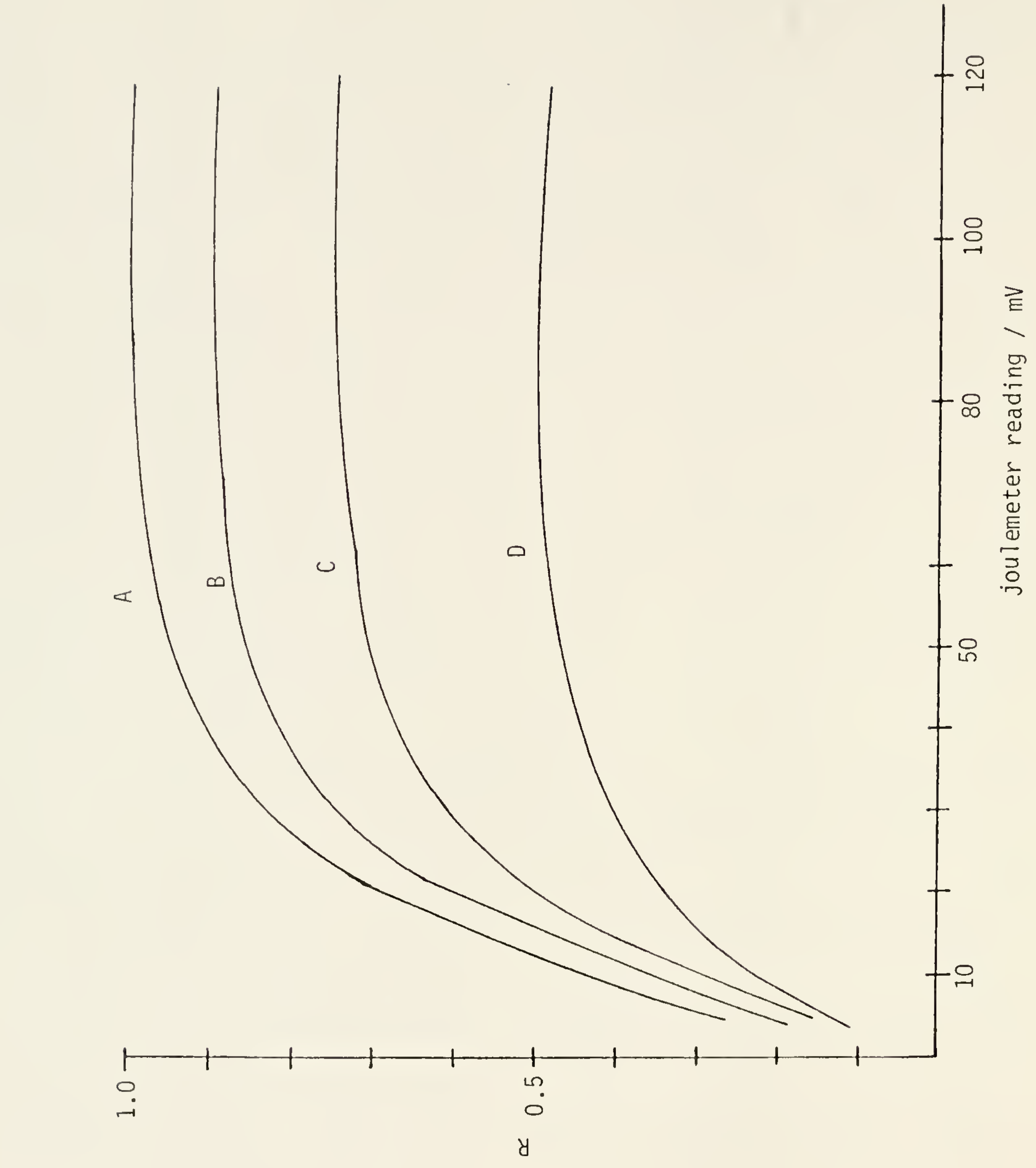
R
1.0
0.5
10
50
80
100
120
joulemeter reading / mV
A
B
C
D

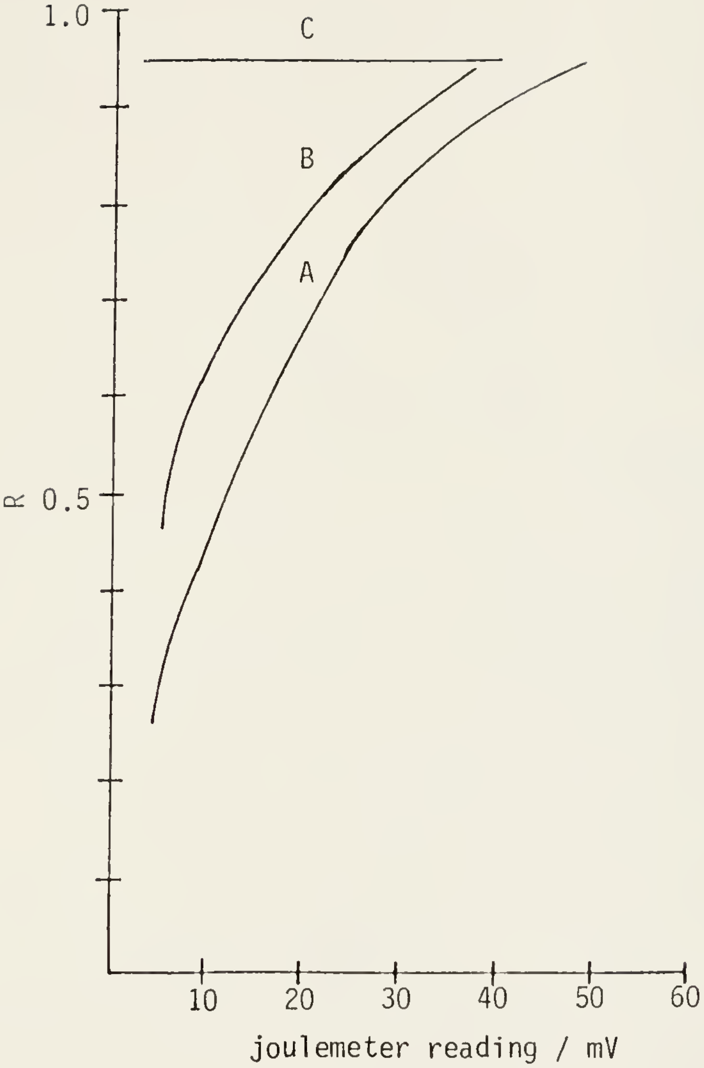

Figure 2.5. Illustration of Effects of Variation in Laser Beam Profile on Measured R value (see text for details)

represents the result if a is constant as assumed. In Figure B, a is varied with $E(\lambda)$ according to the relationship:

$$a = a_0 + rE(\lambda)$$

and a_0 is set equal to 0.5; r is set equal to 0.01. The physical interpretation of this is that the beam has a diameter of 0.5 if the laser lases at all and that it increases with increasing $E(\lambda)$. The quantity R is calculated from Equation 2.29, with $K'\sigma$ assumed to be 1×10^{-4}, and $\rho(\lambda)$ set equal to $E(\lambda)/a$. The quantity R is plotted versus $E(\lambda)$. observed. Figure C results if a is proportional to $E(\lambda)$. Curve C is highly unrealistic. However, Curve B is barely distinguishable in form from Curve A, but the quantitative difference in apparent $K'\sigma$ is marked.

This model is chosen arbitrarily to demonstrate that serious systematic errors might go undetected in these experiments and to illustrate the difficulty of obtaining reliable absolute cross sections in the icr apparatus. To do so one would need to know precisely the size and spatial distribution of the ion population in the icr cell at all times. Further, one would need to know the size and intensity profile of the laser beam for each shot. Given the fluctuating nature of even the grossest experimental variables there seems to be little hope of refining these experiments sufficiently to yield accurate absolute cross sections. One can only hope that systematic errors, if important at all, are consistent enough from experiment to experiment to yield reliable relative results.

CHAPTER 3
THE INSTRUMENT

Introduction

The pulsed icr used in these studies was built largely at the University of Florida. The flashlamp pumped dye laser was purchased commercially and assembled in our laboratory. The instrument consists of four main sections: the vacuum system, the optics, the digital electronics, and the computer data-logging system. Two of these, the optics (39) and the digital electronics have been described in detail (42). The vacuum system is standard for icr operation (43). A functional description of all three follows. The final sections of this chapter are devoted to a detailed description of the computer data-logging system and an evaluation of its performance.

The Vacuum System

Figure 3.1 is a diagram of the icr vacuum system. The entire system was fabricated in the shops of the Chemistry Department of the University of Florida. All components are

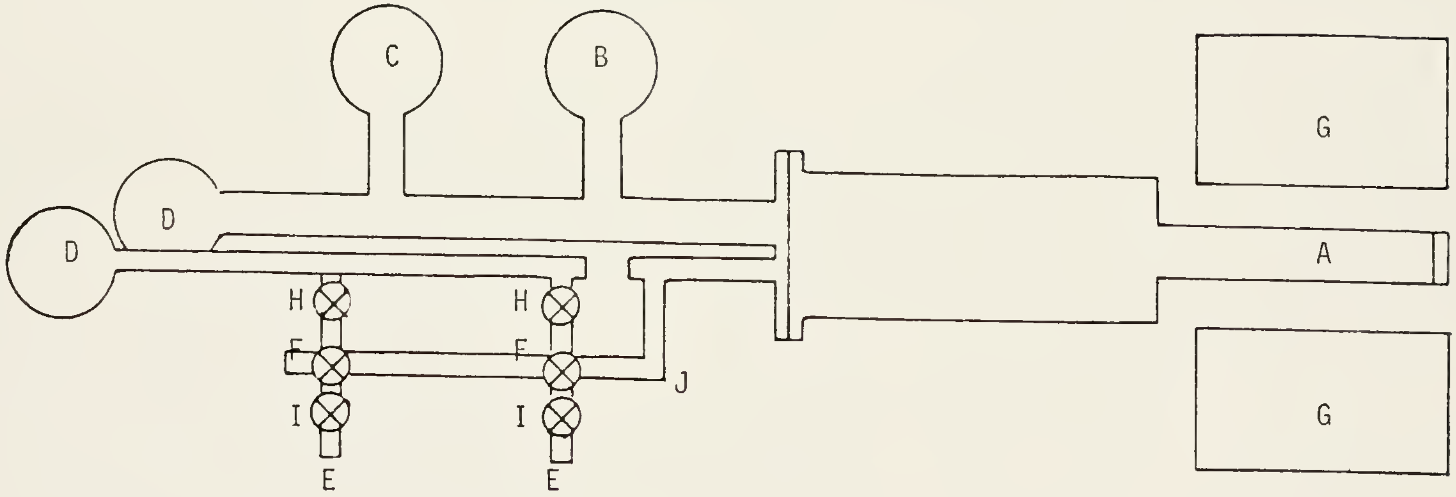

Figure 3.1. Diagram of Vacuum System

A. vacuum can
B. ionization gauge
C. titanium sublimation pump
D. diffusion pumps
E. sample inlet
F. control leak valves
G. magnet
H. valves
I. valves
J. discharge gauge

stainless steel with the exception of the ionization gauge which is glass. The entire system is wrapped with heating tape and can be baked-out at temperatures exceeding 100°C. Background pressures as measured on the Bayard-Alpert ionization gauge (44) (factory calibration) are routinely less than 5×10^{-8} torr. During experiments the reaction chamber is pumped using a 2-inch oil diffusion pump with a liquid nitrogen trap. When experiments are not underway the vacuum chamber is pumped by the Vac Ion titanium sublimation pump.

Samples are routinely freeze-pump-thaw purified two to three times on the inlet vacuum line before introduction into the icr. The normal procedure for sample introduction is to pump the foreline up to the sample bulb stopcock for 10 to 20 minutes. Typically pressures of 1×10^{-6} torr to 5×10^{-6} torr as measured by a cold cathode discharge gauge are obtained. Valves H (Figure 3.1) are then closed and the sample bulb stopcock opened. After several minutes the valves at I (Figure 3.1) are closed. The sample is thus trapped between Valves I and H. Samples handled in this way are less likely to be contaminated by air leaks at the connection between the metal inlet system and the glass sample bulb (Figure 3.1.E) and usually provide samples adequate for 4 to 8 hours of operation. With water samples the sample bulb stopcock and Valve I must be left open to maintain adequate sample pressure but this is the lone exception to the normal procedure. While experiments are in progress the sample pressure of one or two gases is maintained using the control leak valves (Figure 3.1.F). Usually 10 to 15 minutes is required for the sample pressure to stabilize but once set they remain stable within a few percent for a matter of hours.

The Optical System

The light source used in these studies is a flashlamp pumped dye laser (45). The laser head is mounted in a box made of copper screen to shield the m.o. detector from radio frequency noise from the flashlamp discharge. Tuning over the spectral region between 700 nm and 450 nm is achieved by changing dyes and using a diffraction grating at one end of the optical cavity. The grating is moved by a sine arm drive. A diagram of the optical system is shown in Figure 3.2.

In our instrument an intracavity technique (39) is used to maximize the photon flux through the sample. The optical cavity of the laser extends from A to B in Figure 3.2 and the sample region is located at H. The window surfaces on the coaxial flashlamp (D) and vacuum can (C) are antireflectivity-coated to minimize intracavity losses. A small portion of the beam is reflected off a clean microscope slide (E) into a 0.5 m monochromator (G) to

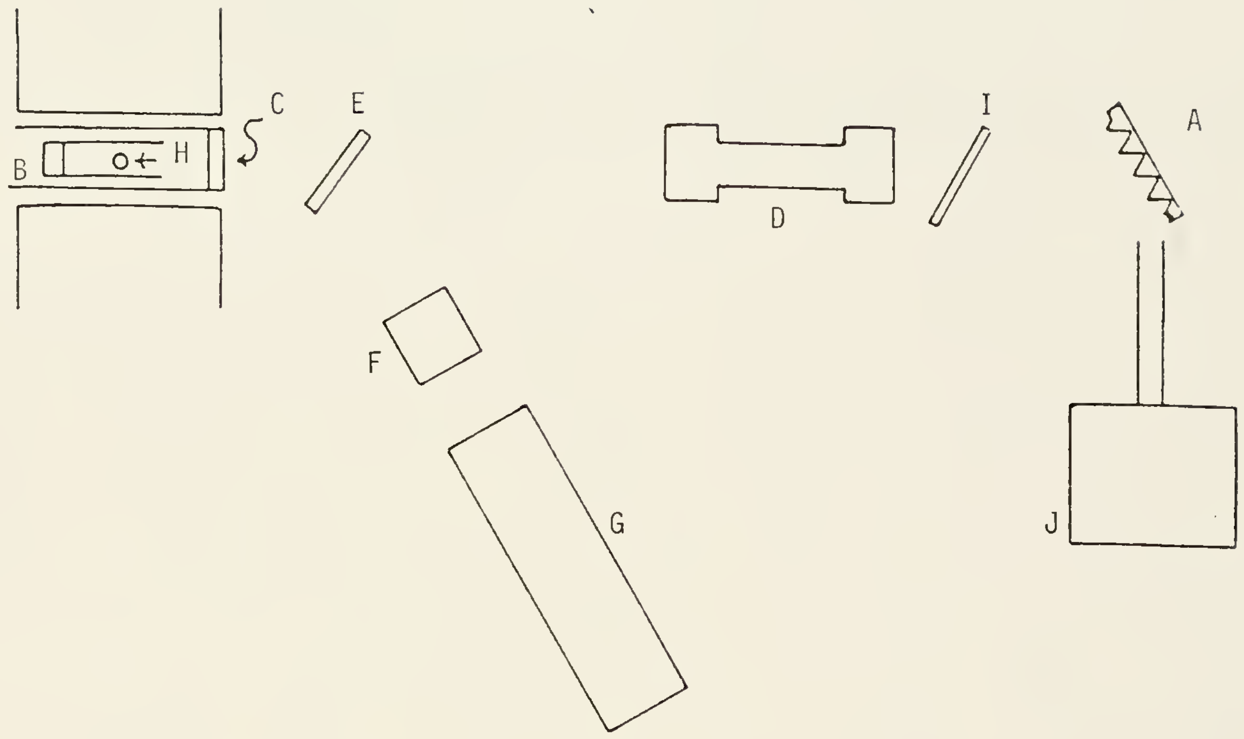

Figure 3.2. Diagram of the Optical System

A. grating

B. mirror

C. anti-reflectivity coated window

D. flashlamp

E. microscope slide

F. joulemeter

G. monochromator

H. sample

I. microscope slide

J. sine arm drive motor

measure the wavelength. The monochromator is calibrated with a helium-neon laser and a mercury lamp.

Once the wavelength has been established the Gen Tec (F) (46) fast response joulemeter is placed to intercept the reflected portion of the laser beam to obtain a measurement of the laser intensity. The transient from the Gen Tec (see Figure 3.3.A) is displayed on an oscilloscope. The energy of the laser pulse is proportional to the peak voltage of the transient. During an experiment this value is read from the oscilloscope and recorded manually each time the laser triggers.

To measure the energy output of the laser it was necessary to determine the fraction of the laser beam diverted by the microscope slide. This quantity was measured by replacing the grating at A in Figure 3.2 with a 90 percent reflecting mirror. Fifteen laser shots were fired with the Gen Tec intercepting the light reflected by the microscope slide and then fifteen more were taken with the Gen Tec measuring the throughput of the 90 percent reflecting mirror. This experiment was then repeated. The throughput of the 90 percent reflectance mirror was taken as 10 percent of the intracavity energy and the light reflected from the microscope slide was compared to it. In the first run the ratio of energy measured off the microscope slide to the throughput of the mirror was 0.48 and for the second run 0.54. Thus, approximately 5 percent of the intracavity

Figure 3.3. Typical Transients Generated by the Experiment

A. Transient from Gen Tec

B. Transient from m.o.

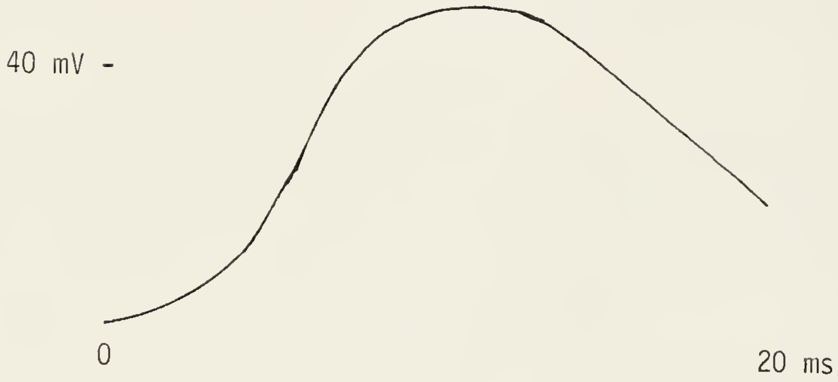

A

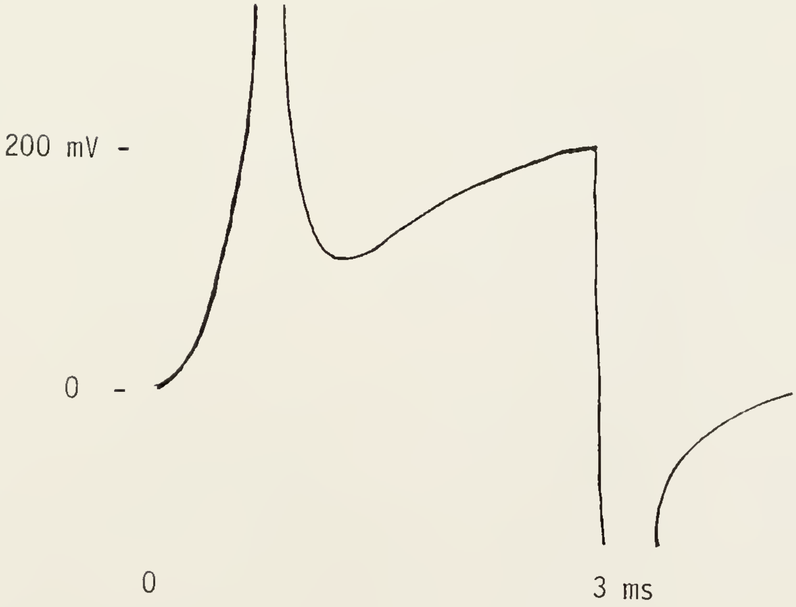

B

energy was reflected to the Gen Tec. This number and the calibration data supplied by Gen Tec were used to estimate the energy output per laser pulse.

Laser performance depended greatly on the dye used and the quality of the optical alignment. The laser manufacturer claims an output pulse duration of 1 μs. The bandpass was on the order of a few tenths of a nanometer and could be measured to ± 0.4 nm with the monochromators used. Energy output ranged from 40 mJ per pulse to over 200 mJ per pulse depending on the dye and the wavelength. Variation in laser output from one shot to the next ranged from 5 percent to 25 percent depending on dye, wavelength, and lamp voltage. In those experiments where the laser output was varied the output was changed both by varying the lamp power supply voltage and inserting dirty microscope slides into the laser's optical cavity at I (Figure 3.2). It was determined that identical results were obtained in a given sample at a give laser intensity no matter which method was used to modify the laser output. At least once in every experiment several experimental cycles were run with the laser firing but the window of the vacuum can was covered so that no light entered the sample region. The ion signal was seen to be unaffected by the laser discharge under these conditions.

The Digital Electronics

A one-of-a-kind digital timer system (42) was constructed at the University of Florida to control the formation trapping and detection of ions with a series of electronic pulses of specified widths and occurring at preset intervals. The m.o. detector was assembled at the University of Florida following the design of McIver (40). This detector is a fixed-frequency design; ions are brought into resonance by changing the magnetic field strength. The magnet is a Varian V-3400, 9-inch low impedance electromagnet with a V-FR2500, 7-kw power supply and a "Fieldial" Mark I controller. A set of regulated power supplies was constructed to provide the d.c. trapping voltages applied to the plates of the cell.

The first pulse of an experimental cycle is the precondition pulse which initializes all the counters and "clamps" them until the start pulse. The start pulse is the reference pulse for all delays and is the zero in all time measurements. A crystal-controlled clock oscillator is used to control the delay time between the start pulse and the sample, grid, quench, detect, ω_2, and free pulses. These delays and the widths of the grid, quench, ω_2, and detect pulses are also controlled by the crystal clock using a system of binary-coded-decimal thumbwheel switches on the front panel of the control unit. The accuracy of the pulse delays and widths is that of the clock oscillator or 10 ppm at constant temperature.

Ion formation occurs during the grid pulse. Electrons ejected from a resistively-heated rhenium filament maintained at a preset potential between 0 V and -50 V are prevented from entering the sample region by a grid biased 5 V negative of the filament. During the grid pulse the grid is biased 5 V positive of the filament and electrons are accelerated into the cell by the negative voltage on the filament. Across the cell they are collected through a hole in the side plate by a plate biased to about +12 V. The electron current is amplified so that an electron current of 1×10^{-6} A yields a signal of 1 V. Under typical operating conditions electron currents of 5×10^{-8} A to 3×10^{-7} A were employed.

The ω_2 pulse is used to gate a radio frequency oscillator for the double resonance ejection experiment (47). Typically an Ailtech function generator was used in the gated mode to apply a burst of radio frequency oscillation to the upper plate of the cell. The frequency of this oscillation is chosen to excite the cyclotron motion of a particular ion to such an extent that it is driven from the cell.

The free pulse is a +5 V pulse with a duration of about 1 ms. A pulse with an amplitude of 180 V with a rise time of 1.8 μs is required to trigger the laser. This pulse is provided in the following fashion. The free pulse (or, under computer control the result of a logic AND with a computer address, see below) is passed through a optoisolator chip. The optoisolator protects the control electronics from transients produced when the laser fires. The output of the isolator is passed to a Schmitt trigger to decrease the rise time. This fast pulse then triggers an SCR circuit that provides the high voltage trigger for the laser.

The detect pulse gates the amplifier in the limiter branch of the m.o. circuit. As McIver mentions in the original article describing the design of this circuit (40), the transient output of this detector (Figure 3.3.B) contains two spikes caused by the mismatch between the reference circuit and the cell circuit. The actual power absorption transient appears between the spikes. These spikes are eliminated by using a switched integrator and delaying the switch pulse until after the first spike has passed and turning the integrator off before the second spike (42). A sample pulse from the control electronics is triggered by the falling edge of the detect pulse to gate a sample/hold module for the 2 ms required to read the output of the switched integrator. The output of the sample/hold module is displayed on a chart recorder or digitized for computer logging as described below.

The final pulse of the experimental cycle is the quench pulse. During this time a 10 V d.c. level

Figure 3.4. Sketch of Typical D.C. Output of Switched Integrator

A. Manual Operation

B. Computer Operation

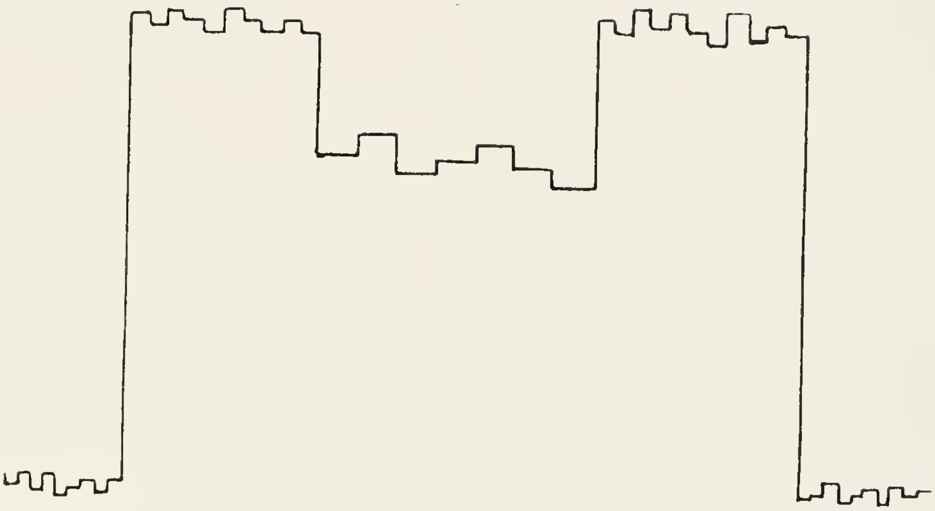

A

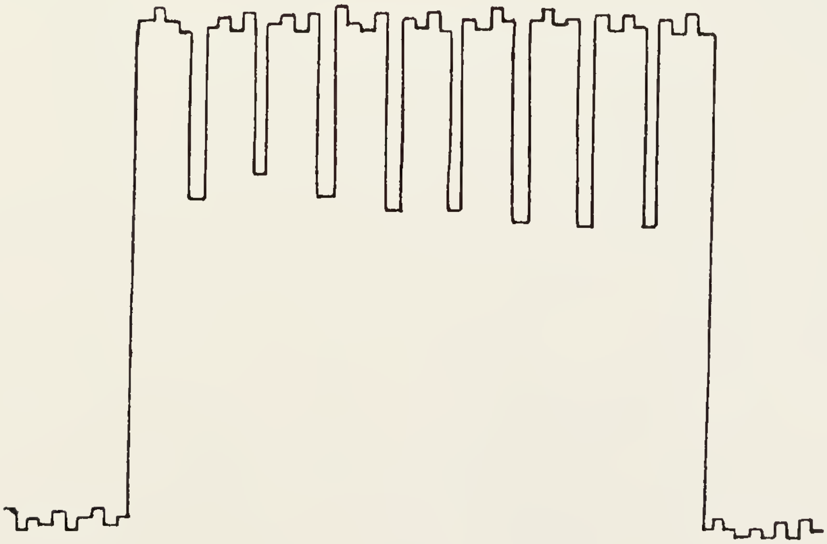

B

is added to the upper cell plate to sweep all ions from the cell.

An experimental cycle can be initiated in three ways: single-cycle trigger, fixed-rate trigger, and automatic trigger. The single-cycle trigger is a pushbutton on the front panel of the control electronics. The fixed-rate trigger causes a cycle to occur once every 20 ms to 5 s in a 1,2,5 sequence chosen by a front panel switch. The automatic trigger causes a cycle to be triggered 175 ms after the end of the quench pulse. In noncomputer experiments the instrument was run in the single-cycle trigger mode when the laser was flashing and in a fixed-rate mode with a duty cycle of 2 s or 5 s when the laser was not flashing. Under computer control the fixed-rate trigger with a 2 s duty cycle was used exclusively.

Interfacing the Pulsed icr with a KIM-1 Microprocessor

The next stage in the development of the pulsed icr/laser instrument was the design and implementation of a microprocessor-based digital data acquisition system. The principal advantage of such a system is that data collection and reduction is greatly simplified. A second advantage is that data can be taken more quickly. Prior to the implementation of computer control the duty cycle of the icr was limited by the minimum duty cycle of the laser--approximately 10 s. Using the computer to control the laser it was possible to collect "laser off" ion level data between laser shots and thus decrease the time needed to run an experiment.

The first stage of interfacing is the manipulation of the transient signals generated by the pulsed instrument into signals sufficiently stable to be digitized. Since each experimental cycle yields two pieces of data--an ion level signal and a laser intensity signal--it is necessary that each be routed to the analog to digital converter (ADC) in its proper turn and then stored in computer memory in a systematic manner so that it can be retrieved later for further processing. The combination of hardware and software used to accomplish these tasks is described in this section. No mention is made of the higher level data processing because the system to carry this out is still under construction. One spectrum calculated from data which had passed through the digital data system was obtained by hand manipulation of the stored data simply to test the reliability of the system.

The m.o. power absorption signal has already been put into a form suitable for digitization by the switched integrator-sample/hold system discussed above. The sample/hold device was observed to maintain the same d.c. level for several seconds, allowing rather leisurely digitization of the ion intensity. The transient output of the Gen Tec fast response joulemeter has to be passed through a peak detector circuit. Since the droop rate on this circuit is much faster than that of the sample/hold module, the laser intensity has to be digitized rather soon after it is measured. In addition, a reset pulse must be applied to the peak detector on each cycle to return it to zero.

Once the data have been manipulated into a stable d.c. level suitable for digitization, it is necessary to route each signal in its turn to the ADC and on into computer memory. The data routing is under computer control so the computer must be "told" that the experiment is under way and that data will soon be arriving. This is accomplished by sending a pulse from the icr's digital timing system on the interrupt request line (IRQ) of the microprocessor. Upon receiving an interrupt the microprocessor jumps to a preset location in memory and begins excecuting the program contained there. From the computer's point of view the experiment consists of long periods of "waiting around" and periodic interrupts followed by a burst of activity routing the analog signals into the ADC and filing the digitized data in memory. In practice the same pulse is used as the interrupt pulse and the laser trigger pulse. The first stage of the program is a timed wait for the rise time of the Gen Tec (25 ms) so that the computer does not look for data before they are there.

Hardware

The microprocessor used as the "brain" of the data collection system is a KIM-1 manufactured by MOS Technology. The central processing unit is a 6500 monolithic CPU chip. As installed in our application the computer has either 4 or 8 kilobytes (K) of memory depending on the configuration used. Contact between the computer and the outside world is maintained through two eight-bit input/output (I/O) ports and the IRQ. In this application only one I/O port (the A port) is used.

The interface was custom built; a block diagram appears as Figure 3.5. KIM's access to the interface is through the A data port (PAD). PAD is treated like any other memory address by the computer except that its contents are determined by (input) or determine (output) the logic level of a peripheral device. Whether a given bit of PAD is an input or an output is determined by the contents of a second memory location--the Port A data direction register (PADD).

Since KIM needs to send and receive data along more than eight individual lines, four eight-channel, three-bit multiplexers are connected directly to the A port. In all applications the lowest four bits of PAD, (PA0, PA1, PA2, PA3) are used as outputs to control these mutiplexers. Pins 4 through 7 of the A port are inputs and outputs as the need arises. PA0 is attached to the "inhibit" line of

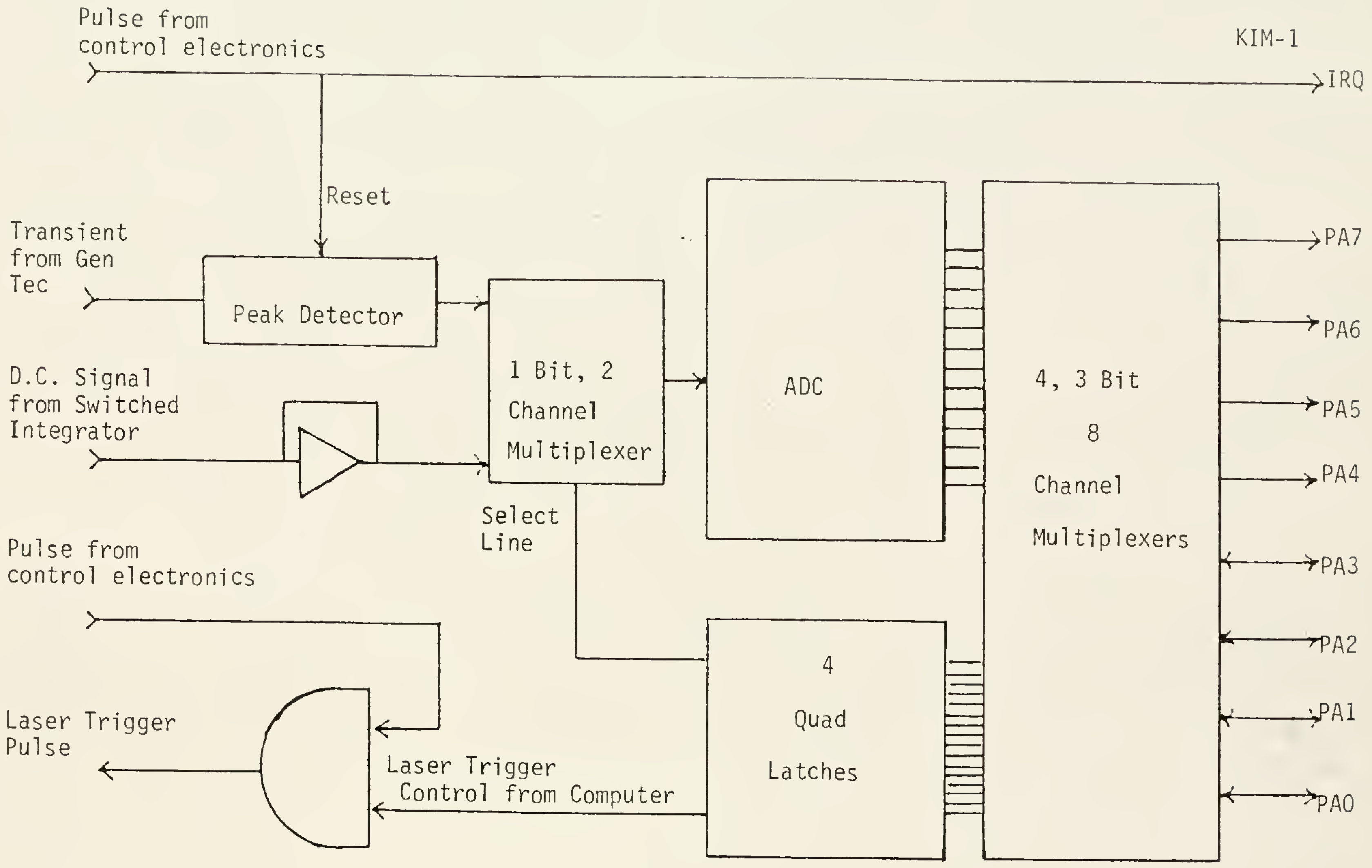

Figure 3.5. Block Diagram of icr/KIM-1 Interface

each of the four multiplexers. If the contents of PA0 are a logic high then no signals pass through the multiplexers; only when the logic level of PA0 is low do signals pass into or out of the KIM. The three Pins PA1, PA2, and PA3 are connected to the control lines of each of the multiplexers. The number (from 0 to 7 binary) that appears on these lines determines which of the eight channels of each multiplexer is passed. The output line of each multiplexer is connected to one of the four remaining pins on PAD.

Some of the time a control signal output from the KIM cannot be maintained at the proper level for the entire time that is required because the KIM must move on to do something else. The system of four quad latches in the interface is used to hold such signals when the computer is needed elsewhere. Each latch has a "clock" line. When the clock line is low the output is constant no matter what the input. When the clock line is raised to a logic high the output is the same as the input. If the clock line is then dropped low again the new output is maintained no matter what the input. In this way more than four external logic levels can be maintained by the computer using only four I/O lines.

A twelve-bit ADC is used to convert the analog signals from the icr into digital data that can be read by the computer. The ADC is operated in the free-run mode and is thus restricted to certain timing requirements.

The minimum conversion time is 25 ms. During that 25 ms the signal on the input line is ignored. Thus, to ensure that a given signal is digitized it must be held on the input line for about 30 ms. At some point (and possibly twice) during that time the ADC will read the data and commence digitizing it. When digitization is complete the digital data are displayed on the output pins of the ADC. These data are maintained there throughout the next conversion cycle, i.e., for 25 ms. During this time they must be read by the computer. Since in this application there is plenty of time, data are routed through the ADC at a rate controlled by the computer's internal clock and paced to be sure that each set of data is held on the input pin for at least 30 ms, collected by the computer 25 ms later, and that one ADC cycle elapses before the next data point is sent through.

Which of the two data points, laser output or ion intensity, is digitized is controlled by the computer through a one-bit, two-channel multiplexer. The "1" channel sends the laser output signal from the peak detector to the ADC and the "0" channel sends the ion intensity signal through. These channels are selected by the computer through the latches subject to the timing requirements discussed above.

Finally, the computer controls the laser by applying a logic level through a latch to one input pin of an AND gate. The laser trigger pulse from the control electronics is applied to the other input pin. The result of the logic AND is passed to the laser trigger shaping circuit. If the logic level from the computer is a "1" the laser trigger pulse is passed and shaped to the proper specifications to trigger the laser.

Software

The software used to drive this interface and collect the experimental data was written in 6502 assembly language. No higher level language is available for the KIM and assembly language is the language of choice for direct hardware control. Timing for the experiment was provided by the icr digital control electronics and it is necessary to synchronize the operations of the computer with those of the icr. The interrupt programming capabilities of the KIM are ideally suited to this purpose. The interrupt is "maskable"; that is, whether or not the computer responds is under program control. It is also a "vectored" entity, meaning that the response to an interrupt is under program control. In addition, the "return from interrupt" allows the program to return to the same point at which it was interrupted, facilitating loop programming.

The program was designed to step-through the entire sequence of a complete spectroscopic data point consisting of three sets of measurements: the zero level of the m.o. (m.o. level with the icr tuned so that no ion is in resonance), the intensity of an ion signal without the laser flashing, and the intensity of the ion signal with the laser flashing. There is a main program which counts the number of experimental cycles run and signals the operator when it is time to enter a new phase of the experiment. There is a common program for all phases of the experiment except that different values of various counters are used. The main program initializes these counters and otherwise consists of a series of jumps into and out of subroutines. Such subroutine programming makes writing and debugging the program easier because the work is broken down into more manageable units and it makes the program relatively easy to modify.

A "step-through" of the operation of a typical experiment (as diagrammed in Figure 3.6) illustrates how the main program works. Assuming that all adjustments have been made to the laser and the icr, the operator powers up the KIM and loads the program from a tape cassette. He then punches "AD"--meaning address--"0200" and then "GO." The computer lights up with "0005 0A." Address 0020 is the start of the routine that loads a set of registers needed by the program. These include setting the interrupt vectors so that when the icr interrupts the computer it will respond correctly. The routine sets the initial address at which data are to be stored and initializes the "data index" which controls the destination in memory of each byte of data. The default values for the number of data

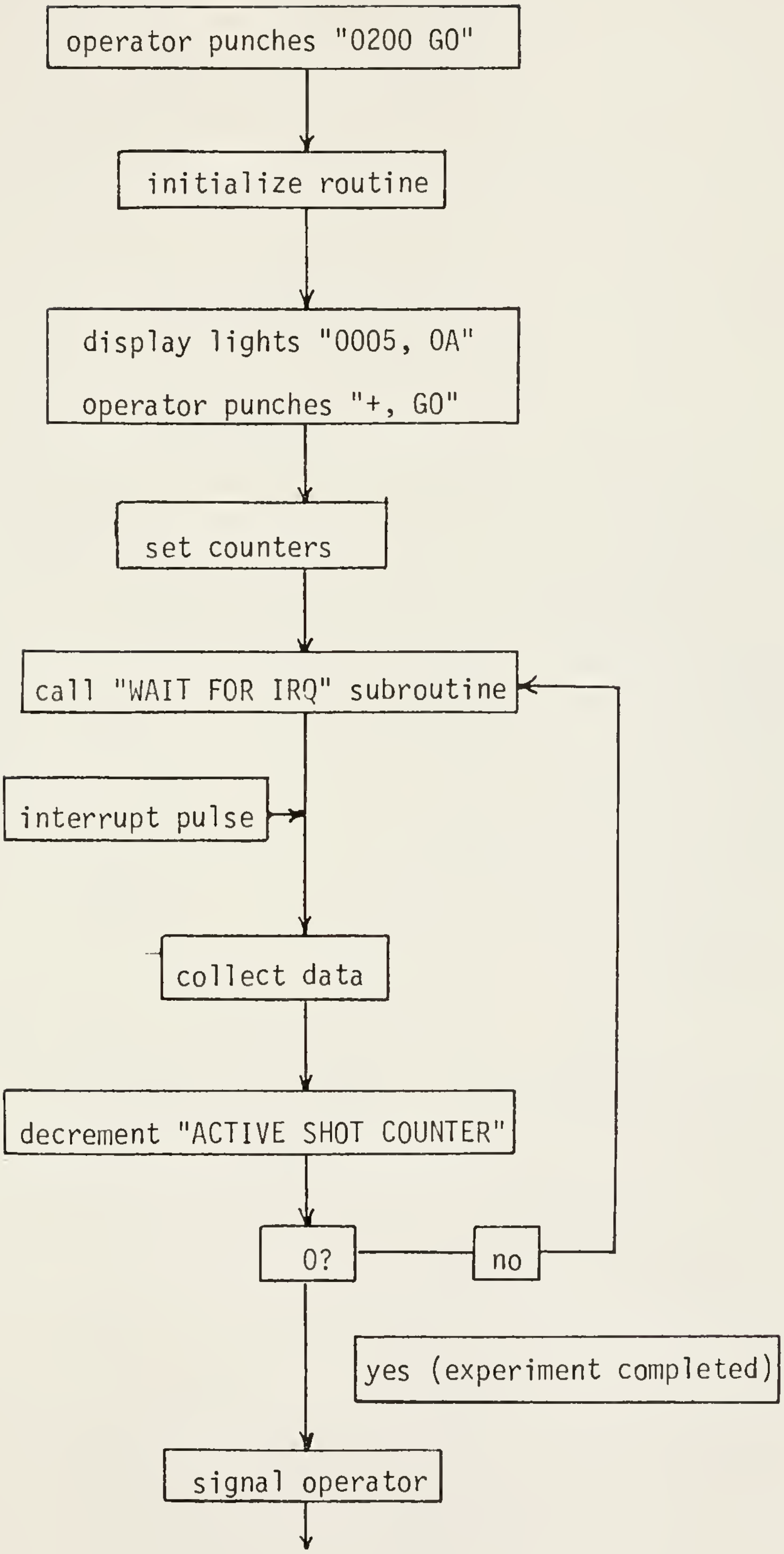
operator punches "0200 GO"
initialize routine
display lights "0005, 0A"
operator punches "+, GO"
set counters
call "WAIT FOR IRQ" subroutine
interrupt pulse
collect data
decrement "ACTIVE SHOT COUNTER"
0?
no
yes (experiment completed)
signal operator

Figure 3.6. Flow Chart of Main Program

points to be taken, and the "ratio counter"--the number of laser off ion level measurements to be taken between each laser shot--are also specified at this time.

The numbers "0005 0A" signify that Address 0005 contains 0A, which is the hexadecimal equivalent of 10. This means that 10 measurements of the ion zero level are to be made. The operator may change this number. Once the operator punches "+" then "GO" the computer loads the number of "zero" points to be taken into the "active shot counter." This is the address where the number of points taken, the number of interrupts, is counted by decrementing the contents and taking a program branch when zero is reached. The "laser trigger counter" is set so high that the laser will not trigger during this phase of the experiment. The interrupt is then enabled and the computer jumps to the "wait" subroutine.

Once the specified number of interrupts has occurred the computer lights up with "0009 0A" where 0A, 10, is the number of times the laser is to trigger. The operator now "tunes in" the ion and turns up the laser. Upon the pushing of "+" and then "GO" by the operator the computer computes a new active shot counter from the ratio counter and the laser shot counter. Should this value exceed "FF" (256) an error message "FFFF FF" appears on the KIM's display. The "trigger" counter is set so that the laser will fire at an interval determined by the ratio counter. The computer interrupt is then enabled and the computer again jumps to the "wait" subroutine. It again services the required number of interrupts and returns to display "0005 0A." The operator makes the necessary adjustments to the icr and continues.

The computer's response to an interrupt is the same each time it is interrupted. As the flow chart (Figure 3.7) indicates the computer first sets the two-channel multiplexer to pass the photodetector signal; it then waits for the data to be digitized. When data are ready the computer calls the "read ADC" subroutine which stores the data. Data are stored at an address calculated by the computer. The address is determined by the contents of Memory Locations 0001, 0002, and 0003. The address is given by the contents of 0002 plus those of 0001 (low-order byte) and 0003 (high-order byte). Data from the photodetector are read into the page determined by the high-order byte of the "data destination register" (0003) and ion intensity data are on the next page (a page consists of 256 memory locations). A page of laser data is thus alternated with a page of ion data beginning at an address specified by the operator.

Once the photodetector data have been read and stored the two-channel multiplexer is set to pass the ion signal. While waiting for it to be digitized the computer adjusts the data destination. Once the ADC has been read the data destination is reset. The data index is then incremented

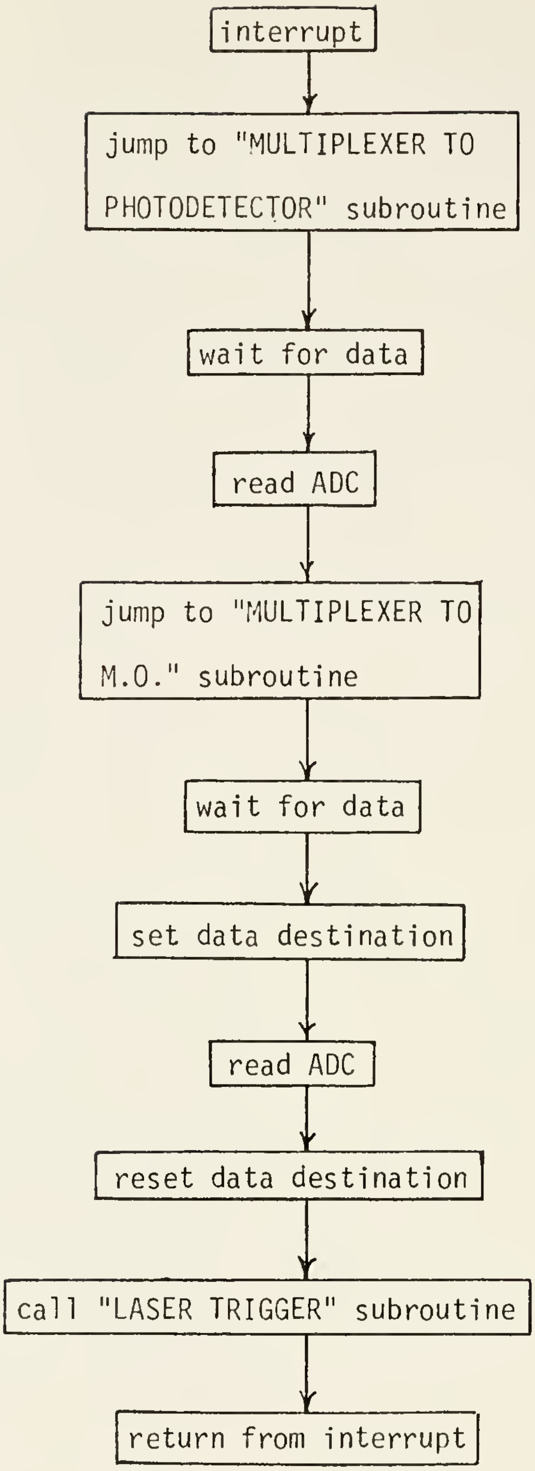
interrupt
jump to "MULTIPLEXER TO PHOTODETECTOR" subroutine
wait for data
read ADC
jump to "MULTIPLEXER TO M.O." subroutine
wait for data
set data destination
read ADC
reset data destination
call "LASER TRIGGER" subroutine
return from interrupt

Figure 3.7. Flow Chart of IRQ Routine

in anticipation of the next set of data, and if the resulting value is greater than "FF" the high-order byte of the data destination is incremented twice so that more than 256 bytes of data can be stored without stopping. Since each experimental cycle produces 2 bytes of ion data and 2 bytes of laser data, whether the laser fires or not, this means that more than 128 experimental cycles can be run without stopping. The number of cycles that can be run is limited by the amount of memory available to store data.

Finally, the laser trigger counter is decremented, and if it reaches zero a logic high is put on one input pin of an AND gate. On the next icr cycle the laser trigger pulse from the control electronics will be passed through the AND gate and on to the pulse shaping circuitry. The trigger counter is derived from the ratio counter that the operator sets.

This program does not represent the final stage of software development. One obvious improvement would be to discard much of the laser output data recorded when the laser does not fire, retaining only enough to calculate a reliable baseline. This would streamline memory requirements considerably. One worthwhile feature of the program is that the operator need only concern himself with the contents of a few addresses: the data destination (0002, 0003), the laser shot counter (0009), the zero counter

(0005), the data index (0001), and the ratio counter (000E). The operator need not specify any of these if he is satisfied with the default values provided by the program or he may change them to suit his needs. If the operator wants to know where the next byte of data will be stored, he need only examine the data index and the high-order byte of the data destination. They are the low- and high-order byte, respectively, of the address where the next byte of data will be stored. This is especially useful when manual data manipulation is to be employed.

Evaluation of the Performance of the Computer Data System

Although the hardware and software for higher level processing of the data stored in the KIM has not yet been assembled and consequently the manipulation of computer-logged data is still very inconvenient, it is worthwhile to compare data that has passed through the digital data system with data recorded in the normal manner. During the study of the photodissociation of 1,3,5 hexatriene reported in Chapter 7, the instrument was set up so that data could be recorded simultaneously by hand and on the KIM. Figure 3.8 is a plot of the spectrum obtained from the computer data. Data from the same experiment processed in the normal manner are presented in Figure 7.2.

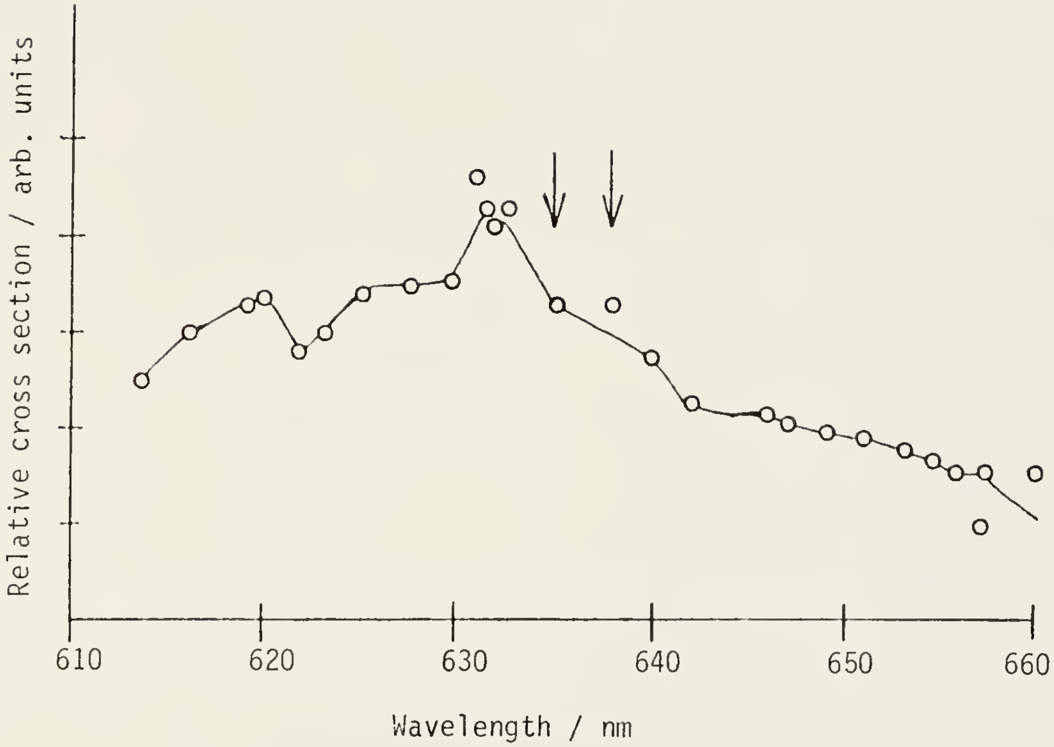

Figure 3.8. Photodissociation Spectrum of 1,3,5 Hexatriene Obtained in Computer Controlled Experiment

There is very good agreement between the two spectra; however, two of the points (indicated by arrows in Figure 3.8) are markedly different in the computer analyzed spectrum. The reason for this becomes apparent when Figure 3.9 is examined. In a different experiment, the intensity of the laser was measured both by hand and by computer at a variety of laser intensities. A plot of the decimal equivalent of the computer-stored data versus the peak height of the Gen Tec as recorded manually clearly shows that below 30 mV of Gen Tec signal the computer system is nonlinear in laser intensity.

Ignoring the two data points calculated with erroneous values for the laser intensity a more detailed analysis of the data revealed good agreement between the two data sets. Each spectral point is the average of ten experimental cycles. Within each set of ten there was good agreement between the computer-logged data and the data obtained manually. In each of six sets studied the median, largest, and smallest cross section were calculated from the same "raw" data.

A comparison of the hexadecimal numbers in the computer memory to the data obtained manually again reveals good agreement. The two sets of laser data have already been compared and shown to be linear over a limited range. The scatter observed in Figure 3.9 is probably due to the large reading error associated with reading the Gen Tec transient from the oscilloscope screen. The relationship

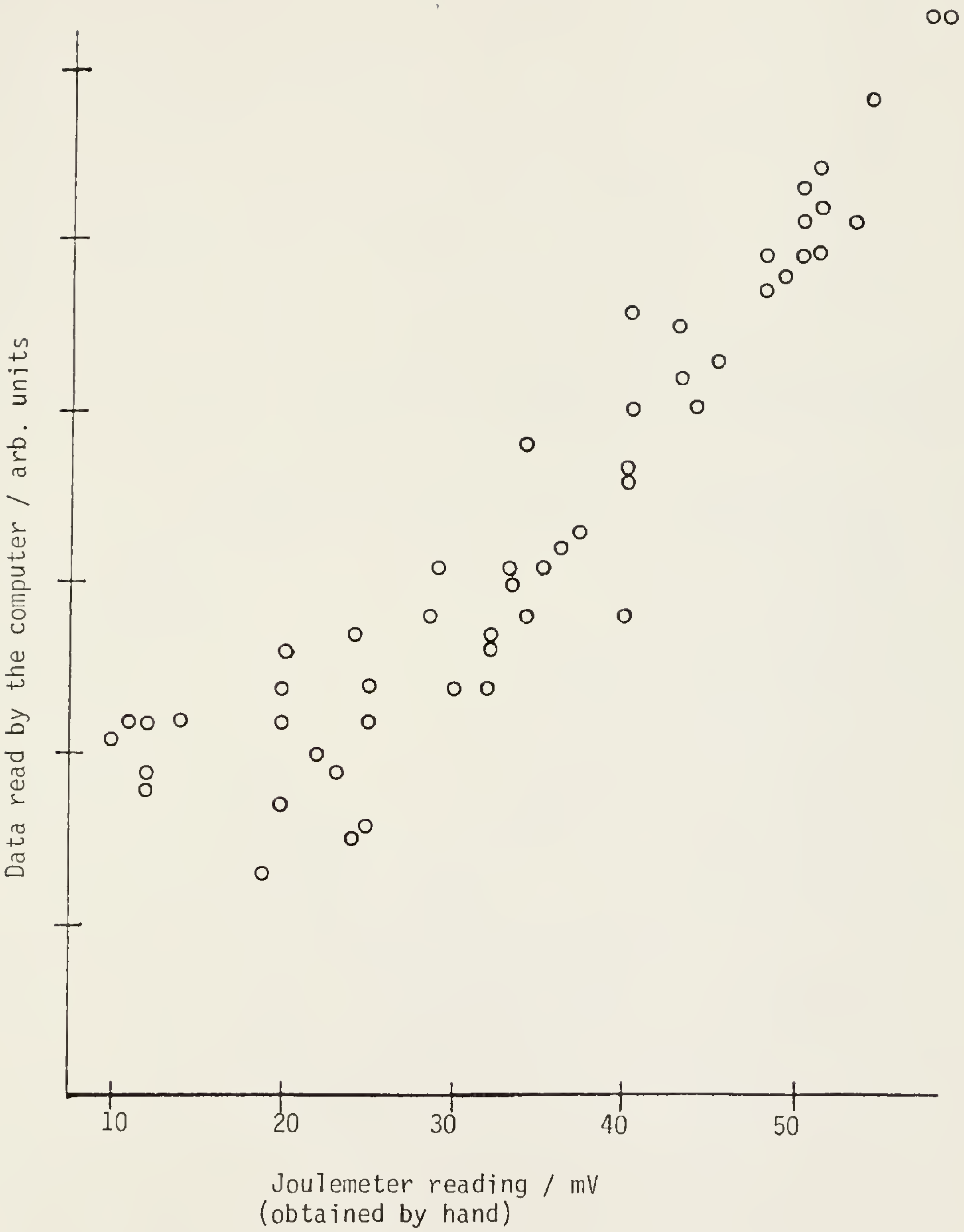

Figure 3.9. Comparison of Laser Energy as Measured by Computer and Manually

between ion intensity data displayed on the chart recorder and the decimal equivalent of the numbers stored in the computer memory is shown in Figure 3.10. Clearly, the relationship is linear.

Since the results obtained from the computer-logged data generally agree with those obtained manually it can be concluded that the computer data routing system works. Also, the linearity of the computer-measured ion intensity suggests that the analog to digital converter works. The nonlinearity in the computer-logged laser output data would appear to indicate that the peak detector circuit is not functioning properly.

Figure 3.10. Comparison of Ion Signal From Digital (Computer) and Analog Circuits

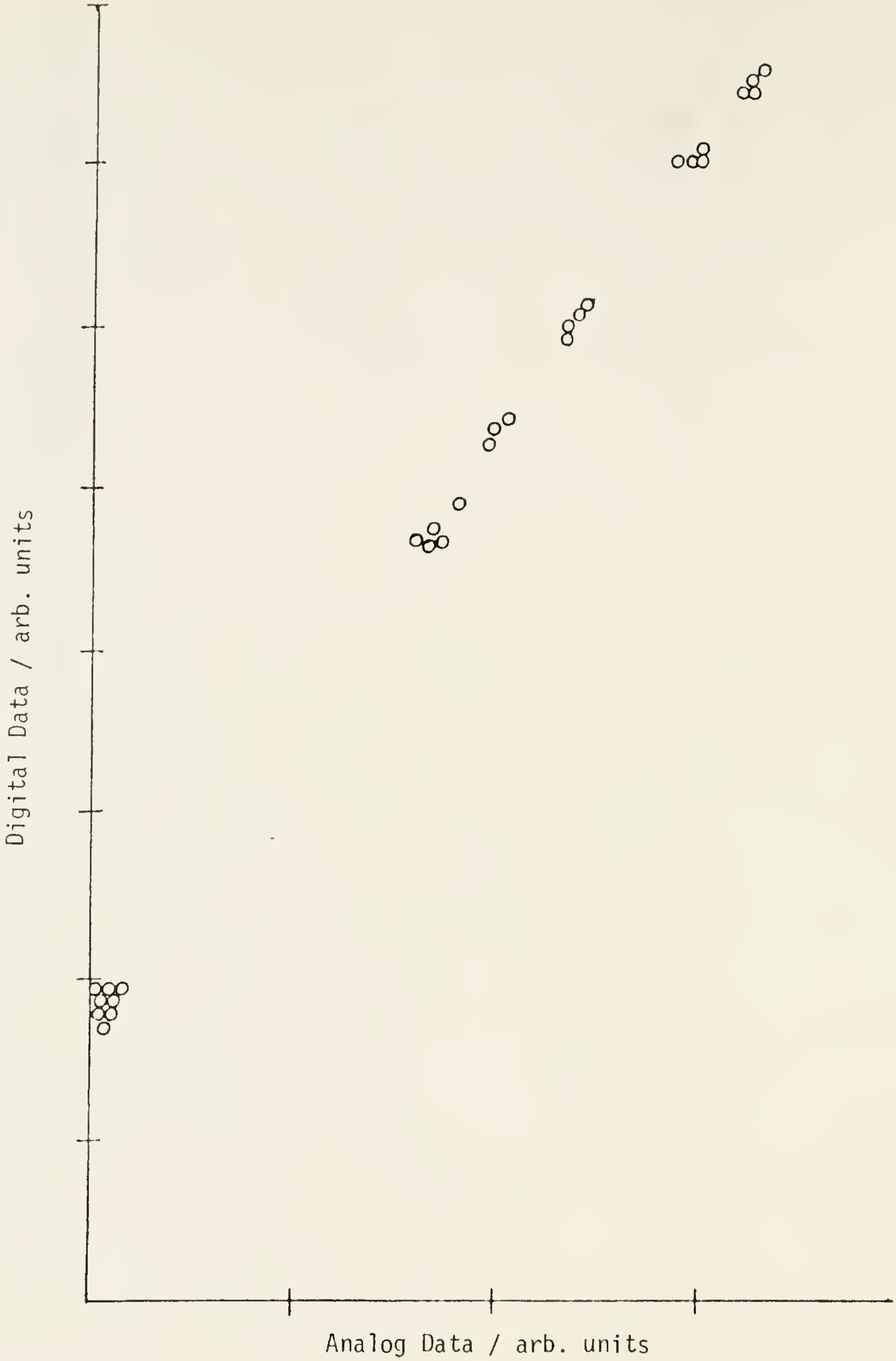
Digital Data / arb. units
Analog Data / arb. units

CHAPTER 4
STUDIES OF THE PHOTODETACHMENT OF OH^---STANDARDIZATION OF THE CELL

Introduction

Obviously, the preceding theoretical discussions do not provide adequate justification for having faith in the results of these experiments. A means of assessing experimentally the behavior of the instrument under the influence of the many experimental variables had to be found. Ideally, one would hope to study an ion with no vibrational energy modes, i.e., an atomic ion. However, several experimental considerations favored the use of a "compromise" ion: OH^-.

The cross section for the photodetachment of OH^- has been shown to be large and nearly constant between 450 nm and 630 nm (30)--a range encompassing most of the wavelengths of interest here. In addition, OH^- is easily formed from a readily obtained sample,water. The actual process for the formation of OH^- is via Reactions 4.1 and 4.2.

$$e^- + H_2O \rightarrow H^- + OH \qquad 4.1$$

$$H^- + H_2O \quad OH^- + H_2 \qquad 4.2$$

The first reaction is dissociative electron attachment to water and is most efficient for electrons with ca. 7.0 eV of translational energy. Reaction 4.2 is extremely efficient, occurring on essentially every collision (48). The use of an ion formed by such a scheme has the advantage that Reaction 4.2 restricts to some extent the possibility of internal excitation in the OH^- ion.

It must be noted that the interpretation of these results requires the assumption that the photodetachment cross section of OH^- is constant at any given wavelength at all times and that all variations in the measured cross section are due to instrumental effects. Two studies of the photodetachment of OH^- have been carried out in beam instruments (30,31) and neither has revealed any effects of internal excitation on the cross section. Furthermore, at photon energies above the detachment threshold such effects should be negligible. The photon energies used in this study were all greater than 0.25 eV above the photodetachment threshold. It must also be assumed that studies of a negative ion are valid for comparison to those of a positive ion. Since the motion of a negative ion in the icr cell is the same as that of a positive ion (except that all oscillations have the opposite "handedness") (17) this assumption seems reasonable.

Experimental

The Effects of Variations in icr Operating Conditions

The effect of magnetic field strength on the apparent cross section for the photodetachment of OH^- was studied.

The potential was maintained at +1.0 V on the end, upper, and lower plates of the cell; the side plate trapping potential was -1.5 V. The sample pressure was 2.8 x 10^{-6} torr of H_2O. Pulse Sequence 1 in Table 4.1 was used and the irradiating wavelength was 580 nm.

In order to vary the magnetic field strength it was necessary to vary the m.o. frequency. Three frequency settings were used: 153.5 kHz (100 G/amu), 306.6 kHz (200 G/amu), and 615.0 kHz (400 G/amu). These corresponded to resonant field strengths of 1,727 G, 3,450 G, and 6,850 G, respectively. The percent detachment of OH^- versus laser intensity was measured at each field strength.

The effect of changes in the trapping, upper, lower, and end cell plate potentials on the apparent photodetachment cross section was also studied. A sample pressure of 2.5 x 10^{-6} torr of water and Pulse Sequences 2 and 3 of Table 4.1 were used. The m.o. frequency was 615.0 kHz and hence the resonant field was 6,850 G.

Three sets of potentials were tested:

1. Side plate trapping potentials of -1.0 V--upper, lower, and end plate potentials of

Table 4.1. Pulse Sequences Used in the Study of OH^- Photodissociation

Pulse Sequence Number	Grid Pulse		Laser Pulse		Detect Pulse	
	Delay (ms)	Width (ms)	Delay (ms)	Width (μs)	Delay (ms)	Width (ms)
1	0	12	19	1	20	2.0
2	0	15	34	1	35	2.0
3	0	15	49	1	50	2.0
4	0	25	149	1	150	2.0
5	0	25	249	1	250	2.0

+1.0 V,

2. Side plate trapping potentials -1.5 V--upper, lower, and end plate potentials of +1.5 V, and
3. Side plate trapping potentials of -2.5 V--upper, lower, and end plate potentials of +2.0 V.

These potentials were chosen as typical of normal operating conditions. Ion signal quality was independent of cell plate potentials over this range. The use of potentials much different than these led to poorer ion signal-to-noise ratios. Percent detachment versus laser intensity was measured at each set of trapping potentials.

In some samples the magnitude of the ion signal was seen to vary considerably from one experiment to the next due to irreproducibility of the emission current. Several types of filaments were employed at various times in this research. In one experiment the ion intensity was varied by about a factor of four by changing the current through the filament. The m.o. frequency was 615.0 kHz; sample conditions, pulse sequence, and trapping potentials were identical to those used to study the effect of magnetic field strength. The apparent photodetachment cross section was measured at both signal intensities.

The Effect of Time

One of the principal aims of this research was to exploit the time resolution of the pulsed icr to obtain information about the dynamics of changes in the structure of molecular ions using photodissociation spectroscopy as a probe. Time-resolved studies of the photodetachment of OH^- were carried out to examine the nature and magnitude of time-dependent instrumental artifacts.

Experiments were carried out at three sample pressures: 2.5×10^{-6} torr H_2O, 5.0×10^{-6} torr H_2O, and 1.0×10^{-5} torr H_2O. In each case Pulse Sequences 1 through 5 in Table 4.1 were used. The m.o. frequency was 615.0 kHz so OH^- was in resonance at a magnetic field strength of 6,850 G. The irradiating wavelength was 620 nm and kiton red S dye was used. The dependence of the percent detachment on laser intensity was measured in each sample using each pulse sequence.

The Effects of Variations in Laser Parameters

This study of the variation in the apparent photodetachment cross section of OH^- was carried out during a period of several months. Results were collected with several dyes and at several different laser alignments. Great pains were taken to maintain the same icr operating conditions from experiment to experiment. The pulse sequence, trapping potentials, and sample pressure were the same as those previously described for the study of the influence of magnetic field strength. The m.o. frequency was 615.0 kHz for all of these experiments corresponding to a resonant magnetic field strength of 6,850 G. The conditions were chosen to provide a standard for comparison to the data obtained with chloroethane as reported in the following chapter (Chapter 5). The experimental conditions, including field strength, were as close to those used in the study of chloroethane as was feasible.

Results

The Effects of icr Operating Conditions

The plot of percent disappearance of OH^- versus laser intensity at three magnetic field strengths is shown in Figure 4.1. Each point is the result of one laser shot. Curve A was obtained at a field strength of 6,850 G; Curve B at 3,450 G, and Curve C at 1,727 G. Clearly the apparent cross section increases with increasing field. However, the form of the dependence on field strength is not obvious from this experiment, nor is it obvious from the theory. Changes in the cell plate potentials and the magnitude of the ion signal made no difference in the measured cross section.

For each pressure listed above and for Pulse Sequences 1 through 5 listed in Table 4.1 the dependence of percent detachment on laser intensity was measured. The results

Figure 4.1. Effect of Magnetic Field Strength on the Apparent Photodetachment Cross Section

A. Field = 6,850 G

B. Field = 3,450 G

C. Field = 1,727 G

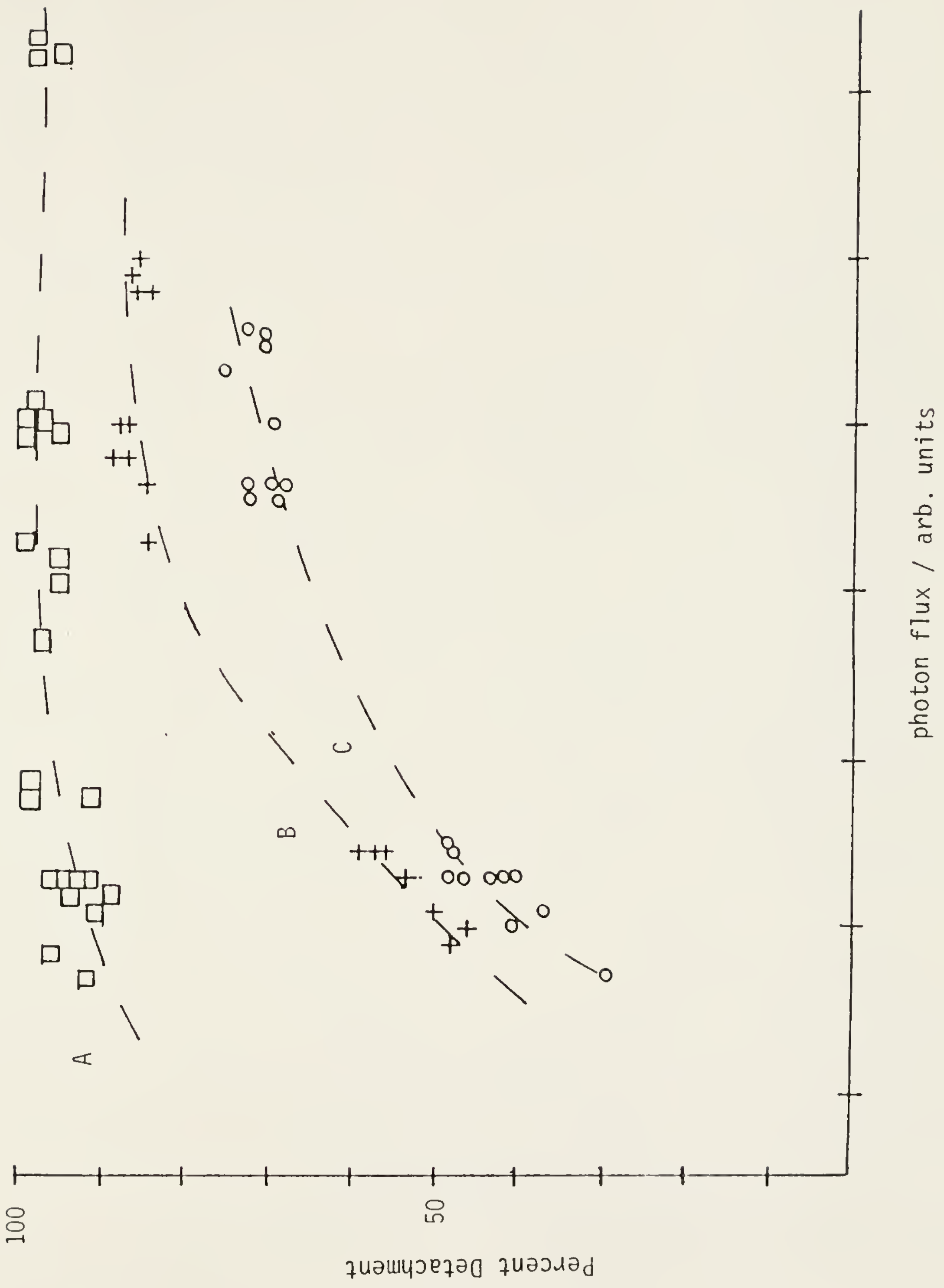
Percent Detachment
100
50
photon flux / arb. units
A
B
C

obtained at 2.5×10^{-6} torr are shown in Figure 4.2.A, those obtained at 5.0×10^{-6} torr are shown in Figure 4.2.B, and those obtained at 1.0×10^{-5} are shown in Figure 4.2.C. The data are plotted as laser energy versus percent detachment. Each point represents the average of five laser shots of approximately the same energy. A plot of the percent detachment at a laser energy of 45 mJ versus detect delay time is shown in Figure 4.3. Again Curve A refers to the 2.5×10^{-6} torr sample, Curve B to the 5.0×10^{-6} torr sample, and Curve C to the 1.0×10^{-5} torr sample.

An indication of the physical basis of this effect is obtained by comparing the percent detachment at 45 mJ versus the "mean collision number," N_C, as in Figure 4.4. The rate constant for orbiting collisions between an ion and a molecule or atom (49), k_L, is given by:

$$k_L = 2\Pi(\alpha e^2/\mu)^{1/2} \qquad 4.3$$

where e is the charge on the ion, α is the polarizability of the neutral species, and μ is the reduced mass of the collision partners. The frequency of orbiting collisions, Z_1, is:

$$Z_1 = k_L N. \qquad 4.4$$

Figure 4.2. Percent Detachment of OH^- Versus Laser Energy at Various Pressures and Ion Residence Times

A - Pressure = 2.5×10^{-6} torr Water

B - Pressure = 5.0×10^{-6} torr Water

C - Pressure = 1.0×10^{-5} torr Water

θ - t = 25 ms; o - t = 35 ms; ∆ - t = 50 ms; □ - t = 150 ms;

X - t = 250 ms

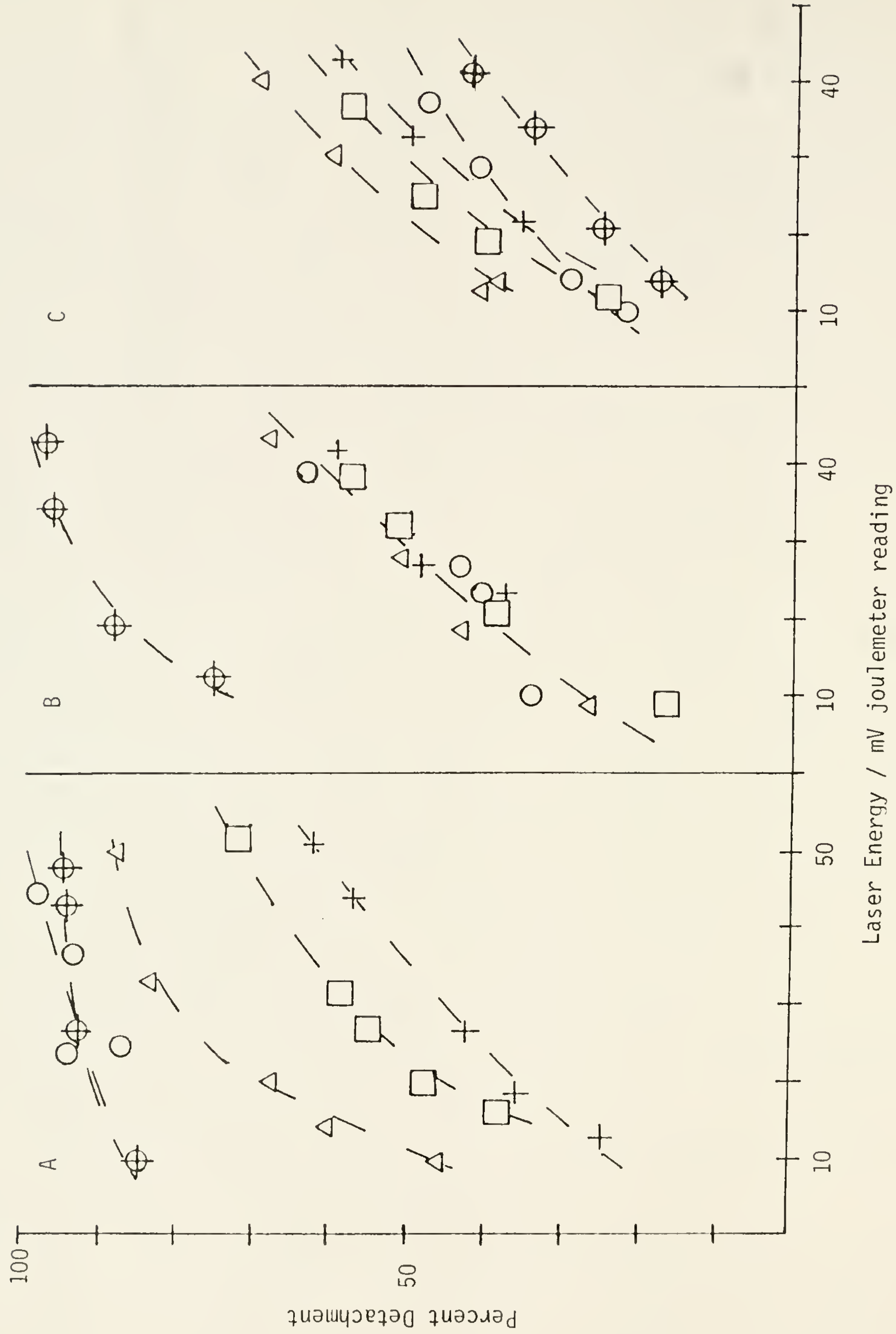
Percent Detachment
100
50
A
B
C
10
50
10
40
10
40
Laser Energy / mV joulemeter reading

Figure 4.3. Percent Detachment of OH^- Versus Time at Constant Laser Energy

A. 2.5×10^{-6} torr Water

B. 5.0×10^{-6} torr Water

C. 1.0×10^{-5} torr Water

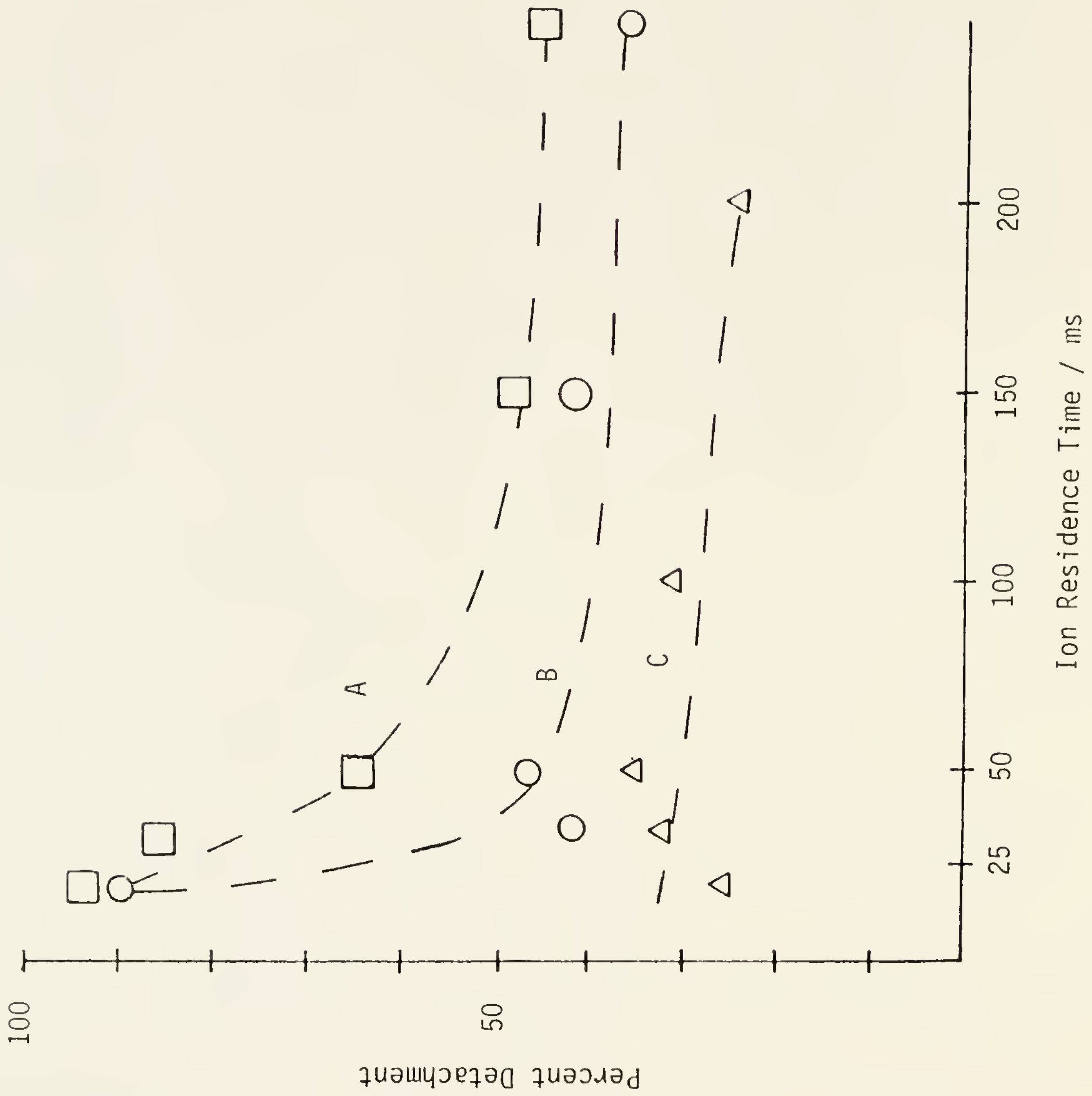
Percent Detachment
100
50
Ion Residence Time / ms
25
50
100
150
200
A
B
C

Figure 4.4. Percent Detachment of OH^- Versus "Mean Collision Number"

□ = Data Obtained with 2.5×10^{-6} torr Water

o = Data Obtained with 5.0×10^{-6} torr Water

Δ = Data Obtained with 1.0×10^{-6} torr Water

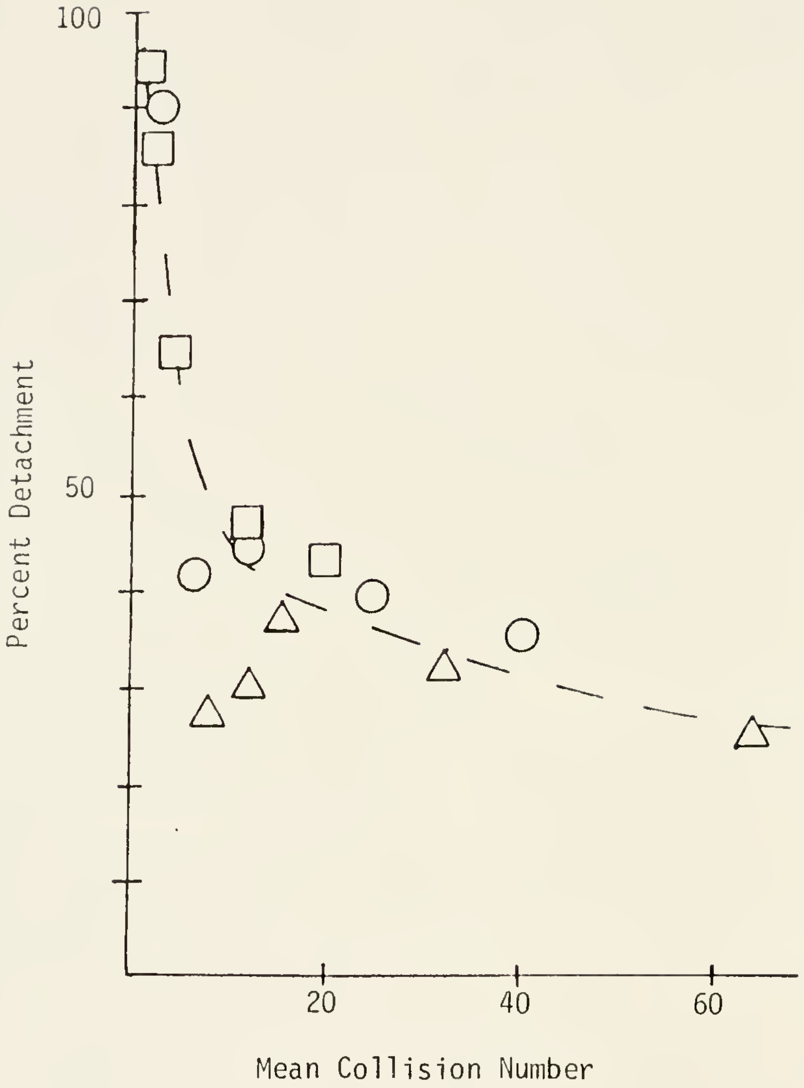
100
50
Percent Detachment
20
40
60
Mean Collision Number

The number density of the neutral gas, N, is calculated from the ideal gas law. The "mean collision number," N_c, is:

$$N_c = Z_1 t_d \qquad 4.5$$

where t_d is the detect delay time. It is then the number of orbiting collisions an ion moving through an ideal gas of the pressure of the neutral sample undergoes between initiation of the experiment and photolysis and detection. It has been shown that the trapping and drift potential fields in the trapped ion icr cell accelerate the ion only a small fraction above its thermal speed (17). It can clearly be seen that the three curves obtained at the three different pressures become nearly identical when percent detachment is plotted against "mean collision number." This suggests that the time-dependence of the apparent photodetachment cross section is related to the collisional equilibration of the sample. This appears to occur very rapidly--the greatest change in percent detachment occurs in the first four collisions.

Effects of Variation in Laser Parameters

Figure 4.5 shows two curves (A and B) obtained with the same dye (rhodamine 6 G) at different wavelengths and with the same laser alignment. Curve C is the result obtained under identical conditions to those used to

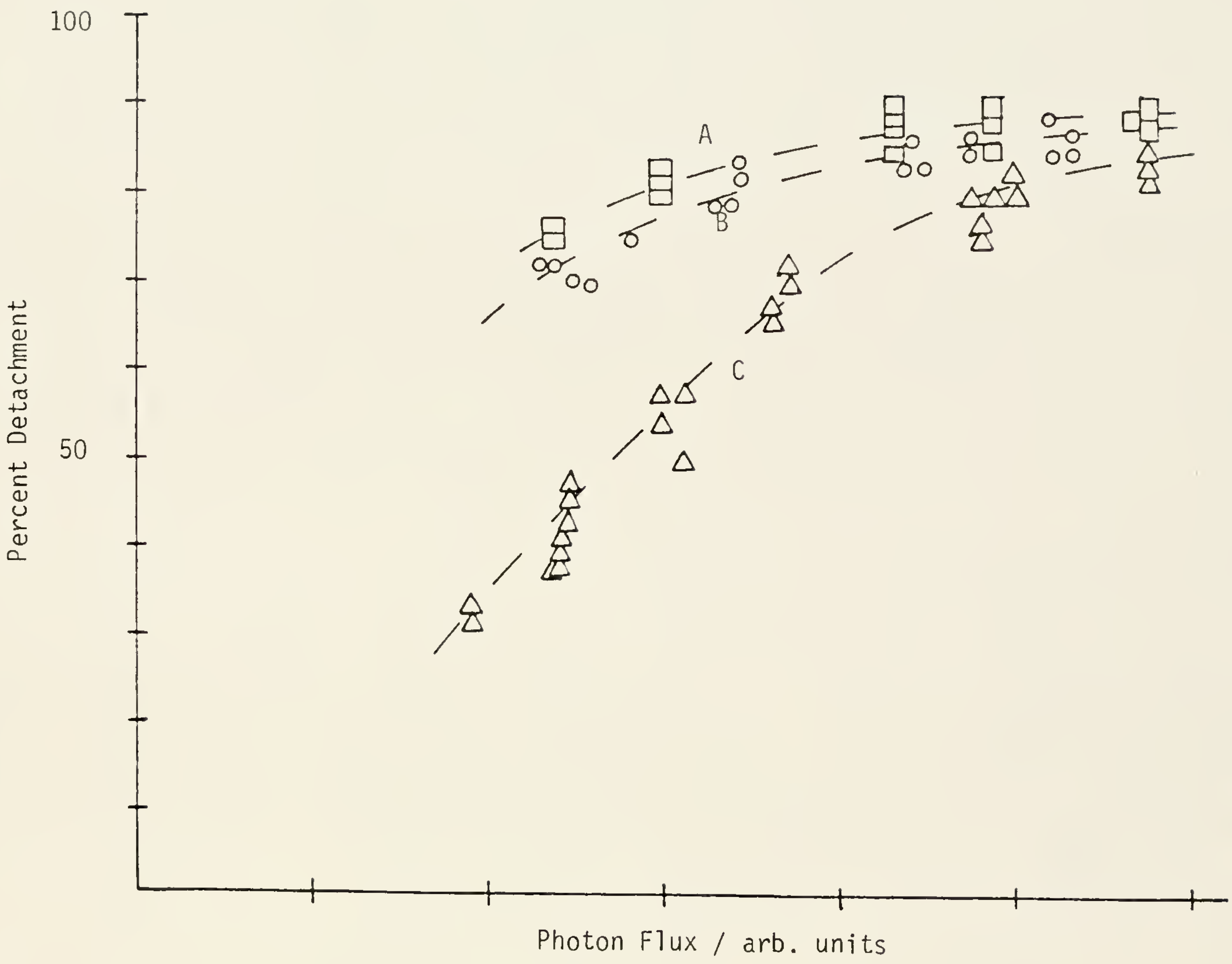

Figure 4.5. Percent Detachment of OH^- Using Rhodamine 6 G (see text for details)

obtain Curve A except that the vertical alignment of the laser grating was changed slightly. Figure 4.6 shows three curves obtained using three different dyes. Curve A of Figure 4.1 was obtained with the same dye used in all of Figure 4.5 and Figure 4.3.A but under a third set of alignment conditions. Figures 4.3.A and 4.3.B were obtained with different dyes (rhodamine 6 G and rhodamine 110) with essentially the same optical alignment. Each curve is a plot of percent decrease in the ion signal versus $E(\lambda)$ and each point represents the result of one laser shot.

Discussion

Curve Fitting

It can easily be seen by comparison of the data in this chapter with the theoretical curves in Chapter 2 (Figures 2.3 and 2.4) that the dependence of the percent detachment of OH^- on laser intensity is similar to that predicted in Equation 2.32. The results of some curve fitting (50) of the experimental data to Equation 2.32 are shown in Figure 4.7. The open points are the experimental data for the photodetachment of OH^- (taken from Figure 4.2. A). The data [R and $E(\lambda)$] were fit to:

$$R = f[1 - \exp(-k'E(\lambda)\lambda)]. \qquad 4.6$$

Figure 4.6. Percent Detachment of OH^- Using Various Laser Dyes

A. Rhodamine 6 G

B. Rhodamine 110

C. LD 490

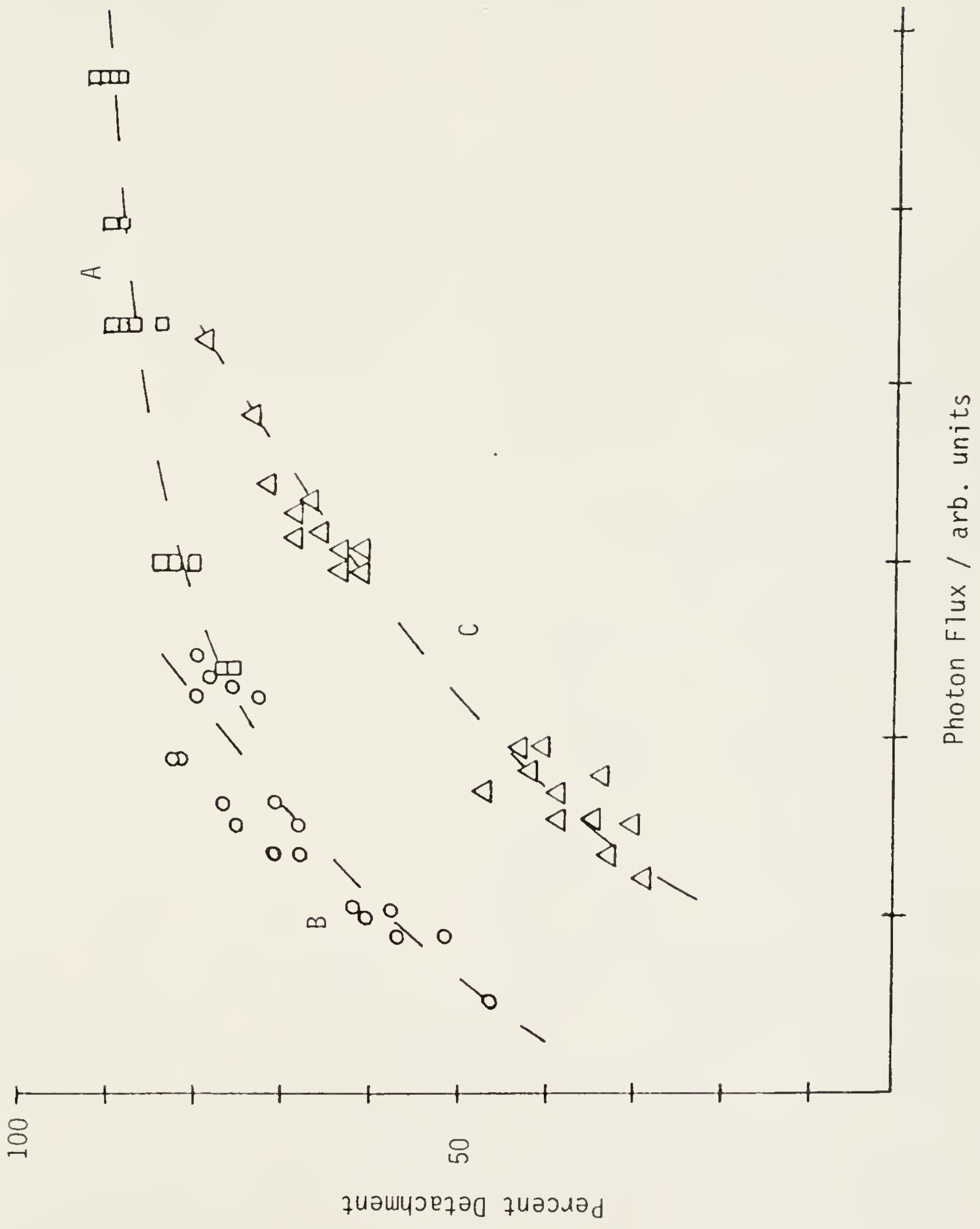
Percent Detachment
100
50
Photon Flux / arb. units
A
B
C

Figure 4.7 The Results of Curve Fitting to the Experimental Data

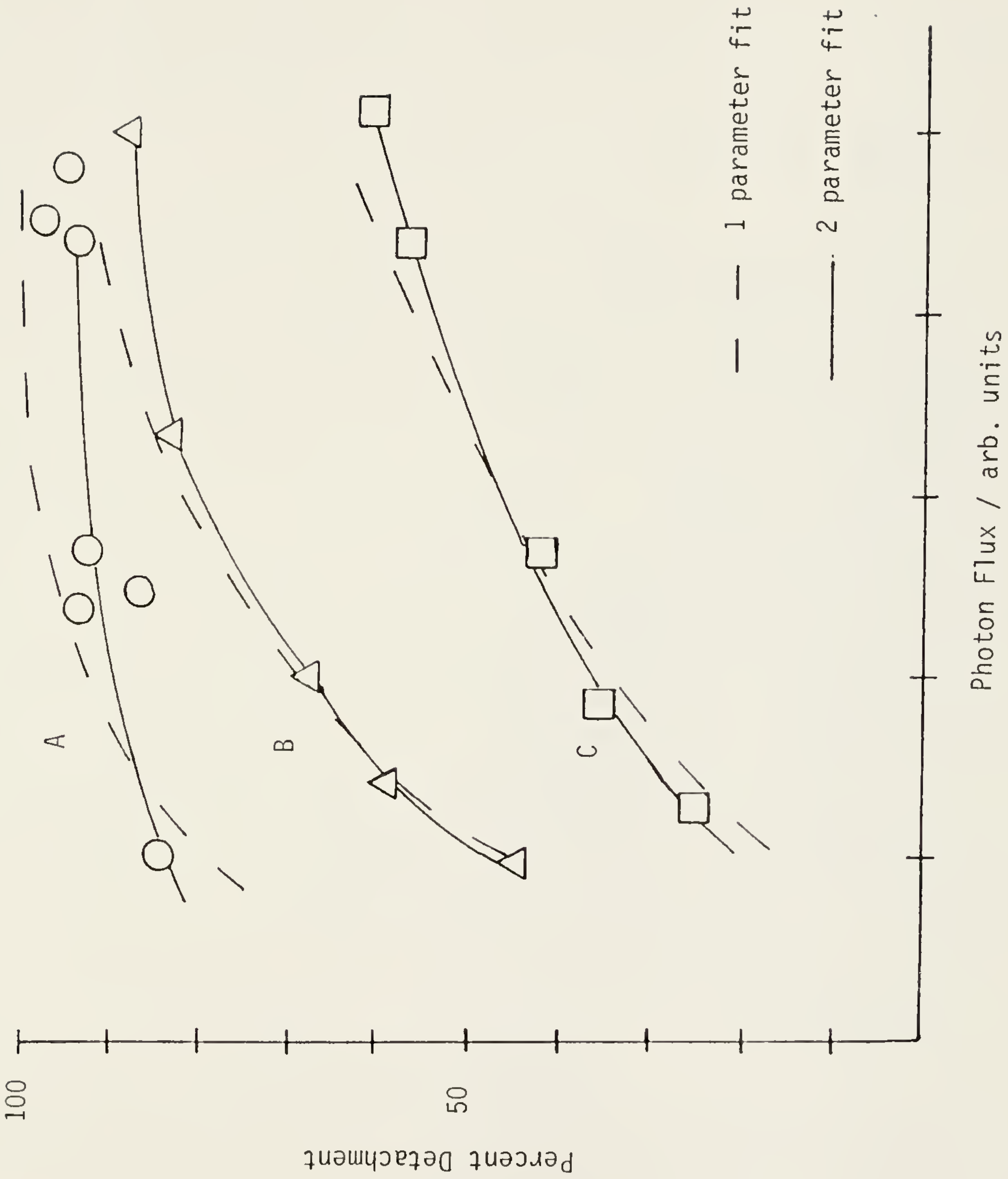
Percent Detachment
100
50
Photon Flux / arb. units
A
B
C
1 parameter fit
2 parameter fit

The dashed lines represent the curves obtained when one parameter, k', was allowed to vary and f was held equal to 1.0. The solid lines represent the curves obtained when both k' and f were varied. Obviously the two-parameter fit looks better than the one-parameter fit. However, application of the standard F test (51) to the variance between the observed and calculated curves reveals that there is no significant difference between the two fits. A value of f of 1.0 is consistent with these results.

A crude method of obtaining a value of f was also applied to Curves 4.1.A, 4.6.A, 4.2.B, and 4.2.C. Since all such measurements at a given wavelength should yield the same cross section, K'σ was calculated from all the data on these curves with f varying. The best value of f was obtained by minimizing the relative standard deviation in K'σ. In all cases the best value of f was between 0.95 and 1.0. Since such a small variation of f has little effect on the calculated cross section, f was taken to be 1.0. The ratios of K'σ obtained in these calculations were used to normalize the data on the photodissociation of $C_2H_5Cl^+$ to constant cross section relative to the cross section for the photodetachment of OH^- as described below.

Standardizaiton of the Experiment

In general the observed probability for a photoinduced process in an ion is related to the absolute cross section for that process times the density of photons and the density of ions integrated over time and space (15). If the absolute cross section depends on wavelength, an integration over the light source wavelength distribution must be carried out. Should the absolute cross section depend on any other variable, such as the internal energy of the ion, an integration over the distribution of that variable must also be carried out. In order to determine the absolute cross section experimentally the distribution of all these experimental variables must be known. In the trapped ion icr cell the spatial and temporal distribution of the ion population is complicated (17). The spatial and temporal distribution of photons depends on the laser operating conditions. One can only speculate about the internal energy states of the ion population. In principal, one might design experiments to determine the distribution of all these variables, but some of these experiments would be exceedingly difficult. The computation of an absolute cross section based on these distributions would also require a prodigious effort. Although the independent determination of absolute cross sections by the pulsed icr technique may not be impossible it is certainly prohibitively difficult.

The experiments described in this chapter represent a crude attempt to investigate the distribution of the many variables that relate the absolute cross section to the apparent cross section measured here. None of these distributions is determined directly--rather, the effect of changes in various experimental conditions on the apparent cross section was studied. Among the experimental conditions varied were the icr operating conditions: cell plate potentials, magnetic field strength, number of ions, and ion residence time. In addition, the laser operating conditions of alignment and dye were varied and their effects on the apparent cross section were studied. The qualitative effect of these experimental conditions on the distributions of the physical variables of the system is estimated from theory.

The percent detachment was observed to be independent of cell plate potentials and the magnitude of the ion signal within practical operating limits. Nonetheless, a concerted effort was made to reproduce all experimental conditions as much as possible. Among the studies reported in Chapters 5, 6, and 7 significant variations in signal intensity were observed only in those involving $C_2H_5Cl^+$. This was due in part to the difficulty of obtaining any signal of $C_2H_5Cl^+$ at all and in part to the rather long span of time over which that study was carried out. Furthermore, by the time the two most recent studies (those of benzyl chloride and 1,3,5 hexatriene) were carried out a single type of filament was in use and signal intensities were reasonably reproducible.

Variations in magnetic field strength, the number of collisions suffered by an ion, laser alignment, and laser dye produced a marked change in the apparent photodetachment cross section of OH^-. The magnetic field strength and the number of collisions probably affect the spatial distribution of the ion sample. However, it is not possible to separate these two effects based on the data presented here. At a fixed field strength the apparent cross section decreases rapidly in the first few collisions and it decreases slowly after that. At early times the apparent cross section decreases with decreasing field. It may be that the effect of field strength and collisions are coupled. One explanation might lie in the dependence of the frequency of the oscillation in the shape of the ion population on magnetic field strength. If that motion is damped by collision or space charge the distribution of the ion population in space at any given time could depend on the number of such oscillations completed and hence on the magnetic field strength. The effect of collisions could be related to the "thermalization" of the translational energy distribution of the ion population. Changes in the translational energy of the ions would be expected to change the distribution of the ions in space. Yet another explanation of this collisional effect is diffusion of the ions away from the region of the cell where they were originally formed.

The data suggest that the dependence on dye and alignment are in fact coupled. Figures 4.6.A and 4.6.B were obtained with two different dyes at the same alignment. There is good agreement between the apparent cross sections obtained in those two experiments. Figures 4.1.A and 4.6.A were obtained with the same dye but at different alignments. In this case there is no agreement between the results. This seems reasonable because changes in dye and alignment tended to accompany one another. Often the grating had to be moved a considerable amount to reflect the widely varying output wavelength of different dyes. Thus, the changes observed in the apparent cross section with changes in laser dye probably reflect changes in the optical alignment.

It was possible to align the grating very precisely but the 100 percent reflecting mirror and the sample chamber had to be moved whenever the filament was replaced. Two different procedures were used to standardize the results when the vacuum chamber was opened. Either a set of observations of the apparent photodetachment cross section of OH^- was obtained with each alignment or several data points were repeated under identical conditions of sample, wavelength, and icr operating conditions. Where both methods were used simultaneously, as with chloroethane, the results obtained by both procedures were the same. That is, the apparent cross sections for photodisappearance of OH^- and $C_2H_5Cl^+$ were observed to change by the same factor from one alignment to the next.

Conclusions

The studies of the photodetachment of OH^- confirmed that the experimental data fit the theory reasonably well. Application of the standard χ^2 test (51) indicated that for all the data fit to Equation 4.6 the calculated values are within the 99 percent confidence limit of the observed values--assuming a normal error distribution. The recurrence of an f value of 1.0 suggests that all of the ions in the cell are irradiated by the laser at all times. The apparent cross section for a photoinduced process changes greatly in the first four collisions but there is little evidence of change after that. The change in the apparent cross section with laser alignment is reproducible from sample to sample indicating that straightforward standardization procedures are valid. This study provides a basis of comparison for results obtained in other molecular systems.

CHAPTER 5
PHOTODISSOCIATION OF CHLOROETHANE MOLECULAR CATION

Introduction

Experimental studies of molecular ions have contributed much to the development of the theory of unimolecular chemical reactions for both ionic and neutral systems. In particular, the sensitivity of mass spectrometric techniques has permitted the study of many processes, among them unimolecular dissociation, in a variety of ionic systems at low pressures where truly unimolecular processes predominate (8 ,52). The principal techniques used in these studies have involved ionization and excitation of the molecules by electron impact (4), photoionization (3), or charge exchange reactions (53).

Recently the technique of photodissociation spectroscopy has been used to study the decomposition of many molecular ions (54). This technique involves ionization of a molecule by electron impact and then excitation of the molecular ion by a light source. Originally conventional light sources were employed but most recent studies have employed lasers as excitation sources. The obvious advantage of laser sources is their narrow energy bandwidth which allows the deposition of a precisely known amount of excitation energy in the ion.

Several photodissociation studies of alkyl halide molecular ions have been carried out previously using both ion cyclotron resonance (35) and beam techniques (55,56,57). In the case of chloromethane and bromomethane only low resolution studies have appeared as yet but at least one of these (55) indicates that dissociation occurs directly from an excited electronic state on a time scale shorter than that of molecular rotations or vibrations. Also, a high resolution photodissociation study of the iodomethane (57) molecular ion has revealed well-resolved fine structure in the first band, indicating that the first excited electronic state of that ion is predissociative. In both of these cases the only dissociation channel observed, or indeed allowed by energetics, is loss of the halogen atom.

The unimolecular decomposition of ethyl halide ions differs from that of the methyl halides in that several molecular elimination processes (elimination of hydrogen halide and elimination of molecular hydrogen) occur with lower activation energy than elimination of the halogen atom. Several studies of the unimolecular decomposition of the chloroethane molecular ion have been reported using a variety of techniques (3,4,53). In those studies where ions were formed with less than 1.5 eV of energy above the ionization threshold molecular elimination of HCl was observed (14) while in studies (3,53) where more than 1.5 eV of excitation energy was deposited in the parent ion a more complex, excitation energy dependent fragmentation pattern emerged.

This study falls into the latter category; the excitation energy ranged from 1.7 eV to 2.7 eV. The study is unique among those involving unimolecular decay in chloroethane ions in that the excitation energy is very precisely known (± 0.002 eV corresponding to ± 0.4 nm) and the excitation involves an optical transition to (an) excited electronic state(s). The results of this study show that while elimination of a chlorine atom is the predominant process, molecular elimination of hydrogen chloride competes with it in a manner strongly dependent upon excitation energy. These results are in general agreement with other studies in the same range of excitation energies (53). However, this study yields detailed information about the energy dependence of the photodissociation cross section and of the competition between reaction channels. These data in turn provide more information about the shape and location of the excited state potential surfaces of the ion than previous studies.

Experimental

Experimental Procedures

Chloroethane (Matheson Gas Company) was used as obtained after freeze-pump-thaw purification on the mass spectrometer inlet vacuum system. Sample pressures were varied between 1.25 x 10^{-6} torr and 3.0 x 10^{-6} torr. At lower pressures the ion signal was too small to be detected with adequate signal-to-noise ratio and at higher pressures ion-molecule reactions removed the parent ion too rapidly to carry out the photodissociation experiment. The ion was formed by electron impact ionization. For the studies reported here, the ionizing electron energy was varied between nominal values of 11.5 and 25.0 eV. The majority of experiments used 12.5 eV as the ionizing energy. This voltage was sufficient to produce an adequate ion signal and yet was low enough to preclude formation of excited electronic states of the ion which are known to have onsets at $>$13.0 eV (58).

A pulse sequence typical of these experiments is shown in Figure 5.1. Only minor variations in pulse sequence were possible because the highly reactive $C_2H_5Cl^+$ ion has only a transient existence even at low pressures and it is possible to achieve adequate signal-to-noise ratios only under a rather limited set of experimental conditions. A typical experiment proceeded according to the following format. Ten to twenty pulse cycles were run with the icr

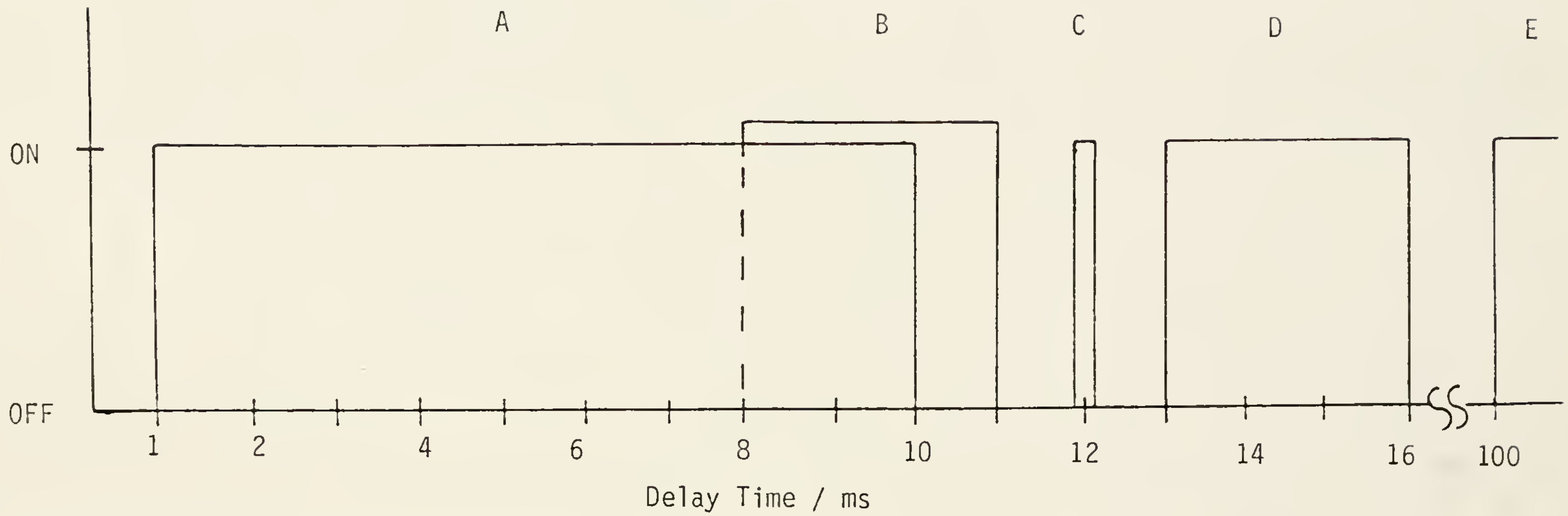

Figure 5.1. A Typical Pulse Sequence

A. Grid Pulse
B. Double Resonance Pulse
C. Laser Pulse
D. Detect Pulse
E. Quench Pulse

tuned so that no ion was in resonance (ion zero level); an equal number were run with the $C_2H_5Cl^+$ ion (m/e = 64) in resonance and the laser off (ion baseline level). Then a minimum of ten cycles were run with the laser firing; the energy of each laser flash was read from an oscilloscope and recorded manually. Ten to twenty more ion baseline level cycles were recorded, then ten to twenty more ion zero levels were taken. It was also necessary to record ten cycles with the icr tuned so that $C_2H_3Cl^+$ (m/e = 62) was in resonance. This value multiplied by 0.32 was subtracted from all $C_2H_5Cl^+$ measurements to correct for that portion of the m/e = 64 signal caused by the presence of $C_2H_3{}^{37}Cl^+$.

The relative cross section was calculated according to Equation 2.32. The quantity R in that equation is calculated as (ion baseline level - ion level with the laser on)/(ion baseline level - ion zero level), where all levels have been corrected for the contribution of $C_2H_3{}^{37}Cl^+$. Here ion baseline level and ion zero level were the average of the twenty to forty measurements of each quantity. A separate value of K'σ was calculated for each laser shot. The results were averaged and treated by standard statistical methods (59).

Standardization of the Spectrum

As the experiments described in Chapter 4 above indicate the measured cross section for a photoinduced process is sensitive to the operating conditions of the instrument, particularly the optical alignment of the laser. Since the optical alignment of the instrument was changed fairly often in the course of obtaining this spectrum, some care had to be taken to ensure consistency from one data set to another. Similar procedures have been reported by other investigators in this field (35). The approach used here seems reasonable on the grounds that two independent experiments were carried out to evaluate the changes in the apparent cross section with changes in optical alignment. The changes observed indicated that both of the cross sections measured changed by the same factor from alignment to alignment making standardization a straight forward matter.

The photodissociation spectrum of $C_2H_5Cl^+$ was obtained in four segments corresponding to four different optical alignments. A total of eight dyes were used to cover the wavelength range from 455 nm to 690 nm; only the region between 500 nm and 520 nm was not examined. The four segments were taken as:

Segment 1. 570-690 nm using rhodamine 6 G (570-608 nm) rhodamine B (600-620 nm), kiton red S (610-640 nm), and a mixture of rhodamine 6 G and cresyl violet (640-690 nm).

Segment 2. 455-500 nm using LD 455 (455-473 nm) and LD 490 (470-500 nm).

Segment 3. 540-600 nm using rhodamine 110 (540-570 nm) and rhodamine 6 G (570-600 nm).

Segment 4. 520-540 nm using coumarin 540.

Within each segment standardization was achieved by measuring the photodissociation cross section of $C_2H_5Cl^+$ at one or more wavelengths where the output range of two dyes overlapped. Within each segment the cross sections measured in this way were always equal within experimental error at any given wavelength independent of the dye used.

The procedure used in standardization between the segments is summarized in Table 5.1. The measured cross section is K'(Segment n)$\sigma(\lambda)$ where K'(Segment n) is the alignment factor for the nth segment of the spectrum and $\sigma(\lambda)$ is the absolute cross section for the photo-process at wavelength λ. Standardization consisted of multiplying K'(Segment n)$\sigma(\lambda)$ by the quantity K'(Segment 1)/K'(Segment n) to obtain K'(Segment 1)$\sigma(\lambda)$ and so put all the measured cross sections on the same relative scale.

Since Segments 1 and 2 were obtained at different wavelengths with no overlap the ratio of K' s was obtained by comparison of the apparent photodetachment cross section of OH^-. Here the ratio of K' s at two different wavelengths (λ and λ') could be determined because the ratio $\sigma(\lambda)/\sigma(\lambda')$ is known independently (30).

Comparison of K'(Segment 1) and K'(Segment 3) was carried out in two ways. The ratio of K' s was obtained at

Table 5.1. Standardization Constants

	Photodetachment Cross Section of OH^- from Ref. 30 $\sigma(\lambda)(\times 10^{18}\ cm^3)$	
A. Segment 1 to Segment 2		
K'σ photodetachment of OH^-		K'(Segment 1)/K'(Segment 2)
Segment 1: 2.0×10^{-4} at 580 nm	11.	2.7
Segment 2: 6.7×10^{-5} at 490 nm	10.	
B. Segment 1 to Segment 3		
K'σ photodissociation $C_6H_8Cl^+$		K'(Segment 1)/K'(Segment 3)
Segment 1: 1.23×10^{-5} at 580 nm		
Segment 2: 7.5×10^{-6} at 580 nm		1.6
Segment 1: 1.23×10^{-5} at 590 nm		
Segment 3: 8.0×10^{-6} at 590 nm		1.5
Segment 1: 1.22×10^{-5} at 595 nm		
Segment 3: 8.0×10^{-6} at 595 nm		1.5
K'σ photodetachment of OH^-		
Segment 1: 2.0×10^{-4} at 580 nm		
Segment 3: 1.2×10^{-4} at 580 nm		1.7
		Average 1.6
C. Segment 4 to Segment 3		
K'σ photodissociation of $C_2H_5Cl^+$		
Segment 3: 1.1×10^{-5} at 540 nm	K'(Segment 4)/K'(Segment 4)	0.55
Segment 4: 2.0×10^{-5} at 540 nm	K'(Segment 1)/K'(Segment 4)	0.90

three wavelengths by comparing the apparent photodissociation cross section of $C_2H_5Cl^+$. A second determination was made by comparing the apparent cross section for the photodetachment of OH^- at one wavelength. As Table 5.1 shows the results are reasonably consistent. The average value was used.

Finally Segments 3 and 4 were compared directly by comparing the observed photodissociation cross section of $C_2H_5Cl^+$ at 540 nm. The ratio K'(Segment 3)/K'(Segment 4) obtained times the ratio K'(Segment 1)/K'(Segment 3) yields the ratio of K'(Segment 4) needed to standardize these data.

The uncertainty in K'σ is taken to be the 95 percent confidence limit based on the mean of between ten and fifty laser shots for each point taken. Both the uncertainty in the ratio of K' s used for standardization and the final uncertainty in the standardized cross section are calculated from this uncertainty using the standard procedures for the evaluation of the propagation of errors (59). The error bars shown in Figure 5.2 represent the 95 percent confidence limits estimated by this procedure.

Measurement of Product Ion Yields--The ω_2 Experiment

Relative yields of product ions from the photodissociation of $C_2H_5Cl^+$ were obtained by measuring the m.o. level at a particular mass with the laser off and then with the laser on. In many instances the product ion (e.g., $C_2H_4^+$) also appeared as a fragment ion from the electron impact ionization of C_2H_5Cl. Such ions could be ejected from the cell by the technique of pulsed double resonance ejection. In these experiments the ω_2 pulse was used to gate a waveform generator which applied a radio frequency oscillation to the upper plate of the cell. The frequency was chosen to eject the suspected product ion from the cell before the laser was fired. Only those ions produced by the photolysis of $C_2H_5Cl^+$ were then detected by the gated m.o. If no ion was seen in the absence of laser irradiation a mass spectral scan of width of ± 1.0 amu about that of the expected product ion was made with the laser firing to determine if the ion in question were formed in the photodissociation of $C_2H_5Cl^+$. No product ions were found in this manner.

Quenching Studies

Several measurements of the effect of an inert gas, argon, (Matheson Gas Company), on the various experimental results were made. The partial pressure of $C_2H_5Cl^+$ was maintained at 1.5×10^{-6} torr and that of argon at 5.5×10^{-6} torr. The wavelength region between 610 nm and 630 nm was studied in both the presence and absence of argon. The relative photodisappearance cross section and the relative photoproduct yield were both studied.

Results

The Identity of the Ion Undergoing Photodissociation

Only one ion, $C_2H_5Cl^+$, was observed to photodissociate in these experiments. $C_2H_3Cl^+$, $C_2H_4Cl^+$, $C_2H_6Cl^+$, $C_2H_4^+$, and $C_2H_5^+$ were all studied for photodissociation effects but none were seen. The relative photodisappearance cross section for $C_2H_5Cl^+$ is plotted against wavelength and excitation energy in Figure 5.2.A. The absolute cross section at 620 nm can be estimated as $1.2 \pm 0.3 \times 10^{-18}$ cm^2 by comparison to the photodetachment cross section of OH^- (30). Neither the presence of argon nor changes in the ionizing electron energy caused any significant change in the photodisappearance cross section.

Identity of the Dissociation Products

Several dissociation pathways are available to $C_2H_5Cl^+$ at the excitation energies reported here. They are listed in Table 5.2 with their endothermicities (60). A search was made for each of the possible product ions listed in Table 1 at at least one wavelength with each dye used. Only Reaction Channels 1 and 3 were observed. Reaction Channel 2 was studied more intensively than any other but no photoproduction of $C_2H_3Cl^+$ was ever observed.

Figure 5.2. A. The Photodissociation Spectrum $C_2H_5Cl^+$ in the Wavelength Region 455-691 nm

B. The Photodissociation Branching Ratio Spectrum

C. The Relevant Portion of the Photoelectron Spectrum of C_2H_5Cl with the States Labelled as They Are in the Text

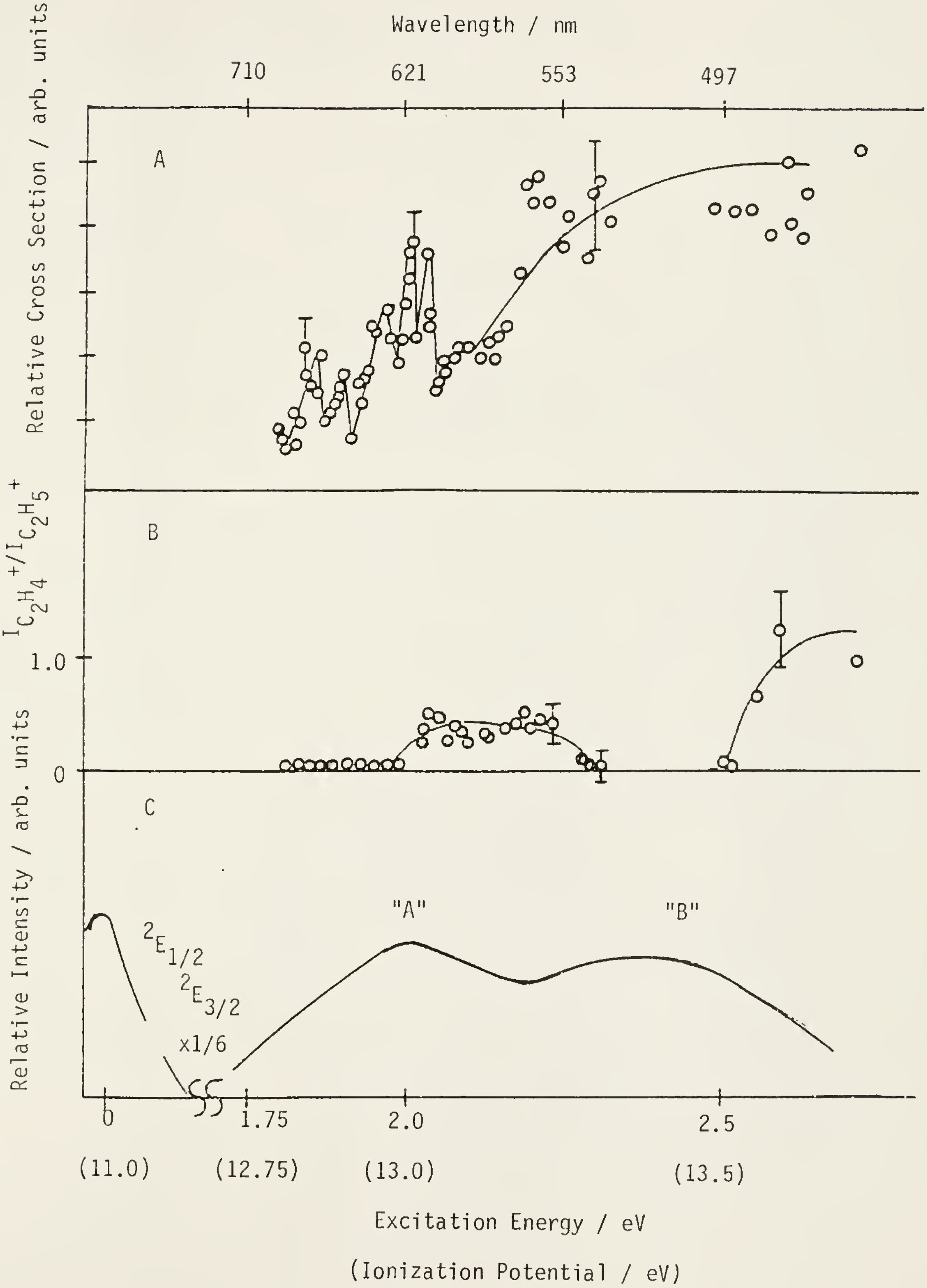
Wavelength / nm
710
621
553
497
Relative Cross Section / arb. units
A
B
$I_{C_2H_4^+}/I_{C_2H_5^+}$
1.0
0
C
Relative Intensity / arb. units
"A"
"B"
$^2E_{1/2}$
$^2E_{3/2}$
x1/6
0
1.75
2.0
2.5
(11.0)
(12.75)
(13.0)
(13.5)
Excitation Energy / eV
(Ionization Potential / eV)

Table 5.2 Dissociation Pathways of $C_2H_5Cl^+$ with Endothermicities of Less than 3.0 eV

Reaction						ΔH (eV)*
1.	$C_2H_5Cl^+$	→	$C_2H_4^+$	+	HCl	0.3
2.		→	$C_2H_3Cl^+$	+	H_2	0.6
3.		→	$C_2H_5^+$	+	Cl	1.0
4.		→	CH_2Cl^+	+	CH_3	2.2
5.		→	HCl^+	+	C_2H_4	2.5
6.		→	CH_3^+	+	CH_2Cl	2.7

*From Reference 60.

Wavelength Dependence of the Photodissociation Pathway

The ratio of the photoproduction cross sections of $C_2H_4^+$ and $C_2H_5^+$ versus wavelength and excitation energy is shown in Figure 5.2.B. The results are plotted as the intensity of the ion signal due to photoproduced $C_2H_4^+$ ($I_{C_2H_4^+}$) divided by the intensity of the ion signal due to photoproduced $C_2H_5^+$ ($I_{C_2H_5^+}$). It is difficult to obtain measurements of the product ion appearance cross section which are independent of disappearance cross section measurements because of difficulties in monitoring the intensities of both parent and daughter ions (having drastically different masses) under equivalent experimental conditions. In any event, the error in the branching ratio may be as great as ± 0.20 so it is difficult to draw any conclusions regarding fine structure in these data or even the threshold for the appearance of $C_2H_4^+$ in each band. However, a distinction can be made between wavelengths where no detectable amount of $C_2H_4^+$ was formed and those where a measurable $C_2H_4^+$ photoproduct ion intensity was observed. The presence of argon as a quencher gas had no measurable effect on the branching ratio. Changes in ionizing electron energy likewise had no measurable effect on the branching ratio.

Discussion

Comparison of the Photodissociation Spectrum to the Photoelectron Spectrum

A number of earlier investigators have found comparison with photoelectron spectroscopy useful in analyzing the results of photodissociation spectroscopy (54). The energies of the excited states of molecular ions can be obtained from their photoelectron spectra, because each peak arises from ionization of a molecule to a different electronic state of its molecular ion. The ionization potentials that appear in the photoelectron spectrum of chloroethane (Figure 5.2.C) (58) are 11.01 eV for the band assigned to the two lowest-lying states ($^2E_{1/2}$, $^2E_{3/2}$) and 13.07 and 13.4 for the next two excited states, here labelled "A" and "B", respectively. These labels are for convenience of discussion only and are not meant to imply any symmetry designation. Chloroethane belongs to the C_s symmetry group and in that group all transitions are symmetry-allowed. Thus, symmetry assignments of the excited states of the molecular ion cannot be made based on the data presented here. Clearly, with an ionizing electron energy of only 12.5 eV it is possible to populate only the low-lying electronic states ($^2E_{1/2}$, $^2E_{3/2}$) to any significant extent upon ionization. The respective populations of these two states cannot be determined under these experimental conditions. Also, the vibrational energy distribution in the molecular ion prior to irradiation cannot be assessed accurately. This offsets to some extent the high resolution advantage gained by using a laser. Although the excitation energy is known to a high degree of certainty, the energy distribution in the initial state is not. However, several considerations suggest that no highly excited ions are present in the sample being dissociated. In the first place changes in pulse sequence, changes in chloroethane pressure, and changes in electron energy had no significant effect on the spectra obtained. Addition of an inert quencher, argon, likewise made no difference; however, in the pressure regime of these experiments this may only indicate the lack of a sufficient number of collisions to relax significantly the internal energy of the parent ion. Furthermore, the presence of several dissociation pathways with very low activation energies makes it unlikely that any highly excited ions survive for more than a few μs. Direct measurements of the unimolecular decay rate in chloroethane show this to be true (4). Although the distribution of vibrational energy in the ion prior to irradiation may not be thermal it almost certainly does not include any ions with more than a few quanta of vibrational excitation.

Direct comparison of the photodissociation spectrum of the ion to the photoelectron spectrum of the parent molecule (58) is presented in Figure 5.2. The lowest I.P. represents ionization of the molecule to the ground state of the molecular ion; it is therefore set as the zero on the excitation energy scale. It can readily be seen that the two major features of the photodissociation spectrum (Figure 5.2.A, namely the peaks between 690 nm and 600 nm and the shoulder between 550 nm and 450 nm) coincide roughly with the second and third bands of the photoelectron spectrum (Figure 5.2.C, i.e., the "A" and "B" excited electronic states of the molecular ion). The differences in appearance of the two bands in the photodissociation spectrum indicate that the two excited states of the molecular ion have markedly different potential surfaces. The band associated with the "A" state appears to have some poorly resolved vibrational structure. This could indicate predissociation or dissociation along a flat potential surface (61). The photodissociation spectrum of the "B" excited electronic state of the ion has no structure, indicating that this state is steeply repulsive (probably involving dissociation along the C-Cl bond).

Examination of the Branching Ratio

The wavelength dependence of the ratio of photoproduct ion intensities raises more interesting questions about the excited state potential surfaces. Ion fragmentation in alkyl halides has often been explained in terms of the quasi eqilibrium theory (Q.E.T.) (8), particularly in those studies involving less than 1.5 eV of excitation energy.

An approximate Q.E.T. calculation (8) of the branching ratio has been carried out. According to the simplest picture of Q.E.T. the rate constant for unimolecular decay is given by (62):

$$K = \frac{F\omega^{\ddagger}(E - E_0)}{d\omega(E)/dE} \qquad 5.6$$

where E is the excitation energy, E_0 is the activation energy, F is a frequency factor, $\omega^{\ddagger}(E - E_0)$ is the density of states in the activated complex, and $d\omega(E)/dE$ is the density of states in the parent molecule. For a given excitation energy, $d\omega(E)/dE$ is the same for all reaction channels. Thus, the ratio of rate constants and the branching ratio is equal to the ratio of $\omega^{\ddagger}(E - E_0)$'s for the reaction channels in question. The value of $\omega^{\ddagger}(E - E_0)$ depends on the structure assumed for the activated complex. In this simple calculation the activated complex was assumed to be the same for all reaction channels considered. It was assumed to be a collection of two harmonic oscillators of frequency 300 cm^{-1}, nine of frequency 1,200 cm^{-1}, and six of freqency 3,000 cm^{-1}. These frequency groupings are similar to the pattern of the fundamental modes of chloroethane and were chosen to simplify the calculation. The number of normal modes in the activated complex is (3N-7) corresponding to the usual number of 3N-6 with one mode subtracted as the reaction coordinate. All frequency factors were assumed to be equal. E_0's for the three channels considered were taken to be the endothermicities of Channels 1, 2, and 3 listed in Table 5.2. The role of rotations was ignored. The ratio of rate constants obtained in this way is then the ratio of the density of vibrational states for the collection of oscillators described above with only the total energy to be partitioned statistically among the normal modes ($E - E_0$) varying from one reaction channel to another.

Obviously such a calculation is simplistic in assuming that the activated complex is identical for all three dissociation channels. However, three salient features arise from such a treatment.

1. $C_2H_4^+$ is predicted in large excess over $C_2H_3Cl^+$ and $C_2H_5^+$. The numerical ratios are roughly 1,000:100:1 at a photon energy of 1.8 eV.
2. The relative amount of $C_2H_5^+$ should increase with increasing photon energy.
3. The dependence of the branching ratio on excitation energy should be a smooth curve.

A brief inspection of the branching ratio obtained in this experiment (Figure 5.2.B) reveals that none of these predictions is borne out. Improvements in the calculations might change the quantitative results but Predictions 2 and 3 are general to Q.E.T. predictions. Based on this Q.E.T.

has been abandoned and other models have been sought for the dissociation of $C_2H_5Cl^+$. The implication of this result is that dissociation of electronically excited $C_2H_5Cl^+$ occurs rapidly compared to internal conversion within the ion. This is in substantial agreement with photodissociation studies of other alkyl halides (55,56, 57).

The fragmentation of chloroethane molecular ion has also been studied by charge exchange mass spectrometry (53) over a wide energy range including that of this study. In the range of excitation energies between 1.0 and 3.0 eV there is substantial agreement between this study and that of Ikuta and co-workers (53). The areas of disagreement can reasonably be attributed to experimental differences. Both studies agree that the principal dissociation product is $C_2H_5^+$, that there is a significant fraction of $C_2H_4^+$, and that no $C_2H_3Cl^+$ is produced. The energy resolution in that study was not sufficient to see the structure in the branching ratio that is reported here. Further, their results suggest that a 15 percent abundance CH_2Cl^+ should be detected in the second band of the photodissociation spectrum. Such a small product ion abundance could not be detected with certainty given the sensitivity of our instrument.

However, the interpretation given to their results by Ikuta et al. is attractive. Based on the results of approximate molecular orbital calculations they propose that $C_2H_5^+$ arises from direct dissociation of the "A" excited electronic state of the ion and that $C_2H_4^+$ arises from dissociation via excited vibrational levels of the ground state. CH_2Cl^+ is thought to be the primary product of the "B" state. However, in their study $C_2H_5^+$ is the principal product in the "B" state region indicating, in their model, substantial internal conversion to the "A" state. Such "A" ← "B" transitions would produce "A" state ions with high potential energy and could thus account for the lack of structure in the "B" state band in the photodissociation spectrum. The structure observed in our branching ratio spectrum would, in this model, indicate enhanced probability for internal conversion to the ground state at the high energy end of each band. This could arise from favorable Franck-Condon overlap on the repulsive potential core of the various electronic states.

Conclusions

From the similarities between the photoelectron spectrum and the photodissociation spectrum one may conclude that the initial step in the photodissociation process is the optical transition to an excited electronic state of the ion. The failure of Q.E.T. to model the subsequent dissociation process suggests that dissociation occurs without substantial partitioning of the excitation energy among the vibrations of the ion. Based on the structure observed in the photodissociation spectrum it is possible to speculate on the shape of the excited state potential surfaces. The results reported here suggest that the second ("A") excited electronic state of $C_2H_5Cl^+$ is weakly bound or flat. The dissociation of ions initially excited to the third ("B") excited electronic state occurs along a potential surface that is strongly repulsive with respect to scission of the C-Cl bond. However, whether that surface is associated with the "B" state itself or the repulsive core of the "A" state cannot be determined. Unfortunately, no definitive explanation for the wavelength dependence of the branching ratio can be offered at this time.

CHAPTER 6
PHOTODISSOCIATION OF BENZYL CHLORIDE MOLECULAR CATION

Introduction

Fu's studies (29) of the photodissociation of benzyl chloride molecular ion ($C_7H_7Cl^+$) revealed some anomalies in comparison to results obtained with other similar compounds. The most striking effect was the apparent inhomogeneity of the parent ion (m/e = 126) sample. Two peaks were reported in the steady state photodissociation spectrum of the benzyl chloride molecular ion; one at 600 nm and another at 440 nm. A high resolution spectrum of the 600 nm peak did not reveal any vibrational structure. Normally an ion irradiated at a wavelength where it dissociates all disappears if irradiated for a long enough time. Under steady irradiation at 440 nm all the benzyl chloride ion disappeared in roughly 20 s. However, irradiation with 600 nm light only caused the ion signal to drop to about 70 percent of its normal intensity in the absence of irradiation. The decrease all occurred in the first 10 s of irradiation and the ion signal was apparently unaffected by the light for 20 s thereafter. The possibility of the parent ion being "reformed" in a reaction between the photodissociation daughter ion and the parent molecule was eliminated by the results of a double resonance experiment. Consequently, Fu concluded that a portion of the parent ion population had rearranged to a chlorotoluene structure. The chlorotoluenes photodissociate at 440 nm but not at 600 nm (29).

In the pulsed experiment the presence of a nondissociating fraction in a given ion population would be revealed by a value of f (Equation 2.32) equal to that fraction of the ion population that is nondissociable. If the photodissociation cross section were large enough this would be revealed in the shape of the intensity dependence of the percent dissociation (see Figure 3.4). A change in the shape of the intensity dependence or even the apparent cross section with time might provide a way of measuring the rate of rearrangement.

Experimental

Benzyl chloride (ACS reagent grade) was used as obtained from Malinkrodt Chemical Company. Sample purity was routinely monitored by mass spectrometry. During the experiments sample pressures were typically between 1.0 x 10^{-6} torr and 5.0 x 10^{-6} torr, as measured by the ionization gauge. Trapping potentials were generally 1.5 V on the side plates and -1.5 V on the upper, lower, and end plates of the cell. The marginal oscillator frequency was 153.7 kHz and the resonant field approximately 12,600 G.

Several intensity dependence measurements were carried out with rhodamine 6 G as the laser dye. A photodissociation spectrum of the region near threshold and other intensity dependence measurements were carried out using kiton red S as the laser dye. Time dependence studies were carried out with both dyes. A variety of pulse sequences were used and they are listed in Table 6.1. The ionization energy was varied between 11.5 eV and 20.0 eV. Data were collected as described in Chapter 5 above except that no isotope correction was necessary.

Results

The most surprising result of this study was the large percent dissociation observed in every experiment. A typical plot of percent dissociation versus laser energy is shown in Figure 6.1. It was obtained with a wavelength of 617.5 nm. Clearly, at sufficiently high laser intensities far more than 30 percent dissociation is observed. This result was reproduced at every wavelength examined. With sufficient laser intensity (220 mJ) as much as 60 percent dissociation was observed. Since this is about the maximum output ever obtained from the laser it is difficult to tell what the limiting percent dissociation was. The large

Table 6.1 Pulse Sequences Used in the Study of the Photodissociation of Benzyl Chloride Molecular Cation

Grid Pulse		Laser Pulse		Detect Pulse	
Delay (ms)	Width (ms)	Delay (ms)	Width (μs)	Delay (ms)	Width (ms)
0	30	34	1	36	2.5
0	30	54	1	56	2.5
0	30	134	1	136	2.5
0	30	234	1	236	2.5
0	30	434	1	436	2.5
0	99	118	1	120	2.5
0	99	240	1	250	2.5
0	99	490	1	500	2.5
0	99	740	1	750	2.5
0	99	990	1	1,000	2.5
0	99	1,240	1	1,250	2.5
0	99	1,490	1	1,500	2.5
0	99	1,990	1	2,000	2.5
0	99	2,490	1	2,500	2.5

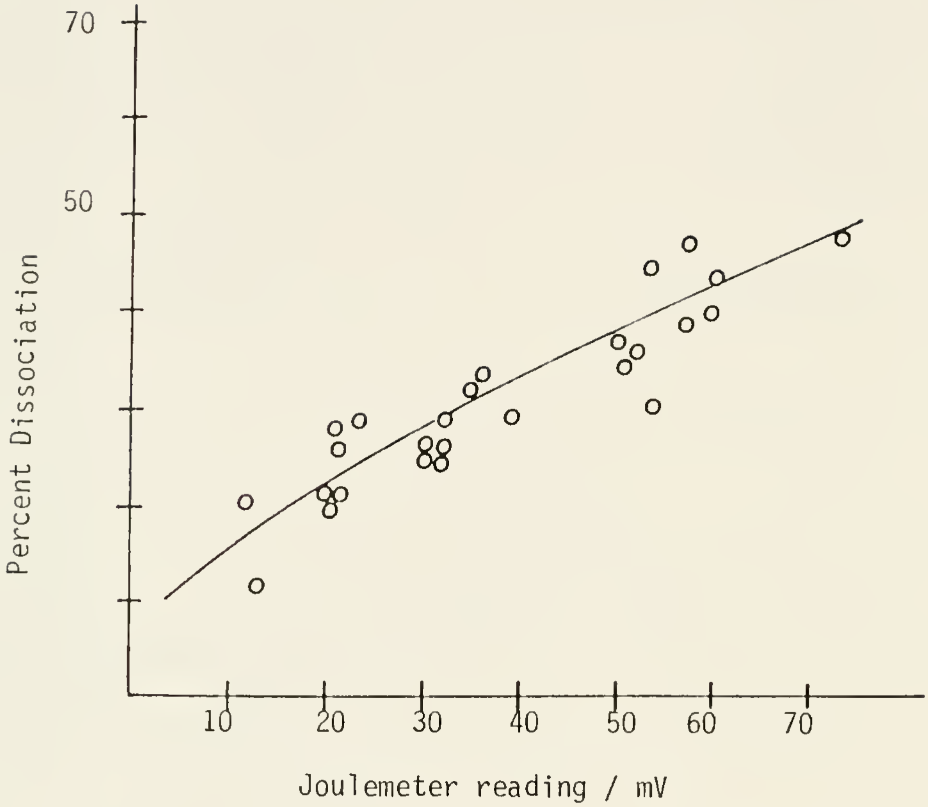

Figure 6.1. Percent Dissociation of $C_6H_7Cl^+$ Versus Laser Energy

percent dissociation was observed at every delay time used (maximum of 2.5 s).

The curve presented in Figure 6.1 was fit to two mathematical functions in the manner described in Chapter 3. A "best" value of f of 0.65 was obtained; however, the quality of the fit was not significantly better than that obtained with f of 1.0. These data cannot be used with any confidence to establish whether or not a portion of the parent ion population has rearranged. The intensity dependence at 595 nm was observed to be independent of ionization energy over the range studied here.

A short spectral scan was taken over the range of 644 nm to 617 nm. The results appear as Figure 6.2. Figure 6.3 shows the apparent cross section at 630 nm versus ion residence time.

Discussion

The shape of the photodissociation spectrum (Figure 6.2) reported here is in good agreement with Fu's results. The smoothly rising cross section suggests that the first excited electronic state of the benzyl chloride molecular ion is steeply repulsive. This behavior is similar to that of the second excited state of the chloroethane molecular ion but represents a distinct contrast to the behavior of the first excited state of that ion.

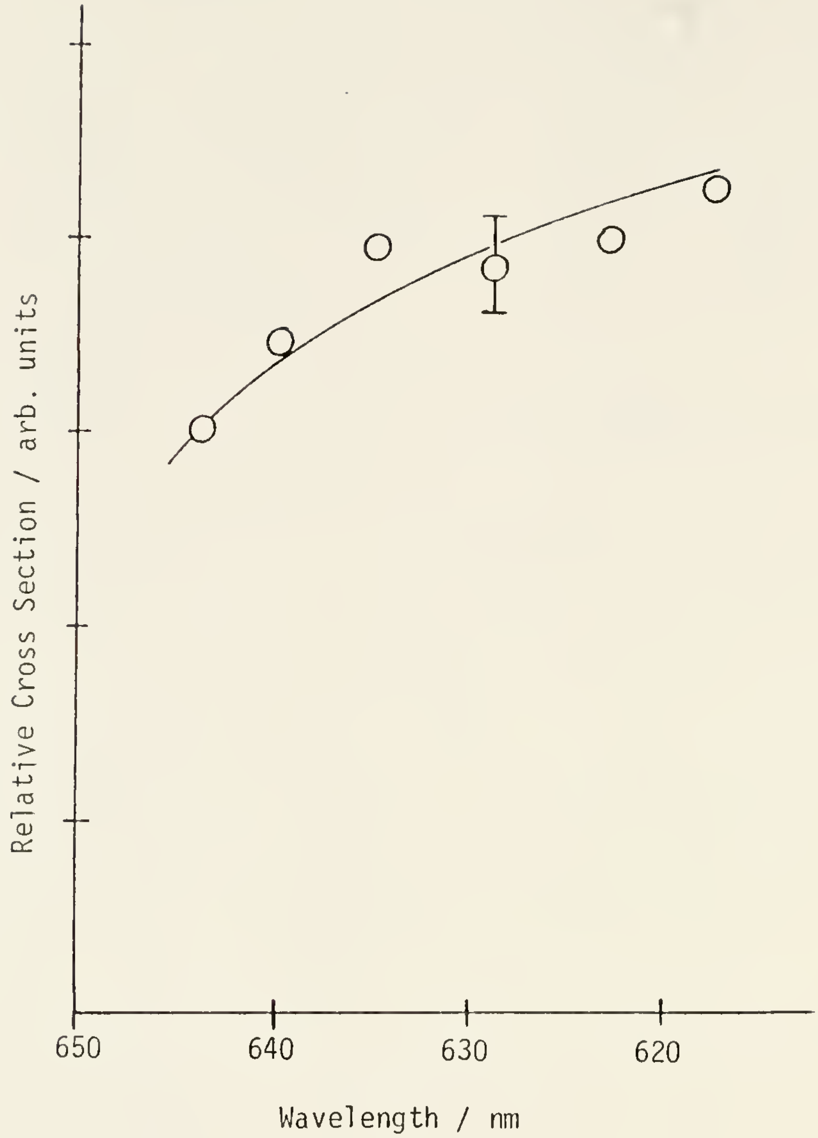

Figure 6.2. Photodissociation Spectrum of Benzyl Chloride Molecular Cation in the Threshold Region

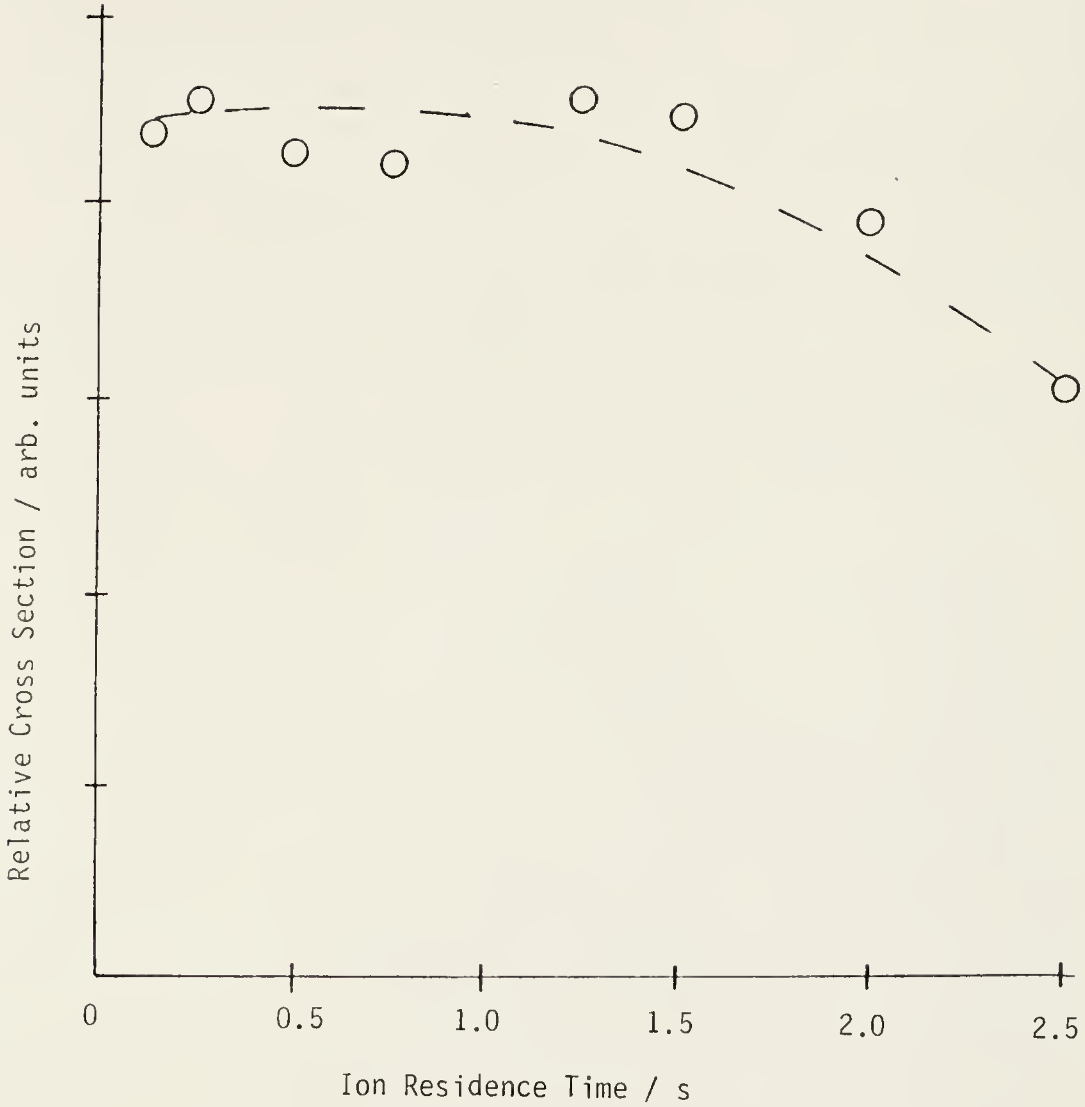

Figure 6.3. Time Dependence of the Apparent Photodissociation Cross Section of Benzyl Chloride Molecular Ion

The maximum percent dissociation observed here is greater by a factor of two than the one reported by Fu. A major difference between the two experiments is the pressure. In this study the pressure was approximately an order of magnitude greater than the pressure employed in the constant intensity experiment. In addition, the instantaneous photon flux in this experiment was at least 10^5 times that in Fu's experiment; however, the irradiation time was roughly 10^{-6} times the irradiation time in Fu's experiment.

One casts about for an explanation of these differences in terms of the kinetics of the apparent rearrangement and photodissociation processes. The results of Fu's double resonance experiment have eliminated the possibility that a reaction between the photodissociation daughter ion and the parent molecule forms the parent ion. Clearly, a fast unimolecular rearrangement can be ruled out as well. Such a process would have yielded identical results in both studies. A rapid collision induced rearrangement can likewise be discarded since more rearrangement, not less, would be expected at higher pressures. An examination of the kinetics of a photoinduced rearrangement in competition with photodissociation reveals that the predicted ultimate percent dissociation is the same for both the pulsed and steady state experiments.

One kinetic scheme that does fit both sets of experimental data is represented as follows:

$A^* \xrightarrow{k_1} B$ (Reaction 1)

$A^* + M \xrightarrow{k_2} A + M^*$ (Process 2)

$A^* \xrightarrow{k_3 I} C + D$ (Process 3)

$A \xrightarrow{k_4 I} C + D.$ (Process 4)

Reaction 1 is the unimolecular rearrangement of Species A*, which is an excited state of Species A, to Species B. Process 2 is the collisional quenching of A* to A. Processes 3 and 4 are the photodissociation of Species A* and A, respectively. With reference to the experiments under discussion here A, A*, and B are all ions with m/e = 126. Species A is the ground state of the benzyl chloride cation and Species A* is an unspecified excited state of that ion formed upon ionization. Species B is the ion of an isomer of benzyl chloride, following Fu's suggestion, a chlorotoluene. M is the benzyl chloride molecule and I is the laser intensity.

The equations describing the kinetics of this system are:

$$dB/dt = k_1 A^*, \tag{6.1}$$

$$dA^*/dt = -k_1 A^* - k_2 M A^* - k_3 I A^*, \text{ and} \tag{6.2}$$

$$dA/dt = -k_4 I A + k_2 A^*. \tag{6.3}$$

These differential equations can be solved analytically to yield:

$$B(t) = (k_1A^*(0)/w)[1 - \exp(-wt)] \qquad 6.4$$

where

$$w = k_1 + K_2M + k_3I, \qquad 6.5$$

$$A^*(t) = A^*(0)\exp(-wt), \text{ and} \qquad 6.6$$

$$A(t) = A(0)\exp(-k_4It) + [k_2A^*(0)/(k_4I-w)][\exp(-wt) - \exp(-k_4It)]. \qquad 6.7$$

The ion signal for a mass of 126 at time t is given by:

$$S(t) = B(t) + A^*(t) + A(t). \qquad 6.8$$

In the continuous irradiation case both $A^*(t)$ and $A(t)$ approach zero at long times. The final ion signal is due entirely to Species B and is given by:

$$S(\infty) = k_1A^*(0)/(k_1 + k_2M_s + k_3I) \qquad 6.9$$

where M_s is the benzyl chloride pressure in the steady state experiment.

In the pulsed experiment Reactions 1 and 2 take place prior to the laser flash, and Reactions 3 and 4 take place only during the laser flash. Reactions 1 and 2 are much slower than the 1 μs laser flash so they can be ignored for that brief time. Assuming sufficient intensity, when the ions irradiated at t_1 are detected at t_d (2 to 10 ms later) the following relationships are true:

$$A^*(t_d) = 0, \qquad 6.10$$

$$A(t_d) = 0, \text{ and} \qquad 6.11$$

$$B(t_d) = B(t_1) = [k_1A^*(0)/(k_1 + k_1M_p)]\{1 - [(-k_1 - k_2M_p)t_1]\} \qquad 6.12$$

where M_p is the benzyl chloride pressure in the pulsed experiment. Note that $k_3I = 0$ prior to the laser pulse.

$$S(t_d) = B(t_d) = B(t_1) \qquad 6.13$$

assuming that $\exp[(-k_1 - k_2M_p)t_1]$ is very small:

$$S(t_d) = k_1A^*(0)/(k_1 + k_2M_p). \qquad 6.14$$

In Fu's experiment:

$$S(\infty) = 0.7\ S(0) \qquad 6.15$$

and since $B(0) = 0$,

$$k_1A^*(0)/(k_1 + k_2M_s + k_3I) = 0.7[A(0) + A^*(0)]. \qquad 6.16$$

If it is assumed that $A^*(0)/[A(0) + A^*(0)] = 0.85$ and that k_3I is very small, then:

$$0.18\ k_1 = k_2M_s. \qquad 6.17$$

If the same assumption about $A^*(0)$ is applied to the pulsed experiment where

$$M_p = 10M_s, \tag{6.18}$$

and consequently,

$$1.8k_1 = k_2M_p. \tag{6.19}$$

The ion signal observed after photolysis is,

$$S(t_d) = 0.30\ S(0), \tag{6.20}$$

in general agreement with the maximum percent dissociation and the best value of f observed here.

Conclusions

It appears that the pulsed icr and the continuous icr techniques give similar results when applied to spectroscopic problems. The two techniques complement each other for the study of dynamics. The kinetic model presented above is not necessarily the only one that would explain the differences between Fu's study and this one; however, it clearly demonstrates that the two results can be reconciled with a reasonable kinetic model.

CHAPTER 7
TIME-RESOLVED PHOTODISSOCIATION SPECTROSCOPY OF THE 1,3,5 HEXATRIENE MOLECULAR CATION

Introduction

The spectroscopy of the 1,3,5 hexatriene molecular cation ($C_6H_8^+$) has been more widely studied than that of most polyatomic ions. Both steady state photodissociation (35,63) and pulsed emission (34) spectra have been published. In addition, the photoelectron spectrum (64) of the parent compound has appeared in print. There is general agreement between these studies as to the location of the excited electronic states of the ion. However, subtle differences in the results obtained by these three techniques suggested that this ion might be a good one to probe for time-dependent phenomena.

Hexatriene exists in two isomeric forms--cis and trans (65). It would be expected that the electronic energy levels of the two isomers, particularly the low lying π molecular orbitals, would be similar. This result has been confirmed by Beez and his co-workers (64). The predicted orbital energies differ somewhat between the

the two structures but between the threshold of ionization at 8.3 eV and 12.0 eV the photoelectron spectra are identical. The photodissociation spectra and the emission spectra agree with the photoelectron spectra with regard to the location of the lowest excited state of the two isomers.

Two distinct structural isomers would be expected to have different vibrational spectra. This has been observed by Allan and Maier (34) in their study of the emission from trans (C_{2h}; $A^2B_g \rightarrow X^2A_u$) and cis ($C_{2v}$; ${}^2A_2 \rightarrow X^2B_1$) 1,3,5 hexatriene radical cations. The 0-0 transition of the trans ion was observed at 630.2 nm and that of the cis isomer at 631.3 nm. Moreover, the emission from the trans isomer was approximately twenty times as intense as that of the cis isomer. It was suggested that this reflected the higher probability of nonradiative de-excitation of the cis isomer.

The photoelectron spectrum (64) also reveals some vibrational structure, but in this case, the spectrum is identical for each of the two isomers. However, the energy resolution of the photoelectron spectrum may be insufficient to distinguish the small difference in energy involved here.

Under steady state visible irradiation the wavelength dependence of the photodissociation cross section of the trans isomer is identical to that of the cis isomer. The 0-0 transition under these conditions is at 631.8 nm for both isomers. The magnitude of the cross section is the same for both samples and the ion population is dissociated with only one cross section. The difference between the emission spectra and the steady state photodissociation spectra can be reconciled by differences in the experimental conditions. The emission spectra were recorded on a time scale of 10^{-8} s while the steady state photodissociation spectra were obtained over several seconds. Since many unimolecular reactions occur rather rapidly it is conceivable that two ions with different structures immediately after ionization might rearrange to an identical structure on the time scale of a few seconds. In both experiments ionization energies sufficient to cause considerable structural changes were employed.

The pulsed icr instrument has a time resolution of a few milliseconds. If the structural identity of the two isomers were maintained on this time scale differences would be expected in the photodissociation spectra of the two isomers. It is also possible that the rate of change of the structure from the distinct isomer to the common form might be obtained.

The application of photodissociation spectroscopy to differentiate structural isomers of molecular ions is not unique. For example, Orth and Dunbar (22) have recently reported a study of the structure of chloropropene ions produced in several ion-molecule reactions. Specific isomers of the reactively produced $C_3H_5Cl^+$ were identified by their photodissociation spectra. In part the study reported here is an extension of this concept into a time-resolved mode of operation. Unfortunately the results reported here suggest either that the rearrangement occurs too rapidly to be monitored by the pulsed icr technique or the spectral differences between the two structures are beyond the optical resolution of this instrument.

Both the emission spectrum and the photodissociation spectrum reveal an intense hot band at 646 nm corresponding to the 1-0 transition of a 350 cm^{-1} skeletal bending mode in the ground state of the ion (34,35,66). The 0-1 transition of this mode is identified with a peak at 615.7 nm by Allan and Maier and one at 617 nm by Dunbar and Teng. In the two spectra reported by Dunbar, the ratio of the intensity of the 1-0 peak to that of the 0-1 peak is different by better than a factor of two. One possible explanation for this is that the lower value reflects longer ion residence time in the sample region (although Dunbar is rather vague about his experimental conditions) and relaxation of vibrationally "hot" ions formed on electron impact. In view of this, the time-dependent behavior of the 1-0 and 0-1 transitions was studied in the hope of obtaining information on vibrational relaxation in this system.

Collisional de-excitation of vibrationally excited species has received considerable attention in the last several years (67,68,69). Much work has involved diatomics because they can be treated theoretically. A second well studied group of systems is those molecules exhibiting laser action from their excited vibrational states. Relatively little work has been carried out on large (more than six atoms) polyatomic molecules. Even less information exists on collisional de-excitation of vibrationally excited molecular ions.

The bulk of the information that does exist has been obtained by steady state irradiation of molecular ions in an icr mass spectrometer under conditions where two-photon dissociation occurs. Several studies (23,36,37) have reported the occurrence of photodissociation at photon energies below the thermochemical dissociation threshold. Using a technique that has been misnamed "time-resolved photodissociation spectroscopy" (23), the kinetics of these processes under continuous irradiation have been studied and found to be consistent with a two-photon process. The observed data fit a simple kinetic model, namely:

$$A^+ \underset{k_3(A)}{\overset{k_1}{\rightleftarrows}} A^{+*} \xrightarrow{k_2} B^+ + C. \tag{7.1}$$

The process characterized by k_1 is thought to include absorption of a photon and excitation to an excited electronic state followed by internal conversion to high vibrational levels of the ground state. In this model k_3 is the rate constant for quenching of the vibrationally excited ions.

Values of k_3 have been reported for the quenching of $C_6H_6^+$, $C_6H_5Br^+$, and $C_6H_5CN^+$ by their respective parent molecules ("self" quenching) and $C_6H_6^+$ by CH_3CN. All of the rate constants for "self" quenching have been reported as roughly 1.0×10^{-9} cm^3 $molecule^{-1}$ s^{-1} which corresponds to quenching on every collision. The rate of quenching of $C_6H_6^+$ by CH_3CN is about a factor of four less than that of quenching by the parent molecule. It is suggested that "self" quenching occurs by resonant charge transfer, i.e., that a vibrationally excited neutral molecule is produced.

This study represents the first attempt to use photodissociation spectroscopy to monitor directly the population of the excited vibrational levels of an ion. Full use was made of the time resolution of the pulsed icr/pulsed dye laser instrument to sample the fractional population of the excited vibrational state at different times after ion formation. Studies were carried out in pure 1,3,5 hexatriene and mixtures of 1,3,5 hexatriene and argon. At the lower ionization energy employed (9.0 eV) the rate constant for quenching of vibrational excitation in the ion by the parent molecule was measured to be 9 x 10^{-11} cm^3 $molecule^{-1}$ s^{-1}. At the higher ionization energy of 11.0 eV this process was characterized by a rate constant of 4 x 10^{-10} cm^3 $molecule^{-1}$ s^{-1}. This dependence on the ionization energy has not been observed before and may support the observation that the structure of the ion is not the same as that of the molecule.

The rate constant for quenching by argon was roughly 1 x 10^{-11} cm^3 $molecule^{-1}$ s^{-1} at both electron energies. Quenching by argon is about an order of magnitude slower than "self" quenching, but it is still far more rapid than similar quenching of vibrationally excited neutrals.

Experimental

Sample Handling and Analysis

As received from the supplier (K & K Pharmaceuticals) the sample of 1,3,5 hexatriene was a 3:2 mixture of the trans and cis isomers as determined by gas chromatography. Sample analyses were carried out on a Perkin Elmer 810 gas chromatograph equipped with twin 12 ft by 1/8 in E-20 carbowax KOH 5 percent columns. A thermal conductivity detector was employed with helium as the carrier gas. The two isomers were eluted 1 min apart at a column temperature of 70°C. The ratio of the peak areas obtained from the sample as received from the supplier was 3:2. Since this is the isomeric ratio reported in the literature (65) the larger peak was taken to be due to the trans isomer. Subsequent chemical manipulations of the sample confirmed this identification when compared to the literature. A sample enriched in the trans isomer was obtained by flash-freezing the sample on a glass filter then slowly thawing it to -25°C while applying a gentle vacuum. The cis isomer melted at a lower temperature than the trans and was drawn through the filter. The solid remaining was predominantly the trans isomer. A sample with a ratio of 3:1 trans to cis isomer was obtained in this way. A sample of pure cis isomer was obtained by adding an excess of maleic anhydride to the racemic mixture and allowing it to stand for 8 hrs. The trans isomer formed a solid polymer and liquid cis isomer was drawn off. A sample of 99 percent cis isomer was prepared in this manner. All samples were stored under dry ice when not in use. Typical gas chromatograms of the three samples are shown in Figure 7.1. Samples were analyzed before and after each use--no changes in the iosmeric ratio were observed in samples stored under dry ice. Those stored at room temperature returned to the racemic mixture after several weeks.

Experimental Procedures

The wavelength dependence of the photodissociation cross section of the parent ion (m/e = 80) from a racemic

Figure 7.1. Sketch of Typical Chromatograms of Samples of 1,3,5 Hexatriene

A. Racemic Mixture

B. Trans Enriched Sample

C. Cis Enriched Sample

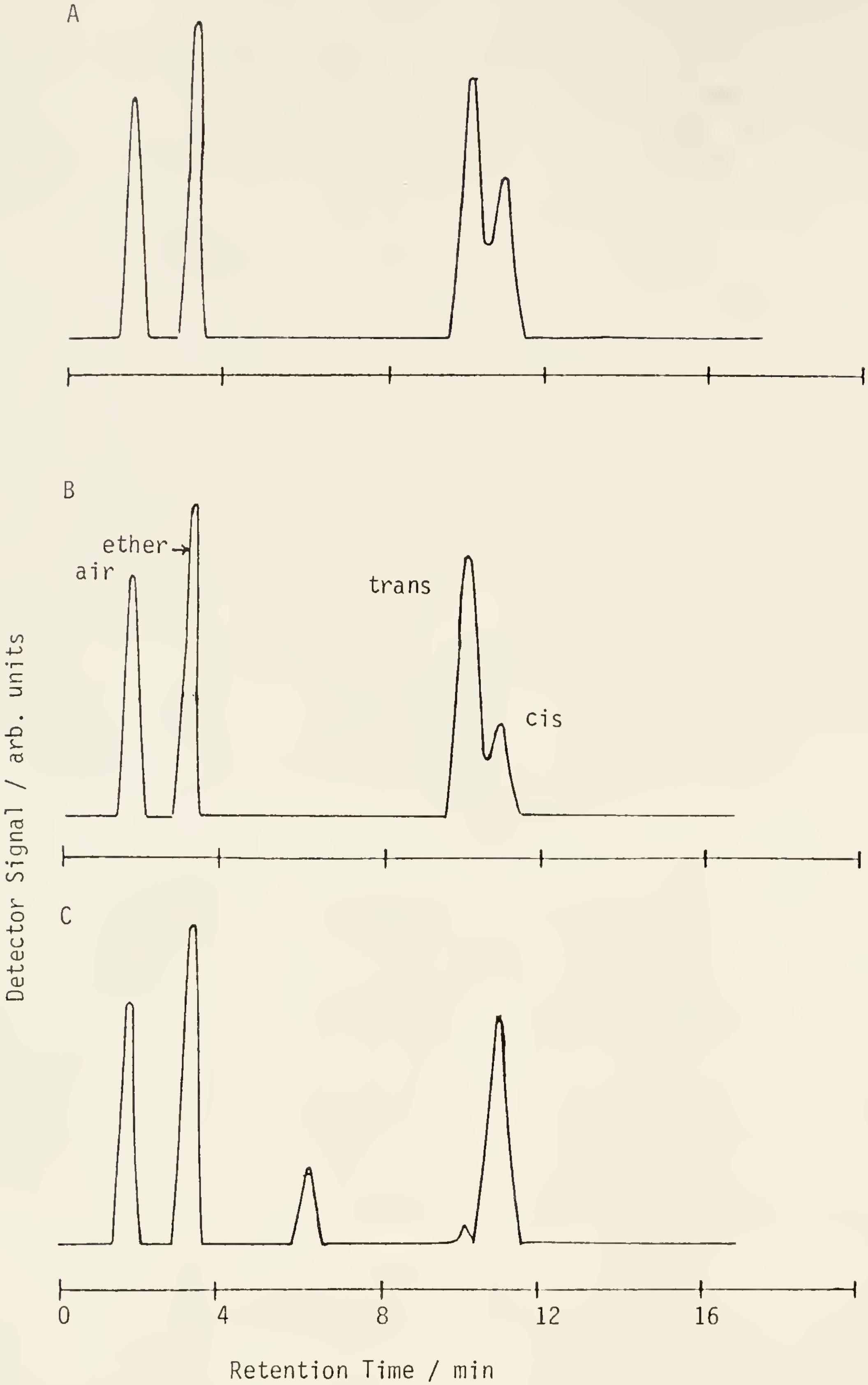
A
B
ether
air
trans
cis
C
Detector Signal / arb. units
0
4
8
12
16
Retention Time / min

mixture of 1,3,5 hexatriene was obtained over the wavelength range of 613 nm to 660 nm. Pulse Sequence 1, 2, 5, 8, and 9 from Table 7.1 were employed. Two dyes were used: kiton red S (613-635 nm) and a mixture of rhodamine 6 G and cresyl violet (635-660 nm). Data points were collected at several instrument alignments. With each change of alignment a set of at least three data points in common with the set obtained under the previous alignment conditions was taken for comparison. In this particular set of experiments all of the data taken under identical conditions of sample and wavelength yielded identical results within experimental error. Only one common point could be taken within the overlap range of the two dyes. Identical results were obtained with both dyes.

The sample pressure was maintained at 7 x 10^{-7} torr of C_6H_8 throughout the experiment and the ionizing electron energy was 9.0 eV. The intensity dependence of the percent dissociation was obtained at several wavelengths and all of the pulse sequences used.

The spectra of the trans and cis enriched samples were obtained using only Pulse Sequence 1 and 3 on Table 7.1. The intensity dependence of the percent dissociation in each sample was obtained at 631 nm using the same two pulse sequences. Sample pressure was 7 x 10^{-7} torr of C_6H_8 and the ionization energy was 9.0 eV.

Table 7.1 Pulse Sequences Used in the Study of 1,3,5 Hexatriene Molecular Ion

Pulse Sequence Number	Grid		Laser		Detect	
	Delay (ms)	Width (ms)	Delay (ms)	Width (μs)	Delay (ms)	Width (ms)
1	0	5	9	1	10	3.3
2	0	5	19	1	20	3.3
3	0	7	29	1	30	3.3
4	0	7	44	1	45	3.3
5	0	10	49	1	50	3.3
6	0	12	59	1	60	3.3
7	0	12	79	1	80	3.3
8	0	25	149	1	150	3.3
9	0	45	249	1	250	3.3

The kinetics of the reaction

$$C_6H_8^+ + C_6H_8 \rightarrow C_6H_9^+ + C_6H_7 \qquad 7.2$$

were examined briefly at a pressure of 7×10^{-7} torr of C_6H_8 and ionization energies of 9.0 eV and 11.0 eV. These experiments were repeated in samples with 7×10^{-6} torr and 7×10^{-5} torr of argon added. All instrumental conditions were kept constant except that the detect pulse delay time was varied. The rate of disappearance of the $C_6H_8^+$ ion was obtained.

The apparent photodissociation cross section of the $C_6H_8^+$ ion (from a racemic mixture) was measured at 619 nm and 646 nm. Pulse Sequence 1, 2, 3, 4, 6, and 7 of Table 7.1 were used. Ionization energies of 9.0 eV and 11.0 eV were employed. The partial pressure of 1,3,5 hexatriene was 7×10^{-7} torr. One sample was run with only hexatriene admitted into the icr. The second sample was run with hexatriene and 7×10^{-6} torr of argon, and the third with hexatriene and 7×10^{-5} torr of argon. A set of data was obtained at both ionization energies, all six pulse sequences, and in all three samples with a wavelength of 619 nm. The experiment was repeated using a wavelength of 646 nm. The data at 619 nm were taken using kiton red S as the laser dye and those at 646 nm were taken using the rhodamine 6 G cresyl violet mixture. In this experiment no attempt was made to standardize the results obtained with the two dyes.

The computer data logging system was used to control the collection of data and the triggering of the laser when the photodissociation spectrum of 1,3,5 hexatriene ion that appears in Figure 7.2.A was obtained. A typical experiment in this mode of operation consisted first of ten experimental cycles with no ion in resonance (ion zero level). Next the ion was brought into resonance by tuning the magnetic field. Once the ion was in resonance, four cycles were run without the laser triggering (ion baseline level), then the computer caused the laser to trigger as described in Chapter 3 (ion level laser on). This four-off one-on sequence was repeated until the laser had triggered ten times and forty-four ion baseline level points had been taken. Then ten more ion zero level points were taken. The quantity R in Equation 2.32, was calculated as the average of the eight ion baseline level readings adjacent to the laser shot minus the ion level laser on reading divided by the average of the same eight ion baseline level readings minus the average of the twenty ion zero level points. The laser intensity was recorded by hand as well as on the computer. In general, the hand recorded data were used because their manipulation was easier in the absence of a complete data system. The spectra of the two isomerically enriched samples and the data on the time and pressure dependence of the cross section at 619 nm and 646 nm were obtained in the same way as the photodissociation spectrum of chloroethane molecular ion described in Chapter 5.

Results

The Spectrum of the Racemic Mixture

The photodissociation spectrum of the parent ion (m/e = 80) from the racemic (3:2 trans to cis) mixture of 1,3,5 hexatriene is shown in Figure 7.2. The spectrum shown was obtained using Pulse Sequence 5 from Table 7.1. Spectra obtained at all other delay times were qualitatively identical. There was a gradual decrease in the apparent cross section with time at all wavelengths consistent with the results reported in Chapter 4 and 6. The cross section at the long wavelength end of the spectrum decreased in a manner discussed below.

According to Dunbar (63) the only photodissociation process observed was:

$$C_6H_8^+ + h\nu \rightarrow C_6H_7^+ + H. \qquad 7.3$$

The photoproduction of $C_6H_7^+$ was also studied in these experiments. The amount of photoproduced $C_6H_7^+$ was seen to equal the amount of $C_6H_8^+$ that was dissociated. Since both of these ions were detected under nearly identical

Figure 7.2. Photodissociation Spectra of Various Samples of 1,3,5 Hexatriene

A. Racemic Mixture

B. Trans Enriched Sample

C. Cis Enriched Sample

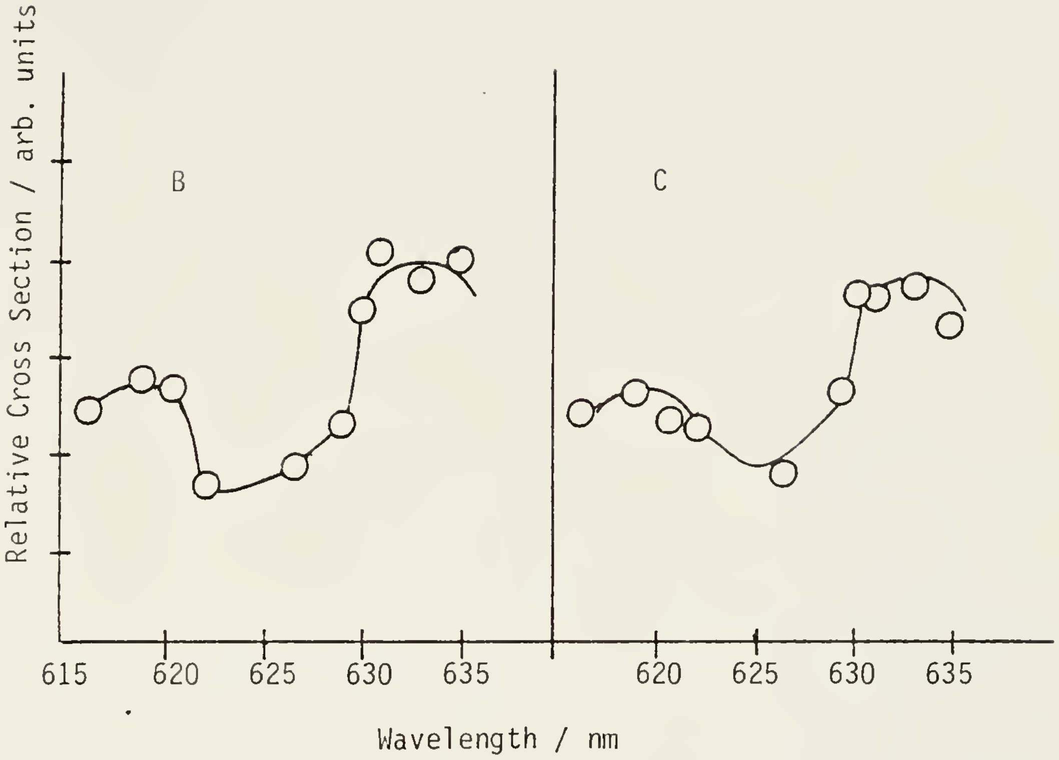
Relative Cross Section / arb. units
B
C
615
620
625
630
635
620
625
630
635
Wavelength / nm

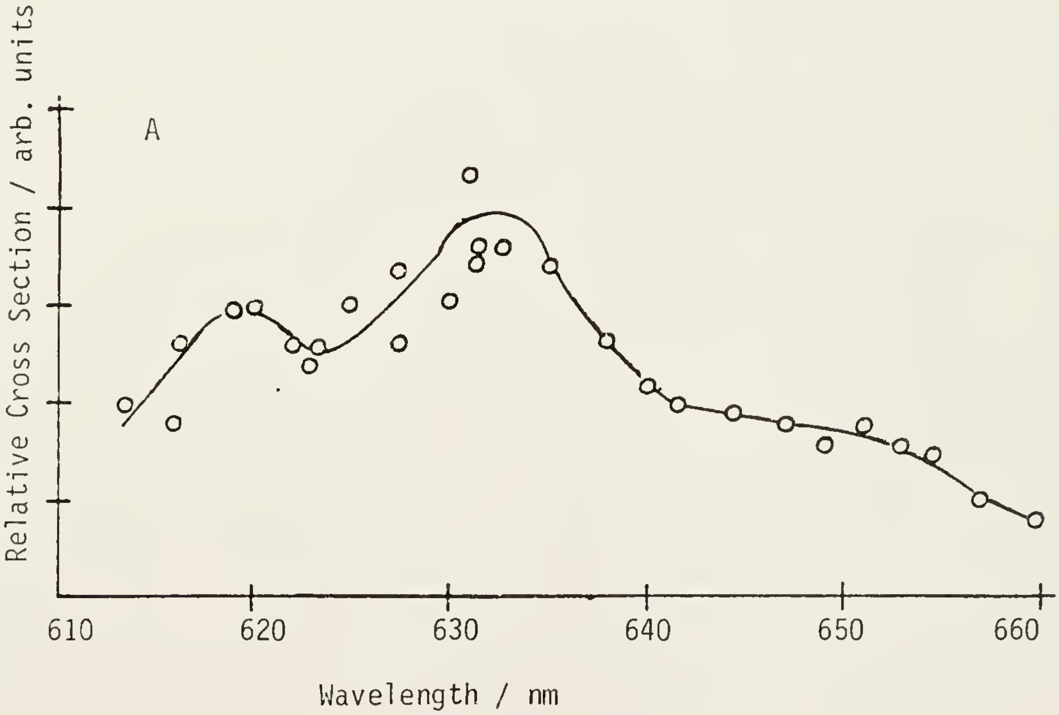
Relative Cross Section / arb. units
A
610
620
630
640
650
660
Wavelength / nm

conditions, such a quantitative comparison is possible. Consequently, no other dissociation products were sought.

The Spectra of the Two Isomers

Figures 7.2.B and 7.2.C are the photodissociation spectra of 3:1 trans to cis and 1:99 trans to cis samples, respectively. Both were obtained using Pulse Sequence 1 (Table 7.1). The 10 ms delay time employed here is essentially the limit of the temporal resolution of this pulsed icr. Clearly, the two spectra are indistinguishable over the wavelength range of 615 nm to 635 nm.

The dependence of the percent dissociation on laser energy at 631 nm is shown in Figure 7.3. Curve A was obtained with the racemic (3:2) mixture, Curve B with the 3:1 mixture, and Curve C with the 1:99 mixture of trans to cis isomer. All three curves were measured at a delay time of 10 ms and again they are indistinguishable. These curves were fitted to several mathematical functions. A one-parameter fit, a two-parameter fit (Equation 4.6), and a three-parameter fit:

$$R = f\{1 - \exp[-kE(\lambda)\lambda]\} + (1 - f)\{1 - \exp[-k'E(\lambda)\lambda]\}. \tag{7.4}$$

The purpose of the one- and two-parameter fits is discussed in Chapter 4. The three-parameter fit was intended to model the situation where two types of ions are dissociated

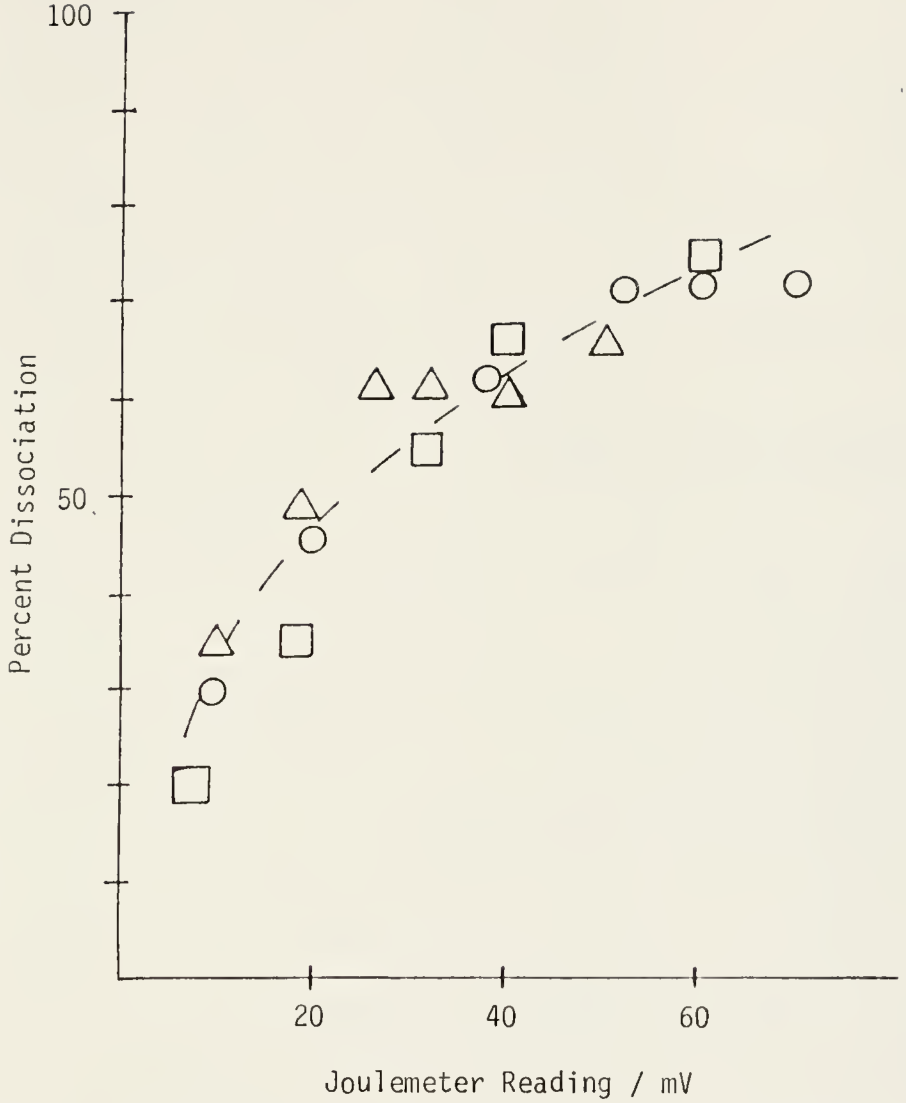

Figure 7.3. Percent Dissociation of 1,3,5 Hexatriene Cation Versus Laser Energy

A = o = Racemic Mixture

B = □ = Trans Enriched Sample

C = △ = Cis Enriched Sample

with distinct cross sections (k and k'). As before, neither of the mulitparameter fits was significantly better than the one-parameter fit, indicating that f (Equation 2.32) is equal to one. The intensity dependence does not indicate that more than one type of ion is present in the sample. The near identity of Figures 7.3.A, 7.3.B, and 7.3.C demonstrates that the apparent photodissociation cross sections of these three samples are quantitatively identical at 631 nm.

The Results of the Time-Resolved Experiment

The ratio of the apparent photodissociation cross section of the 1,3,5 hexatriene ion from a racemic mixture of the parent molecule at 646 nm to that measured at 619 nm versus time is shown in Figures 7.4 and 7.5. These results were obtained under a variety of experimental conditions. Figures 7.4 and 7.5 present the results obtained using ionization energies of 9.0 eV and 11.0, respectively. Curves 7.4.A and 7.5.A were obtained with a sample of 7×10^{-7} torr of C_6H_8 alone. Curves 7.4.B and 7.5.B were obtained with an additional 7×10^{-6} torr of argon present and Curves 7.4.C and 7.5.C were obtained with 7×10^{-5} torr of argon present. Although the cross section observed at 619 nm decreased somewhat with time (see Figure 7.6) in a manner consistent with the results reported in Chapters 4 and 6, the apparent cross section at 646 nm decreased far more rapidly, especially at high pressures.

Figure 7.4. β Versus Time for Samples Formed With an Ionization Energy of 9.0 eV

$A = o = 7 \times 10^{-7}$ torr C_6H_8

$B = \square = 7 \times 10^{-7}$ torr $C_6H_8 + 7 \times 10^{-6}$ torr Argon

$C = \Delta = 7 \times 10^{-7}$ torr $C_6H_8 + 7 \times 10^{-5}$ torr Argon

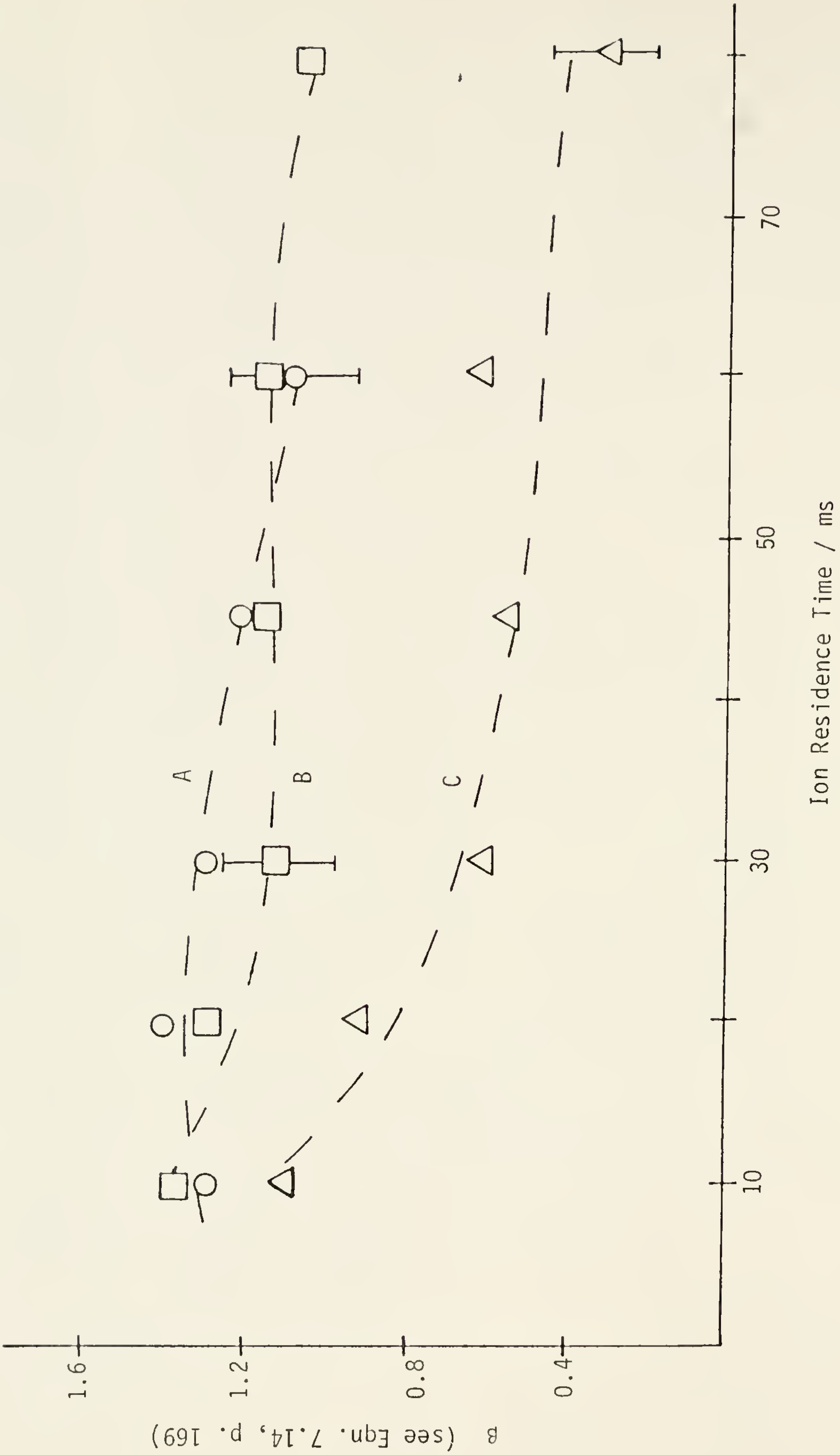
β (see Eqn. 7.14, p. 169)
1.6
1.2
0.8
0.4
10
30
50
70
Ion Residence Time / ms
A
B
C

Figure 7.5. β Versus Time for Samples Formed With an Ionization Energy of 11.0 eV

A = o = 7 x 10^{-7} torr C_6H_8

B = □ = 7 x 10^{-7} torr C_6H_8 + 7 x 10^{-6} torr Argon

C = Δ = 7 x 10^{-7} torr C_6H_8 + 7 x 10^{-5} torr Argon

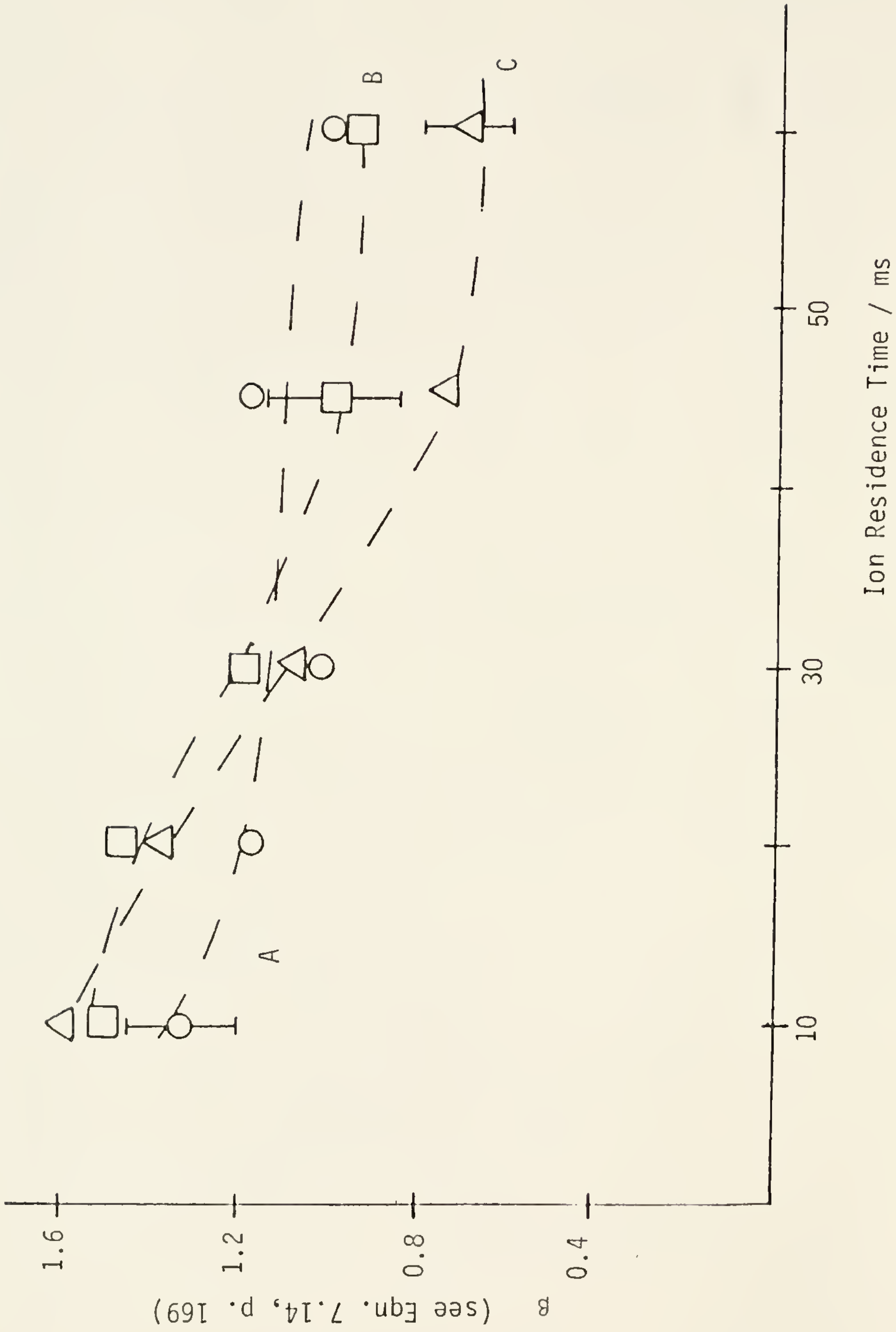
β (see Eqn. 7.14, p. 169)
1.6
1.2
0.8
0.4
10
30
50
Ion Residence Time / ms
A
B
C

Figure 7.6. Photodissociation Cross Section of $C_6H_8^+$ Versus Time

o = 7 x 10^{-7} torr C_6H_8 + 7 x 10^{-5} torr Argon; λ = 619 nm; Ionization Energy = 9.0 eV

□ = 7 x 10^{-7} torr C_6H_8; λ = 619 nm; Ionization Energy = 11.0 eV

Δ = 7 x 10^{-7} torr C_6H_8 + 7 x 10^{-5} torr Argon; λ = 646 nm; Ionization Energy = 9.0 eV

X = 7 x 10^{-7} torr C_6H_8; λ = 646 nm; Ionization Energy = 11.0 eV

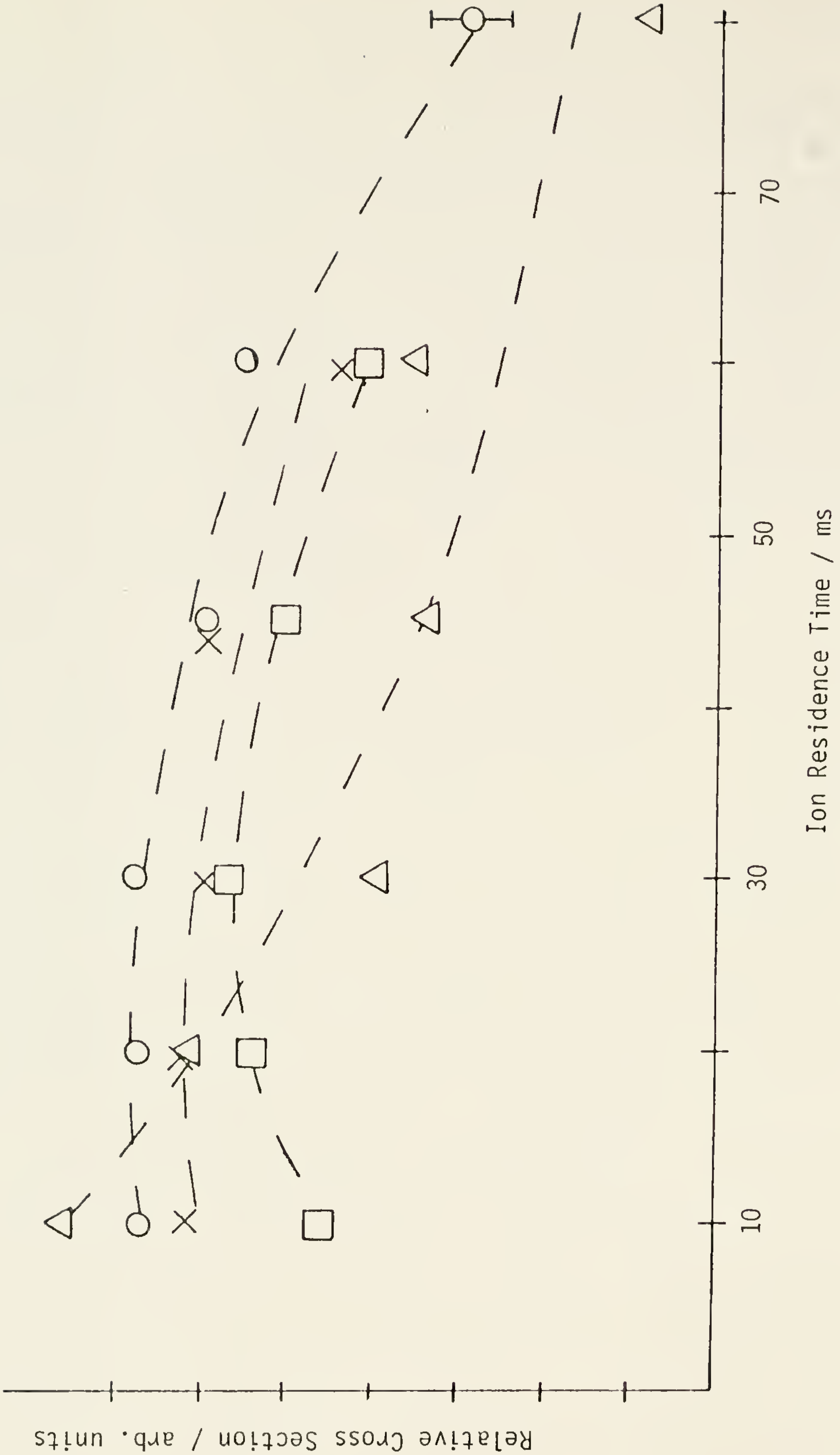
Relative Cross Section / arb. units
Ion Residence Time / ms
10
30
50
70

This decrease relative to the "normal" decrease observed at 619 nm is taken to reflect a change in the absolute photodissociation cross section with time at 646 nm. The rate of change of the photodissociation cross section at 646 nm appears to be exponential in time. The lifetime associated with this apparent exponential decay can be calculated.

Consider a general first-order process of the type:

$$A \rightarrow B \qquad 7.5$$

where A and B represent the initial and final states of the system, respectively. If the concentration of Species A at any given time t is:

$$A(t) = A(\infty) + x \qquad 7.6$$

or

$$A(t) = A(t) - A(\infty), \qquad 7.7$$

then it can be shown that (70):

$$dx/dt = -(1/\tau_{ob})x \qquad 7.8$$

where τ_{ob} is the apparent lifetime of State A.

Rearranging Equation 7.8 and integrating yields:

$$\ln x(t_0)/x(t) = (t - t_0)/\tau_{ob}. \qquad 7.9$$

Thus, a plot of $\ln[x(t_0)/x(t)]$ versus time yields a straight line with a slope of $1/\tau_{ob}$.

If Process 7.5 proceeds by a bimolecular collision, i.e.,

$$A + M \rightarrow B, \qquad 7.10$$

then

$$1/\tau_{ob} = k_{AM}M \qquad 7.11$$

where k_{AM} is the apparent bimolecular rate constant and M is the number density of the collision partner.

The first-order decays and semilog plots for Reaction 7.2 are shown in Figure 7.7. Curves 7.7.A and 7.7.C refer to ions formed with an ionization energy of 9.0 eV in a sample of 7×10^{-7} torr C_6H_8 plus 7×10^{-5} torr of argon. Curves 7.7.B and 7.7.C refer to ions formed at 11.0 eV in a sample of 7×10^{-7} torr of C_6H_8 alone. The reaction of $C_6H_8^+$ with its parent molecule is extremely rapid. It occurs at the same rate in all samples formed at both ionization energies indicating that internal excitation of the ion has little effect on the rate of the reaction. The apparent bimolecular rate constant is 5×10^{-10} cm^3 $molecule^{-1}$ s^{-1} corresponding to reaction on about every other collision.

Figure 7.7. First-Order Decay and Semilog Plot for Reaction 7.2

A. First-Order Decay in a Sample of 7 x 10^{-7} torr C_6H_8:
Ionization Energy = 11.0 eV

B. First-Order Decay in a Sample of 7 x 10^{-7} torr C_6H_8 +
7 x 10^{-5} torr Argon;
Ionization Energy = 9.0 eV

C. Semilog Plot of Data from Curves 7.7.A (□) and 7.7.B (X)

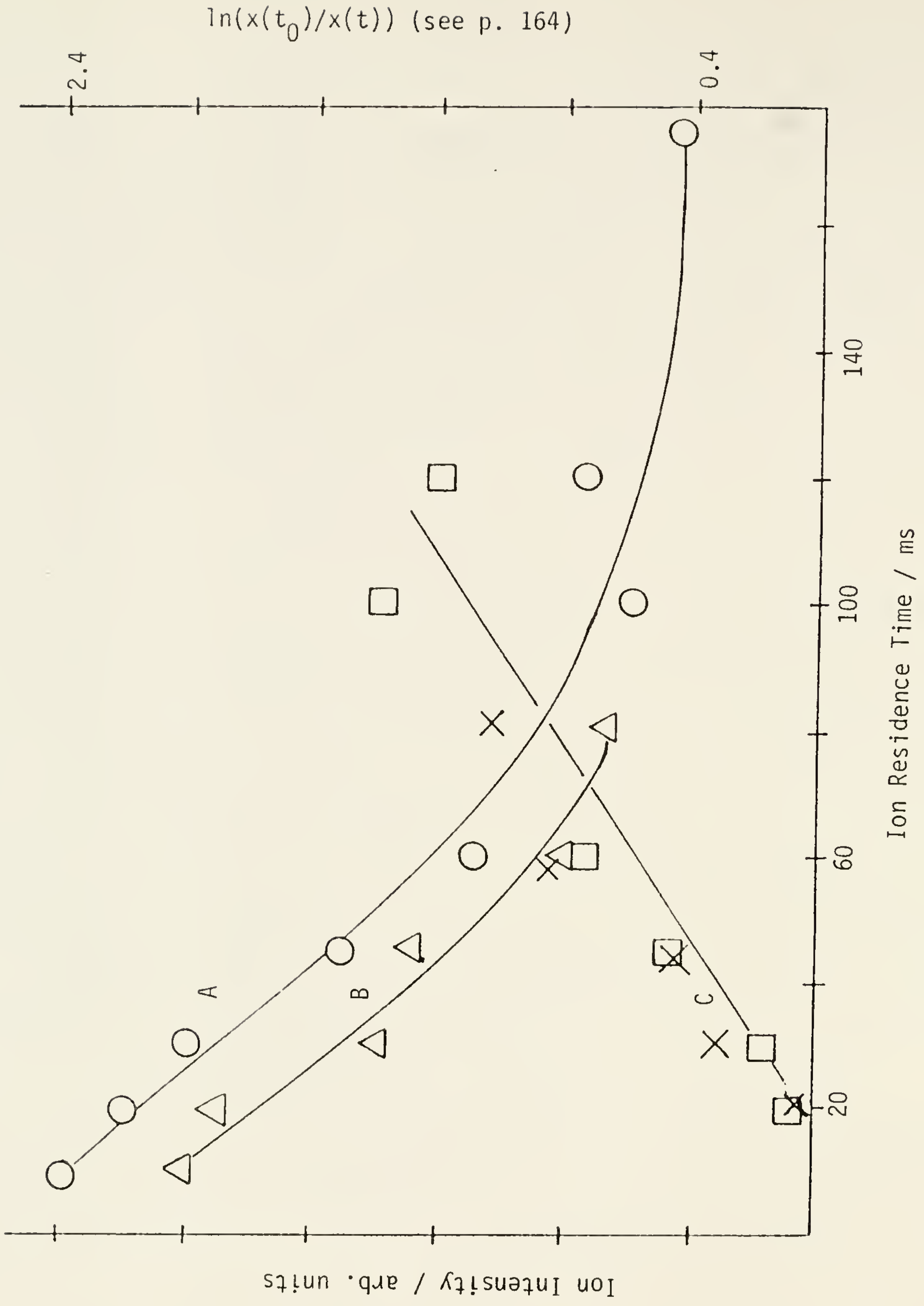
ln(x(t$_0$)/x(t)) (see p. 164)
2.4
0.4
A
B
C
20
60
100
140
Ion Residence Time / ms
Ion Intensity / arb. units

The Quenching of Vibrational Excitation

If the vibrational analysis presented by Dunbar and Teng (35) and by Allan and Maier (34) is correct, the photodissociation cross section at 646 nm should be related to the probability of an ion undergoing a transition from the first (or nth) excited level of the 350 cm^{-1} mode of the electronic ground state of the ion to the zeroeth (or n-1st) level of the 350 cm^{-1} vibration in the first excited electronic state. The photodissociation cross section at 619 nm is related to the probability of an ion undergoing a transition from the nth vibrational level of the ground state to the n+1st level of the first excited electronic state for the 350 cm^{-1} mode. Since only ions in excited vibrational levels can undergo the n to n-1 transition, the cross section at 646 nm is proportional to the population of ions in excited vibrational levels while the cross section at 619 nm is proportional to the total number of ions.

It follows from this that:

$$\sigma(646)/\sigma(619) = N_e/N \qquad 7.12$$

if the transition probabilities for the n to $n\pm1$ transitions are assumed to be equal. Here, N_e is the population of ions in excited vibrational states of the 350 cm^{-1} mode.

Certainly, $N_e/N \leq 1$ and yet, the ratio of apparent cross sections

$$k''\sigma(646)/k'\sigma(619) > 1 \qquad 7.13$$

at some times.

It may be assumed that:

$$N_e/N(t) \propto [k''\sigma(646)/k'\sigma(619)](t) = K[N_e/N(t)] \equiv \beta(t) \qquad 7.14$$

where

$$K = k''/k'. \qquad 7.15$$

Equation 7.15 is the ratio of "alignment factors" for the two dyes.

If one makes the approximation that at equilibrium ($t = \infty$) only the first excited level of the 350 cm^{-1} mode is populated to any significant extent,

$$[N_e/N](\infty) = [N_1/N](\infty) = \exp(-h\nu/kT) \qquad 7.16$$

where ν is the frequency of the vibrational mode, then

$$x(t) = \beta(t) - K\exp(-h\nu/kT). \qquad 7.17$$

The observed ratio of cross section is $\beta(t)$ and $x(t)$ is defined by Equation 7.7.

One can estimate that K is between 1.5 and 2.0 on the following basis:

1. K is at least 1.5 since the maximum value of N_e/N is 1 and the minimum value of K consistent with the largest observed ratio of cross section is 1.5 allowing for experimental error.
2. $$N_1/N(\infty) = 0.18 \qquad 7.18$$

   The minimum ratio of the populations can be no less than this. The maximum value of K consistent with the smallest observed ratio of cross section is about 2.0.

A second estimate of K can be obtained by examining the data presented in Figure 7.2. In that experiment the apparent cross sections were standardized between dyes and the ratio of alignment constants was observed to be 1.0 (see Chapter 7, Experimental Procedures). The ratio $\beta(t)$ observed in that case was 0.80 at 20 ms and 0.70 at 50 ms. The data presented in Figure 7.4.A were obtained with the same sample conditions as the data presented in Figure 7.2 but different alignment conditions. The same alignment was used in obtaining all of the data in Figure 7.4 and 7.5. The ratio of cross sections presented in Figure 7.4.A decreases slowly with time in agreement with Figure 7.2 but the ratio $\beta(t)$ in the case of Figure 7.4.A is 1.4 at 20 ms and 1.2 at 50 ms. If the difference in the observed ratio of cross sections is due to the difference in the ratio of the alignment constants K, then K for those experiments summarized in Figures 7.4 and 7.5 can be estimated as 1.7 at both times. Obviously this is within the range of acceptable values determined above. From this it follows that:

$$x(t) = \beta(t) - 1.7 \exp(-h\nu/kT). \qquad 7.19$$

The first-order plots of $\ln[x(t_0)/x(t)]$ versus time are shown in Figures 7.8 and 7.9 for the data obtained with ionization energies of 9.0 and 11.0 eV, respectively. The observed lifetimes are summarized in Column 3 of Table 7.2.

In order to interpret the results of these time-resolved studies it is necessary to consider the kinetics of the various processes that occur between ionization and photodissociation and to relate these to the quantities actually measured. The processes are represented as Reactions 7.20 through 7.23.

$$A + B \xrightarrow{k_{20}} C + D \qquad 7.20$$

$$A^* + B \xrightarrow{k_{21}} C + D \qquad 7.21$$

$$A^* + B \xrightarrow{k_{22}} A + B^* \qquad 7.22$$

$$A^* + Q \xrightarrow{k_{23}} A + Q^* \qquad 7.23$$

Figure 7.8. Semilog Plot of Data From Figure 7.4

o = 7×10^{-7} torr C_6H_8

□ = 7×10^{-7} torr C_6H_8 + 7×10^{-6} torr Argon

Δ = 7×10^{-7} torr C_6H_8 + 7×10^{-5} torr Argon

Ionization Energy = 9.0 eV

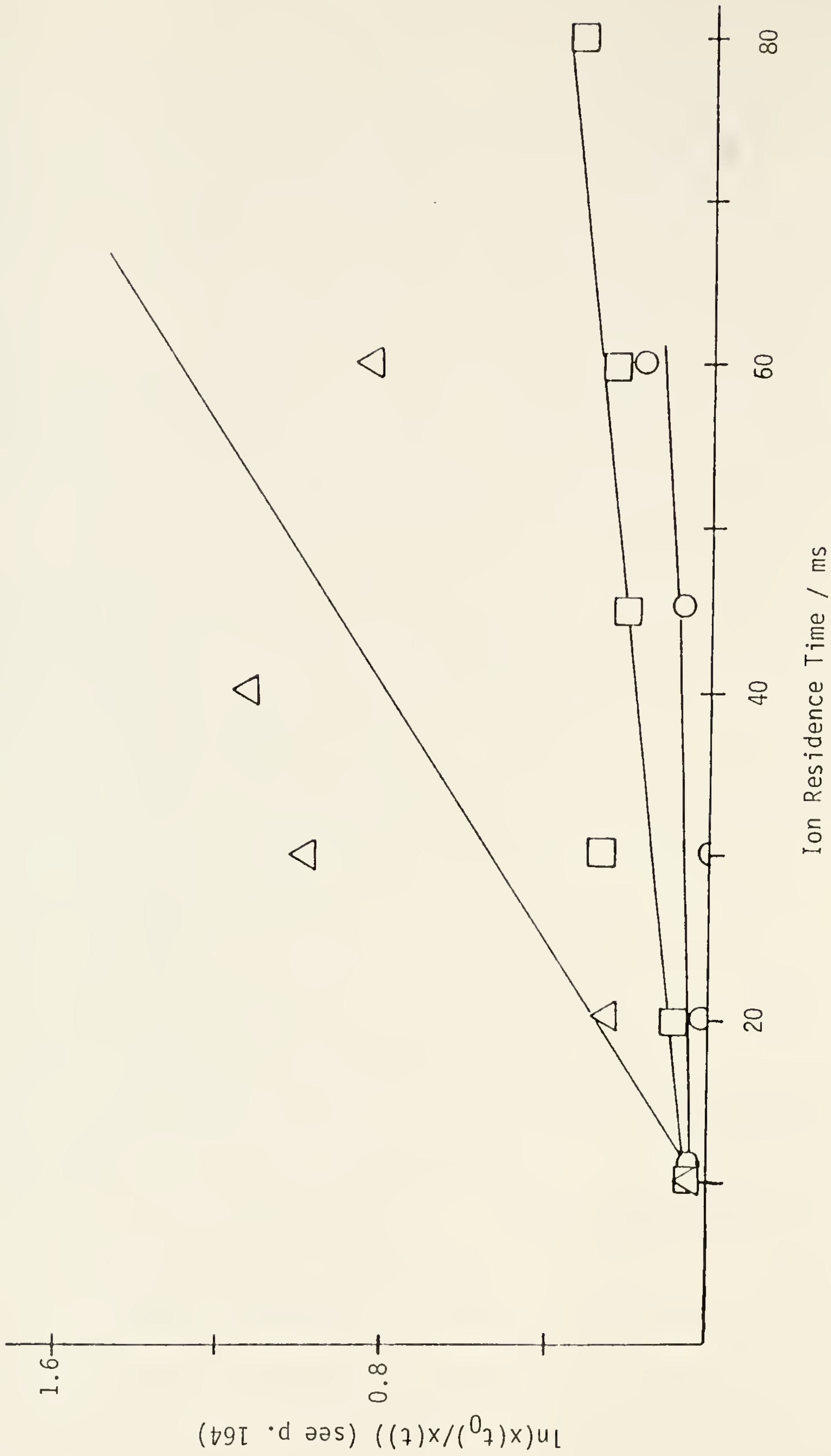
ln(x(t$_0$)/x(t)) (see p. 164)
1.6
0.8
Ion Residence Time / ms
20
40
60
80

Figure 7.9. Semilog Plot of Data From Figure 7.5

o = 7×10^{-7} torr C_6H_8

□ = 7×10^{-7} torr C_6H_8 + 7×10^{-6} torr Argon

Δ = 7×10^{-7} torr C_6H_8 + 7×10^{-5} torr Argon

Ionization Energy = 11.0 eV

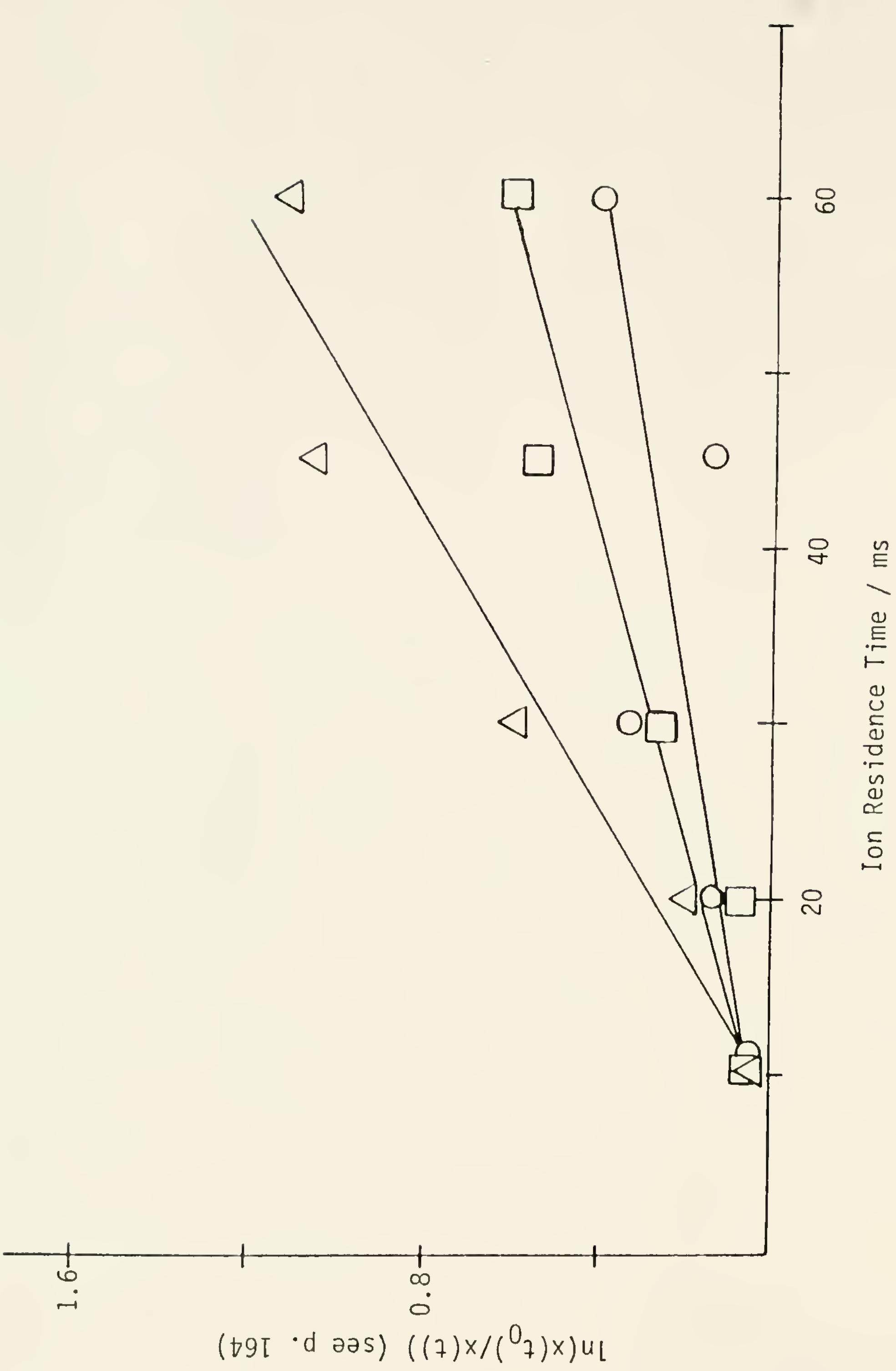
1.6
0.8
ln(x(t0)/x(t)) (see p. 164)
20
40
60
Ion Residence Time / ms

Table 7.2. Rate Parameters for the Quenching of Vibrationally Excited 1,3,5 Hexatriene Molecular Cation

$P_{C_6H_8} = 7 \times 10^{-7}$ torr

Ionization Energy (eV)	P_{Ar} (torr)	τ_{ob} (ms)	k_{22} (cm^3 molecule^{-1} s^{-1})	k_{23} (cm^3 molecule^{-1} s^{-1})	τ_{AB} (ms)	τ_{AB} (ms)	Z_{AB}	Z_{AQ}
9.0	0	500	9×10^{-11}		500		9	
9.0	7×10^{-6}	200		1×10^{-11}		300		40
9.0	7×10^{-6}	40		1×10^{-11}		40		50
11.0	0	130	4×10^{-10}		130		2	
11.0	7×10^{-6}	100		9×10^{-12}		450		50
11.0	7×10^{-5}	40		8×10^{-12}		50		60

Here Reaction 7.20 is the reaction between ground state $C_6H_8^+$ and the C_6H_8 molecule, Reaction 7.21 is the reaction between the vibrationally excited $C_6H_8^+$ ion and the parent molecule, Reaction 7.22 is the quenching of the excited ion by the parent molecule, and Reaction 7.23 is the quenching of the excited ion by argon atoms. The possibility of long-lived electronic excitation of the ion is ignored. In the first place the ionization energy of 11.0 eV is fairly close to the appearance potential for the first excited electronic state of the ion. Surely the cross section for production of that state is relatively small at this energy. It should be noted that Allan and Maier (34) used 20 eV electrons to excite the emission from 1,3,5 heaxtriene ions. In any event, the radiative lifetime of the first excited electronic state is only about 10 ns, far too short for electronic excitation to be important on the time scale of this experiment.

The kinetic equations for this reaction scheme are:

$$dA^*/dt = -k_{21}BA^* - k_{22}BA^* - k_{23}QA^*, \text{ and} \qquad 7.24$$

$$dA/dt = -k_{20}BA + k_{22}BA^* + k_{23}QA^*. \qquad 7.25$$

The pulsed photodissociation technique records the quantity:

$$d[A^*/A + A^*)]/dt = [(A + A^*)dA^*/dt - A^*d(A^* + A)/dt](A + A^*)^{-2} \qquad 7.26$$

$$= (AdA^*/dt - A^*dA/dt)(A + A^*)^{-2}. \qquad 7.27$$

If, as the results of these experiments indicate, $k_{20} = k_{21}$, then:

$$d[A^*/A + A^*)] = -(k_{22}B + k_{23}Q)[A^*/(A + A^*)]dt. \qquad 7.28$$

It follows from this and Equation 7.8 that:

$$1/\tau_{ob} = k_{22}B + k_{23}Q, \qquad 7.29$$

where B is the number density of 1,3,5 hexatriene neutrals and Q is the number density of argon atoms.

In the lowest pressure case Q = 0 and k_{22} can be calculated in a straightforward manner using the number density of hexatriene calculated from the ideal gas law. These values are reported in Column 4 of Table 7.2. Values of k_{23} can then be computed using these values and the number density of argon atoms calculated from the ideal gas law. These are reported in Column 5 of Table 7.2.

The collision number for a bimolecular process, Z_{AB}, is defined as the ratio of the observed lifetime of that process to the orbiting collision lifetime, τ_L, calculated as:

$$\tau_L = 1/k_L M \qquad 7.30$$

where k_L is calculated from Equation 4.3 and M is the number density of the neutral collision partner.

The quantity Z_{AB} is the average number of orbiting collisions between ion A and neutral B required to induce the bimolecular process. It is the inverse of the collision efficiency.

For collisional quenching the collision number is given by (71):

$$Z_{AB} = \tau_{AB}[1 - \exp(-h\nu/kT)]/\tau_L \qquad 7.31$$

where τ_{AB} is the lifetime of the collisional process and the term $[1 - \exp(-h\nu/kT)]$ accounts for the probability of collisional excitation.

The lifetime for the quenching of $C_6H_8^+$ by C_6H_8, τ_{AB}, is just:

$$\tau_{AB} = 1/k_{22}B \qquad 7.32$$

and that for quenching by argon, τ_{AQ}, is given by:

$$\tau_{AQ} = 1/k_{23}Q. \qquad 7.33$$

These values are reported in Columns 6 and 7 of Table 7.2.

The collision numbers for "self" quenching, Z_{AB}, and for quenching by argon, Z_{AQ}, are reported in Columns 8 and 9 of Table 7.2, respectively. These were calculated using Equation 7.31 and assuming that only the first level of the 350 cm^{-1} mode has significant probability of being populated in a collision. The rate constant for orbiting collisions between $C_6H_8^+$ and C_6H_8 was taken to be 1 x 10^{-9} cm^3 $molecule^{-1}$ s^{-1}. This value was estimated based on the value obtained for several compounds of similar size and molecular structure (9). The rate constant for orbiting collisions between $C_6H_8^+$ and argon was calculated from Equation 4.3 using 1.6 x 10^{-24} cm^3 as the polarizability of argon.

The lifetimes, rate constants, and collision numbers reported here are only accurate to within about a factor of two due to the uncertainty in the measured cross sections. The apparent cross sections are uncertain by between 10 and 15 percent (95 percent confidence limit based on the mean of seven to ten laser shots). The corresponding uncertainty in the ratio of the ratios of such quantities is approximately 30 percent. The uncertainty in the logarithm is roughly 30 percent. The final uncertainty in the slope of the line described by such logarithms (from which the lifetimes, rate constants, and collision numbers are calculated) can be estimated to be roughly a factor of two (59). It is interesting to note that the choice of any value of K between 1.0 and 2.0 for use in Equation 7.17 has a much smaller effect on the magnitude of the calculated rate parameters.

Discussion

The Photodissociation Spectrum

The appearance of the spectrum presented in Figure 7.2 is entirely consistent with the steady state spectrum obtained by Dunbar (35,63). The peak between 630 nm and 635 nm is assigned to the 0-0 transition to the first excited electronic state of the ion. The shoulder between 640 nm and 650 nm is consistent with Dunbar's observation of a peak at 646 nm corresponding to the 0-1 transition of a 350 cm^{-1} vibrational mode of the ground state ion. The peak at 619 nm is assigned to the 1-0 transition of a similar mode in the first excited state. There is a 1 nm difference between the wavelength of the 1-0 transition reported here and that reported by Dunbar. This seems most likely to be a result of experimental uncertainty.

The Structure of the Ion

As reported above, the spectra of the three samples are identical both qualitatively (Figures 7.2 and 7.4) and quantitatively (Figure 7.3). This, coupled with the fact that the position of the 0-0 transition in the spectrum of a 3:2 (trans to cis) mixture of the isomers does not change with time, suggests that both isomers of the 1,3,5 hexatriene cation rearrange in the gas phase to some common structure within 10 ms of formation. These results then extend Dunbar's result (that the ions are identical on the time scale of seconds) to a time regime that is shorter by a factor of 100.

A second possible argument is that the two ions have distinct structures but the differences in their spectra cannot be distinguished given the spectral resolution of this instrument. The difference in the position of the 0-0 peak in the two isomers is reported to be 1.1 nm by Allan and Maier (34). Although this is somewhat greater than the spectral resolution that is claimed here (± 0.4 nm), it is at the limit of resolution of this instrument. The large (a factor of twenty) difference in the emission yield of the two isomers reported by Allan and Maier suggests that there ought to be a significant difference in the photodissociation cross section between the two isomers. If the first excited state of the trans isomer is twenty times as emissive as that of the cis isomer then one would expect emission to compete with dissociation in the trans ion resulting in a lower apparent photodissociation cross section in the trans enriched sample. That no such difference is observed in this experiment nor in

Dunbar's strongly suggests that at the time the respective techniques sample the ion population there is a single, identical type of ion in each sample.

Ionization of 1,3,5 hexatriene involves removing an electron from the π bonding molecular orbitals of the molecule (64). Zahradnik and Carsky (72) have calculated the π bond order in the hexatriene molecule and the radical ion. They find a marked decrease in the bond order of the central double bond suggesting a lower barrier to internal rotation in the ion. Since even the "gentlest" ionization involves 0.7 eV of excess energy, sufficient energy could be imparted to the ion to result in rapid rearrangement.

Collisional Quenching of Vibrational Excitation in $C_6H_8^+$

A cursory examination of the rate parameters presented in Table 7.2 reveals that the rate of collisional quenching of vibrationally excited $C_6H_8^+$ by 1,3,5 hexatriene neutrals increases with increasing ionization energy. The rate of quenching in the sample ionized with nominally 11.0 eV electrons is four times that observed in the sample ionized with 9.0 eV electrons. Since the ion is more likely to be highly excited at the higher ionization energy this result is somewhat surprising. The collision number calculated for the sample ionized at 11.0 eV is roughly two. This is lower than the value of one reported in other studies

(23,36,37) of the quenching of excited ions in collisions with their parent molecules. However, it may not reflect less efficient quenching. The collision number for the reaction between $C_6H_8^+$ and the parent molecule is also about two. In other words, about every other orbiting collision is reactive. If every other orbiting collision causes quenching--as in the 11.0 eV sample--then every (apparently) nonreactive collision leads to quenching.

The other studies of collisional quenching (23,36,37) have involved ions that were slow to react with the parent molecule. In every instance quenching of the vibrationally excited ion occurred on essentially every collision with the parent molecule. This result has been interpreted to indicate that quenching occurs via a resonant charge exchange reaction. However, no direct proof of this has yet been produced. In the one case where a second species of polyatomic molecule (36) was introduced into the sample it was found to be only about one fourth as efficient at quenching the vibrational excitation. This may indicate either that quenching occurs by a different mechanism than charge exchange or that charge exchange (in this case nonresonant) is less efficient.

One might speculate that the mechanism of quenching in the 11.0 eV sample is resonant charge exchange since it apparently occurs on every nonreactive collision. The slower rate (again by a factor of four) observed in the

9.0 eV sample may be attributed to either a lower probability for, or complete absence of, charge exchange. If the ions formed with an ionization energy of 11.0 eV are more highly excited than those formed with an ionization energy of 9.0 eV, the difference in rates suggests that charge exchange is a resonant process only for the more highly excited ions. This in turn may indicate that the ion has rearranged from the original molecular structure. It may indicate that charge exchange is a resonant process only for ions distorted from their equilibrium geometry to a structure similar to that of the parent molecule.

The quenching of vibrationally excited $C_6H_8{}^+$ by argon atoms is roughly independent of ionization energy. If there is a trend it indicates that the ions formed at the higher ionization energy require about fifteen more collisions to quench than those formed at the lower energy. This may simply reflect the fact that more energy needs to be carried off, requiring more collisions.

In comparison to similar processes in neutral molecules (69,71) the quenching of vibrational excitation in ions is very rapid. The number of collisions to quench is about two orders of magnitude less for ions than for the corresponding process in neutrals whether the collision partner is a molecule or an atom. Shin (68) has studied the effect of the interaction potential between the collision partners on the collisional efficiency of vibrational to translational energy transfer. He compared a purely repulsive potential to a Lennard-Jones (r^{-12} - r^{-6}) type potential and found that the inclusion of the attractive term decreased the number of collisions to quench by one to two orders of magnitude. One might speculate that the inclusion of a longer range attractive term, such as the Langevin (49) r^{-4} term commonly used to treat ion-molecule reactions, might decrease the number of collisions to quench by yet another order of magnitude. This is roughly the effect that such a treatment has on the calculated collisional efficiency of ion-molecule reactions relative to neutral-neutral reactions (14). Surely such musing must be regarded as highly speculative but worthy of further study.

Conclusions

This study indicates that in favorable cases time-resolved photodissociation spectroscopy can yield detailed information about the dynamics of physical processes in polyatomic ions. The photodissociation spectra of the parent ion of the two isomers of 1,3,5 hexatriene are identical even at the shortest residence time accessible with this instrument. This suggests that either the differences in the spectra are smaller than the spectral resolution of this instrument or that the ions rearrange to a common structure within 10 ms of ionization.

The collisional quenching of the 350 cm^{-1} mode of the $C_6H_8{}^+$ ion from 1,3,5 hexatriene is extremely rapid compared to similar processes in neutral systems. The rate constant for quenching by atomic argon is roughly 1 x 10^{-11} cm^3 molecule^{-1} s^{-1} for ions formed with an ionization energy of 9.0 eV corresponding to about forty collisions to quench. In ions formed with an ionization energy of 11.0 eV the rate constant for this process is roughly 9 x 10^{-12} cm^3 molecule^{-1} s^{-1} corresponding to fifty-five collisions to quench. This difference probably reflects the fact that more energy must be removed from ions formed at the higher ionization energy.

Quenching by the parent molecule competes with an ion-molecule reaction between $C_6H_8{}^+$ and the parent molecule. The rate of de-excitation of ions formed with an ionization energy of 11.0 eV is roughly four times that of ions formed at an energy of 9.0 eV. The respective rate constants are 4 x 10^{-10} cm^3 molecule^{-1} s^{-1} and 9 x 10^{-11} cm^3 molecule^{-1} s^{-1}. The faster process appears to occur on every nonreactive collision, perhaps by resonant charge exchange. If the slower rate in the lower ionization energy case indicates a lower probability for charge exchange it may indicate that the ion's structure is significantly different than that of the molecule.

REFERENCED BIBLIOGRAPHY

1. P. Kebarle, "Ion Molecule Reactions" Vol. 1, edited by J.L. Franklin (Plenum Press, New York, 1972).

2. W.A. Chupka, "Ion Molecule Reactions" Vol. 1, edited by J.L. Franklin (Plenum Press, New York, 1972).

3. P.B. Tsai, A.S. Werner and T. Baer, J. Chem. Phys. 63, 4,384 (1975).

4. K.C. Kim, J.H. Benyon and R.G. Cooks, J. Chem. Phys. 61, 1,305 (1974).

5. J.H. Futrell and T.O. Tiernan, "Ion Molecule Reactions" Vol. 1, edited by J.L. Franklin (Plenum Press, New York, 1972).

6. J.M.S. Henis, "Ion Molecule Reactions" Vol. 2, edited by J.L. Franklin (Plenum Press, New York, 1972).

7. J.D. Baldeschwieler, Science 159, 263 (1968).

8. P.J. Robinson and K.A. Holbrook, "Unimolecular Reactions" (Wiley Interscience, New York, 1972).

9. S.B. Lias and P. Ausloos, "Ion Molecule Reactions, Their Role in Radiation Chemistry" (American Chemical Society, Washington, D.C., 1975).

10. F.H. Field, "Ion Molecule Reactions" Vol. 1, edited by J.L. Franklin (Plenum Press, New York, 1972).

11. W.C. Lineberger, "Chemical and Biochemical Applications of Lasers" Vol. 1, edited by C.B. Moore (Academic Press, New York, 1974).

12. J.T. Moseley, R.A. Bennett, and J.R. Peterson, Chem. Phys. Lett. 26, 288 (1974).

13. R.C. Dunbar and P. Armentrout, Int. J. Mass Spectrom. and Ion Phys. 24, 465 (1977).

14. M. Henchman, "Ion Molecule Reactions" Vol. 1, edited by J.L. Franklin (Plenum Press, New York, 1972).

15. T.F. Thomas, F. Dale and J.F. Paulson, J. Chem. Phys. 67, 793 (1977).

16. J.T. Moseley, M. Tadjaddine, J. Durup, J.B. Ozenne, C. Pernot and A. Tabche Fouhaille, Phys. Rev. Lett. 37, 891 (1976).

17. T.E. Sharp, J.R. Eyler and E. Li, Int. J. Mass Spectrom. and Ion Phys. 9, 421 (1972).

18. R.C. Dunbar and B.B. Hutchinson, J. Am. Chem. Soc. 96, 3,816 (1974).

19. R.C. Dunbar and R. Klein, J. Am. Chem. Soc. 98, 7,994 (1976).

20. D.W. Turner, "Molecular Photoelectron Spectroscopy" (Wiley Interscience, New York, 1970).

21. J.B. Ozenne, D. Pham and J. Durup, Chem. Phys. Lett. 17, 427 (1972).

22. R. Orth and R.C. Dunbar, J. Am. Chem. Soc. 100, 5,949 (1978).

23. R.C. Dunbar and E.W. Fu, J. Phys. Chem. 81, 1,531 (1977).

24. R.C. Dunbar, Spectrochim. Acta. 31, 797 (1975).

25. R.T. McIver, Jr. and R.C. Dunbar, Int. J. Mass Spectrom. and Ion Phys. 7, 471 (1971).

26. J.R. Eyler and G.H. Atkinson, Chem. Phys. Lett. 28, 217 (1974).

27. L.N. Morgenthaler and J.R. Eyler, J. Chem. Phys., In Press.

28. B.S. Freiser and J.L. Beauchamp, J. Am. Chem. Soc. 96, 6,260 (1974).

29. E. Fu, P.P. Dymerski and R.C. Dunbar, J. Am. Chem. Soc. 98, 337 (1976).

30. L.M. Branscomb, Phys. Rev. 148, 11 (1966).

31. H. Hotop, T.A. Patterson and W.C. Lineberger, J. Chem. Phys. 60, 1,806 (1974).

32. J.L. Beauchamp, D. Holtz, S.D. Wood and S.L. Patt, J. Am. Chem. Soc. 94, 2,798 (1974).

33. M. Riggen, R. Orth, and R.C. Dunbar, J. Chem. Phys. 65, 3,365 (1976).

34. M. Allan and J.P. Maier, Chem. Phys. Lett. 43, 94 (1976).

35. R.C. Dunbar and H.H. Teng, J. Am. Chem. Soc. 100, 2,279 (1978).

36. T.E. Orlowski, B.S. Freiser, and J.L. Beauchamp, Chem. Phys. 16, 439 (1976).

37. B.S. Freiser and J.L. Beauchamp, Chem. Phys. Lett. 35, (1975).

38. R.T. McIver, Jr., Rev. Sci. Inst. 41, 555 (1970).

39. J.R. Eyler, Rev. Sci. Inst. 45, 99 (1974).

40. R.T. McIver, Jr., Rev. Sci. Inst. 44, 1,071 (1973).

41. The derivation is based on one presented by K.C. Smyth and J.I. Brauman, J. Chem. Phys. 56, 4,620 (1972) and adapted to the conditions of the pulsed experiment.

42. R.J. Dugan, L.N. Morgenthaler, R.O. Daubach and J.R. Eyler, Rev. Sci. Inst., In Press.

43. The Vacuum System is based on that of a Varian Syrotron Mass Spectrometer, Varian Associates, Analytical Instruments Division, Palo Alto, California.

44. Veeco RX-21X controller, Veeco Instruments Inc., Plainview, New York.

45. Candela Model ED-66M, Candela Corp., Needham, Mass. The dyes used were: (1) cresyl violet, K & K Pharmaceuticals, Plainview, New York; (2) rhodamine 6 G, rhodamine 110, Eastman Chemical Co., Rochester, New York; and (3) kiton red S, coumarin 540, LD 490, LD 455, Exciton Chemical Co., Dayton, Ohio.

46. Gen Tec Model ED-200, Gen Tec Inc., Ste-Foy, Quebec, Canada.

47. R.T. McIver, Jr., Rev. Sci. Inst. 49, 111 (1978).

48. J.F. Paulson, "Ion Molecule Reactions" Vol. 2, edited by J.L. Franklin (Plenum Press, New York, 1972).

49. G. Gioumousis and D.P. Stevenson, J. Chem. Phys. 29, 294 (1958).

50. The curve fitting program was kindly provided by Professor A.E.S. Green of the Interdisciplinary Center for Aeronomy and Atmospheric Science, University of Florida, Gainesville, Florida.

51. B. Ostle and R.W. Mensing, "Statistics in Research" 3rd ed. (Iowa State University Press, Ames, Iowa, 1975).

52. G.M. Wieder and R.A. Marcus, J. Chem. Phys. 37, 1,835 (1962).

53. S. Ikuta, K. Yoshihara, and T. Shiokawa, Bull. Chem. Soc. Japn. 49, 66 (1976).

54. R.C. Dunbar, "Interactions Between Ions and Molecules," edited by P. Ausloos (Plenum Press, New York, 1975).

55. R.C. Dunbar and J.M. Kramer, J. Chem. Phys. 58, 1,266 (1973).

56. M.L. Vestal and J.H. Futrell, Chem. Phys. Lett. 28, 559 (1974).

57. D.C. McGilvary and J.D. Morrison, J. Chem. Phys. 67, 368 (1977).

58. K. Kimura, S. Katsumata, Y. Achiba, H. Matsumoto, and S. Nagakura, Bull. Chem. Soc. Japn. 46, 373 (1973).

59. D.P. Shoemaker, C.W. Garland and J.I. Steinfeld, "Experiments in Physical Chemistry" (McGraw-Hill Book Co., New York, 1974).

60. J.L. Franklin, J.G. Dillard, H.M. Rosenstock, J.T. Herron, K. Draxl and F.H. Field, Nat. Stand. Ref. Data Ser., Nat. Bur. Stand. (U.S.), 26 (1969).

61. M.F. Golde, J. Mol. Spectrosc. 58, 261 (1975).

62. S.E. Butrill, Jr., J. Chem. Phys. 52, 6,174 (1970).

63. R.C. Dunbar, J. Am. Chem. Soc. 98, 4,671 (1976).

64. M. Beez, G. Bieri, H. Bock and E. Heilbronner, Helv. Chim. Acta. 56, 1,028 (1973).

65. J.C.H. Hwa, P.K. deBenneville, and H.J. Sims, J. Am. Chem. Soc. 82, 2,537 (1960).

66. E.M. Popov and G.A. Kogan, Opt. Spectrosc. (USSR) 17, 362 (1964), (English Tranlation).

67. D. Rapp and T. Kassal, Chem. Revs. 69, 61 (1969).

68. H.K. Shin, J. Chem. Phys. 42, 59 (1965).

69. G. Flynn, "Chemical and Biochemical Applications of Lasers" Vol. 1, edited by C.B. Moore (Wiley Interscience, New York, 1974).

70. C.F. Bernasconi, "Relaxation Kinetics" (Academic Press, New York, 1976).

71. F.D. Shields and K.P. Lee, J. Chem. Phys. 40, 737 (1964).

72. R. Zahradnik and P. Carsky, J. Phys. Chem. 74, (1970).

BIOGRAPHICAL SKETCH

Lee Nickey Morgenthaler was born on August 11, 1952, in Carlisle, Pennsylvania. He attended high school at the Baltimore Polytechnic Institute. On the day after receiving his Bachelor of Science from Tufts University, he married Andrea Oppenheim. As his contribution to the "demographic shift" he entered graduate school at the University of Florida. Upon graduation he will be repatriated (temporarily at least) to the North as a research associate at the U.S. Air Force Geophysics Laboratory in Bedford, Massachusetts.

I certify that I have read this study and that in my opinion it conforms to acceptable standards of scholarly presentation and is fully adequate, in scope and quality, as a dissertation for the degree of Doctor of Philosophy.

John R. Eyler

John R. Eyler, Chairman
Assistant Professor of
Chemistry

I certify that I have read this study and that in my opinion it conforms to acceptable standards of scholarly presentation and is fully adequate, in scope and quality, as a dissertation for the degree of Doctor of Philosopy.

Thomas L. Bailey

Thomas L. Bailey
Professor of Physics

I certify that I have read this study and that in my opinion it conforms to acceptable standards of scholarly presentation and is fully adequate, in scope and quality, as a dissertation for the degree of Doctor of Philosophy.

Martin Vala

Martin T. Vala
Professor of Chemistry

I certify that I have read this study and that in my opinion it conforms to acceptable standards of scholarly presentation and is fully adequate, in scope and quality, as a dissertation for the degree of Doctor of Philosophy.

William Weltner Jr.

William ~~W.~~ Weltner, Jr.
Professor of Chemistry

I certify that I have read this study and that in my opinion it conforms to acceptable standards of scholarly presentation and is fully adequate, in scope and quality, as a dissertation for the degree of Doctor of Philosophy.

James D Winefordner

James D. Winefordner
Professor of Chemistry

This dissertation was submitted to the Graduate Faculty of the Department of Chemistry in the College of Liberal Arts and Sciences and to the Graduate Council, and was accepted as partial fulfillment of the requirements for the degree of Doctor of Philosophy.

June 1979

Harry H. Sisler
Dean, Graduate School

UNIVERSITY OF FLORIDA

3 1262 08554 1018